INFRARED RADIOMETRIC MEASUREMENTS OF SURFACE TEMPERATURES GENERATED BY FRICTION OF SLIDING IRON-ON-SAPPHIRE

by

Steven Craig Moyer

Thesis submitted to the Faculty of the

Virginia Polytechnic Institute and State University

in partial fulfillment of the requirements for the degree of

MASTER OF SCIENCE

in

Mechanical Engineering

APPROVED:

M. J. Furey, Chairman

N. S. Eiss

W. C. Thomas

H. L. Wood

February, 1983

Blacksburg, Virginia

INFRARED RADIOMETRIC MEASUREMENTS OF

SURFACE TEMPERATURES GENERATED BY FRICTION

OF SLIDING IRON-ON-SAPPHIRE

by

Steven Craig Moyer

(ABSTRACT)

Experimental measurements of surface temperatures produced during dry sliding contact were made by using an advanced infrared microscope which receives radiation from a very small target area e.g., $1.78 \times 10^{-5} m$ in diameter for a *36X* objective, allowing temperature measurements within a general region of contact.

The sliding system consisted of an Armco iron pin, with a hemispherical end loaded against a rotating sapphire disk. A statistical study was made concerning the effect of environment, load, and velocity on temperature, wear, and coefficient of friction.

The formation of iron oxides and its influence on emissivity and possible correlation with wear and friction is discussed.

Comparison between the experimental results and the flash temperature theories by both Jaeger and Archard is made.

ACKNOWLEDGEMENTS

The author would like to express his sincere gratitude to his major advisor, Dr. Michael J. Furey, for his guidance and understanding throughout this research and in preparation of this thesis. Appreciation is also extended to Dr. Henry L. Wood, Dr. Norman S. Eiss, and Dr. William C. Thomas for their comments, advice, and interest concerning this study.

The author would wish to thank the National Science Foundation for their financial support.

Special thanks is given to Craig A. Rogers, a friend and colleague for his invaluable assistance, suggestions, and encouragement.

Lastly, the author is indebted to his wife, Llewellyn, for her love and sacrifice; without her help, this study would not have been completed.

TABLE OF CONTENTS

TABLE OF CONTENTS (Continued)

TABLE OF CONTENTS (Continued)

LIST OF FIGURES

LIST OF FIGURES (Continued)

LIST OF FIGURES (Continued)

LIST OF FIGURES (Continued)

LIST OF FIGURES (Continued)

LIST OF TABLES

NOMENCLATURE

Q	Heat supply per unit time
q	Heat supply per unit area per unit time
Θ	Surface temperature rise
Θ_m	Mean surface temperature rise
a	Radius of circular contact area
ℓ	Length of square contact area
K	Thermal conductivity
ρ'	Density
c	Specific heat
κ	Thermal diffusivity $(K/\rho' c)$
μ	Coefficient of friction
V	Sliding velocity
W	Normal load
p_m	Material hardness
E	Modulus of elasticity
R	Radius of hemispherically shaped contact
τ	Transmissivity
ρ	Reflectivity
ε	Emissivity

INTRODUCTION

A. The Problem: Importance and Purpose of Study

With the advent of the first machine, man has been in a constant struggle to control the energy-dissipating force of friction and the destructive wear of machine components. Surface temperature is likely to hold a key to greater understanding of the complex mechanisms of friction, the formation of wear particles, and the failure of lubricants. Thus, the study of surface temperature extends into the complete area of tribology, having many practical applications.

Surface temperature has received attention in manufacturing processes, design of machine components, and the development of lubricants. Chao, Li, and Trigger (1) used lead-sulfide photoconductive cells to determine the temperature distribution across a tool-flank surface, aiding better understanding of tool wear. The frictional heating of wires and strips during drawing has been analytically investigated (2), providing important information in reducing undesirable residual stresses produced by high thermal gradients. Beneficial use of the high temperatures produced by friction have been successfully used in production welding.

Design of machine components in relative motion has profited by studies of surface temperature. H. Blok, one of the earliest investigators of surface temperatures, has proposed that gear scuffing occurs when a critical temperature is obtained and has theoretically derived a "flash" temperature equation (3). This concept has also been investigated by others such as Niemann and Lechner (4) who measured surface temperatures of meshing gears using the dynamic thermocouple principle and Al-Rubeye (5) who experimentally applied this principle to a four-ball machine. Both experimental (6) and theoretical (7) treatments of surface temperatures generated between frictional material and metal have been instrumental in improving brake design. In bearing design, Floquet, Play, and Godet (8) have shown the effectiveness of using surface temperature as a design criterion.

Related to Blok's work, the failure of lubricants in elastohydrodynamic (EHD) contact by high temperatures has important implications. Turchina, Sanborn, and Winer (9) have used a thermal radiative technique to measure the steady-state temperature distribution in an EHD contact. The employment of surface temperature in the formation of an antiwear film has been proposed by Furey (10). In this concept, polymer-formers within a lubricant react at sites of high contact temperature, depositing a protective polymer film.

Since surface temperature is an important variable in a wide range of application, earnest investigation has ensued. Various experimental approaches have been attempted, but the difficulty in obtaining accurate surface temperature measurements has led to the general use of theoretical calculations. Even so, relatively large discrepancies exist between theories. Thus, in light of much effort, only moderate progress has been made in the accurate prediction of surface temperatures produced by friction between solids.

B. Present Research at VPI & SU

Within recent years, a system has been developed at VPI & SU to experimentally measure surface temperatures. In this system, an infrared microscope is used to measure radiance emitted from a specimen in sliding contact with a rotating sapphire disk. Given the necessary thermal radiative properties of both the specimen and the sapphire disk, the surface temperature can be readily determined. The unique feature of this system is its capability to resolve small points of contact and to allow examination of the temperature distribution within a general region of sliding contact.

With Dr. M. J. Furey as principal investigator, the design and construction of the rotating disk/infrared microscope system was initiated by J. M. Wiggins (11). Additional refinements to the system and preliminary investigations were performed by D. I. Omori (12), S. H. Li (13), and M. H. Richardson (14). A collective overview of these investigations and a discussion concerning the capabilities and limitations of the system have been presented by Furey (15).

The following experimental study of surface temperature is part of a 27 month investigation funded by the National Science Foundation (16). The objectives of this study were as follows:

1) to measure the generated surface temperatures, wear, and coefficient of friction of an Armco iron specimen loaded against a rotating sapphire disk in dry sliding contact. Iron was selected as the specimen material for several reasons: metals have not been studied before with this particular system, iron is a widely used material in industry, and iron provides

the effects of oxide formation to be observed.

2) to observe the effects of time, load, and velocity on radiance $\left(\text{watts}\cdot\text{steradian}^{-1}\cdot\text{centimeter}^{-2}\right)$ for the iron-on-sapphire system.

3) to develop a technique for measuring emissivity within the wear region.

4) to investigate the effects of oxide formation on emissivity at the interface.

5) to statistically determine the significance of load and velocity on surface temperature, wear, and coefficient of friction.

6) to perform repeat tests in an inert atmosphere (nitrogen).

7) to compare oxide formation in air and nitrogen environments.

8) to determine the statistical significance of environment on surface temperature, wear, and coefficient of friction.

9) to compare the measured values of surface temperature for both environments with major theories, i.e., those proposed by Jaeger and Archard.

REVIEW OF RELATED LITERATURE

A. Experimental Background

A lack of rigorous experimental information on the magnitude of surface temperatures reached during sliding contact has resulted from the difficulty in making such measurements. Numerous attempts to measure surface temperature by embedded thermocouples have been made, e.g., Spurr (17). One major objection to this practice is that disruption of the flow of heat will occur, resulting in an inaccurate measurement. Embedded thermocouples can satisfactorily measure the bulk temperature near the surface; however, their use to measure temperatures at the interface is questionable. The sub-surface temperatures measured by embedded thermocouples have been used to predict the surface temperature by considering the flow of heat through an idealized single asperity (18).

To avoid the induced error caused by embedding thermocouples, Ling and Simkins (19) attempted to measure the surface temperature distribution at the contact region by using thermocouples positioned in the plane of the specimen's surface, perpendicular to the interface. The experiment was designed such that the flow of heat in the specimen would be at most two-dimensional in the plane to the interface. Thus, the temperature along a line parallel to the interface would be approximately the same.

The interference of the heat flow within a specimen has also been circumvented by using the dynamic thermocouple (20). Sometimes referred to as the Herbert-Gottwein method, the dynamic thermocouple consists of two dissimilar metals as the slider and rider. This method has revealed more information concerning the high temperature transients as reported by Furey (21). It was found, however, that the dynamic thermocouple gave results considerably lower than that predicted by Archard's flash temperature theory. The dynamic thermocouple is limited by the fact that it can only measure a kind of average surface temperature, being a function of the number of contacting areas at a given time. Therefore, it is incapable of describing the temperature distribution across the contact region. The dynamic thermocouple has also been used by Uetz and Sommer (22) where the surface temperature measurements were supplemented by determining the phase transformation of the specimen.

In oxidational wear studies, Quinn (23) analyzed the oxide wear debris by x-ray diffraction as an indirect measurement of surface temperature. The estimated temperature was found to be of the same magnitude as that measured by the dynamic thermocouple.

A more advanced method of surface temperature measurement is the use of infrared detectors. In 1948, Parker and Marshall (24) used an infrared-sensitive photoconductive cell to measure the temperature reached between a brake and drum. Later, Bowden and Thomas (25) used a lead sulphide cell to investigate the high, fluctuating temperatures generated between metal pin specimens and a quartz disk. It was found, in general, that the maximum temperature rise was limited by the melting point of the specimen. Another study used the lead sulphide cell to measure the temperature distribution at the flank surface of a cutting tool as it quickly passed over an arrangement of small holes drilled through the workpiece (1).

Early use of infrared detectors received radiation from the total contacting surface; thus, only an average temperature could be measured. Recent advances in infrared detectors and electronics have produced an available infrared radiometric microscope (Barnes Model RM-2A) capable of detecting radiation from extremely small areas (approximately $2.5 \times 10^{-4} mm^2$). This particular microscope has been used to map the temperature distribution across an EHD contact (9) and has also been used in fundamental research of surface temperatures generated in dry sliding contact at VPI & SU (15).

One primary difficulty in using infrared detectors is that one of the specimens must be transparent to infrared radiation. This reduces the free choice of material pairing. Otherwise, holes must be drilled through the specimen to allow the detector to view the surface which disrupts the flow of heat. Another primary difficulty arises when the measured radiance output is converted to temperature. To enable accurate conversion of radiance to temperature, the specimen's emissivity must be known. Since the sliding contact is a dynamic system, knowledge of the emissivity with time presents a very difficult problem. Over thirty potential sources of error associated with the particular system used at VPI & SU have been discussed in detail by Furey (26).

B. Theoretical Background

One of the earliest attempts to analytically derive the surface temperatures generated between two sliding bodies was conducted by Blok (27). The initial work involved the calculation of the temperature rise due to a heat source in contact with a plane body of infinite heat capacity. It was assumed that all the heat is conducted away into the body. Heat sources of various shapes and distributions were dealt with under two condition, (a) stationary, and (b) moving. The cases having particular importance were those developed for a circular heat source having a steady, even distribution.

Under the above given conditions, the temperature rise at the center of the contact was derived for both the stationary case and the moving heat source. For the stationary case, the temperature rise was found to be

$$\Theta_{center} = \Theta_{max} = Q/(\pi K a) = qa/K \qquad \{1\}$$

where the total heat supply per second is given by $Q = \pi q a^2$. For a heat source moving at constant velocity, and assuming no lateral heat flow occurs, the temperature at the center of the contact was derived for both a high and low velocity case.

For high velocities where $V \geq \frac{4\kappa}{a}$,

$$\Theta_{center} \sim \frac{qa}{K}(4\kappa/V\pi a)^{\frac{1}{2}} \qquad \{2\}$$

For low velocities where $V \leq \frac{4\kappa}{25a}$,

$$\Theta_{center} \sim 18a/K\sqrt{\pi} \qquad \{3\}$$

It was noted that the high speed equation will become more accurate as the velocity increases. This effect occurs because the assumption of zero lateral flow of heat is more nearly approximated.

In applying these equations to a protuberance on one body sliding against a plane surface of another body (see Fig. 1), the proportion of heat generated at the sliding interface entering each body must be determined. Thus, if $A_1 Q$ and $A_2 Q$ are the quantities of heat entering bodies *1* and *2*, respectively, it is obvious that $A_1 + A_2 = 1$. To determine the fractions A_1 and A_2, it was assumed that no temperature jump occurs at the region of actual contact between the two bodies. To approximate this condition, Blok equated the average temperature of each body at the interface and determined for the high velocity case that

$$A_2 \sim \frac{1/2(1 - 1/\sqrt{2}) + K_2/K_1 (V\pi a/8\kappa_2)^{\frac{1}{2}}}{1 + K_2/K_1 (V\pi a/8\kappa_2)^{\frac{1}{2}}} \qquad \{4\}$$

and $$A_1 = 1 - A_2 \qquad \{5\}$$

Since the model utilizes friction as the source of heat, the heat supply per unit area per unit time at the contact region may be assumed to be

$$q = \mu WV/a^2 \qquad \{6\}$$

where all of the frictional resistance is converted to heat.

The analytical study of moving heat sources and their application to sliding contacts was further investigated by Jaeger (28). Like Blok, Jaeger dealt with various shapes of uniform plane heat sources moving with constant velocity on the surface of a semi-infinite medium with no heat loss from the surface. Both maximum and average steady temperatures over the area of the source were derived. The temperature equations

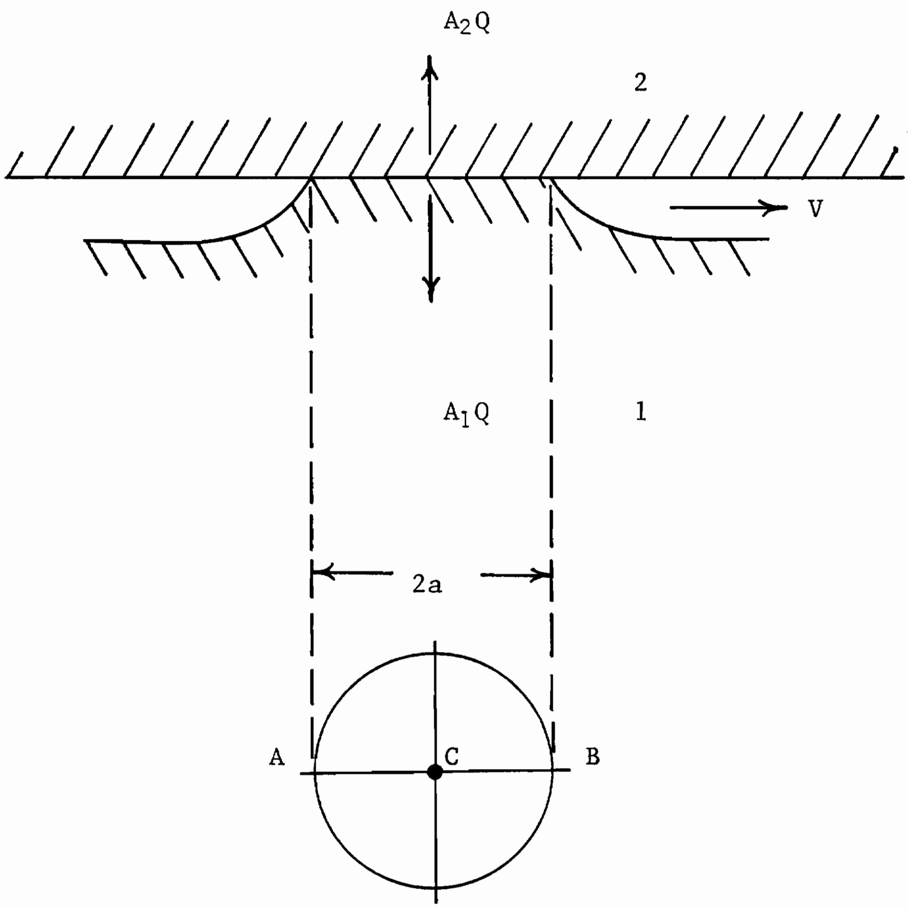

Figure 1 A Round Protuberance on Body 1 Sliding Against the Plane Surface of Body 2

of particular importance are those pertaining to a square source of sides $2l$ in length with heat liberated uniformly at the rate q per unit time per unit area moving at a constant velocity, V. The equation for the temperature at a point (x, y, z) at time t in an infinite solid, initially at zero temperature, due to a quantity of heat Q instantaneously liberated at the point (x', y', z') at zero time as derived by Carslaw (29) to be

$$\Theta = \frac{Q\kappa}{8K(\pi\kappa t)^{3/2}} \cdot \exp\left\{ - \frac{(x - x')^2 + (y - y')^2 + (z - z')^2}{4\kappa t} \right\} \qquad \{7\}$$

From this equation, Jaeger begins his analysis. For stationary square sources, the steady temperature with no heat loss from the surface and q constant was found to be,

$$\Theta_m = 0.946 \ell q/K \qquad \{8\}$$

and

$$\Theta_{max} = 1.122 \ell q/K \qquad \{9\}$$

In the case of moving heat sources, the derivations are much more complicated. To simplify the temperature equations, Jaeger specified three distinct regimes depending upon the dimensionless quantity L, called the Peclet number. The Peclet number is defined as

$$L \equiv V\ell/2\kappa \qquad \{10\}$$

Therefore, for small L $(L < 0.1)$,

$$\Theta_m = 0.946 q\ell/K \qquad \{11\}$$

$$\Theta_{max} = 1.122 q\ell/K \qquad \{12\}$$

These are equivalent to the stationary heat source equations.

For large L $(L > 5.0)$,

$$\Theta_m = 1.064q/K \cdot (\kappa\ell/V)^{\frac{1}{2}} \qquad \{13\}$$

$$\Theta_{max} = 2q/K \cdot (2\kappa\ell/\pi V)^{\frac{1}{2}} \qquad \{14\}$$

For the intermediate range of L $(0.1 < L < 5)$, a graphical method shown in Fig. 2 was developed by Jaeger to simplify the temperature calculations. The curves are a plot of the quantity $(\pi KV/2\kappa q)\Theta$ versus L. Curve *I* is to be used for maximum temperature calculations and curve *II* is to be used for average temperature calculations.

To apply these temperature equations to the problem of a small square protrusion on one body sliding against the plane surface of another body, Jaeger used similar assumptions to Blok's (27). A fraction of heat, A, enters the plane surface and A-1 into the slider. The fraction A was determined upon the assumption that the average temperature over the contact area calculated for a moving source Aq in Body 1 equals the average temperature calculated for Body 2 with a stationary source $(1 - A)q$. Therefore, it was determined that A may be given by

$$A = K_1/(K_1 + K_2) \qquad (L < 0.1) \qquad \{15\}$$

$$A = \frac{K_1(\ell V)^{\frac{1}{2}}}{1.125K_2\kappa_1^{\frac{1}{2}} + K_1(\ell V)^{\frac{1}{2}}} \qquad (L > 5) \qquad \{16\}$$

For the intermediate values of L, the average temperature for Body 1 must be obtained from Fig. 2, curve *II*. It was then found that

$$A = \frac{1.486\ell K_1 V}{1.486\ell K_1 V + \kappa_1 K_2 y} \qquad (0.1 < L < 5) \qquad \{17\}$$

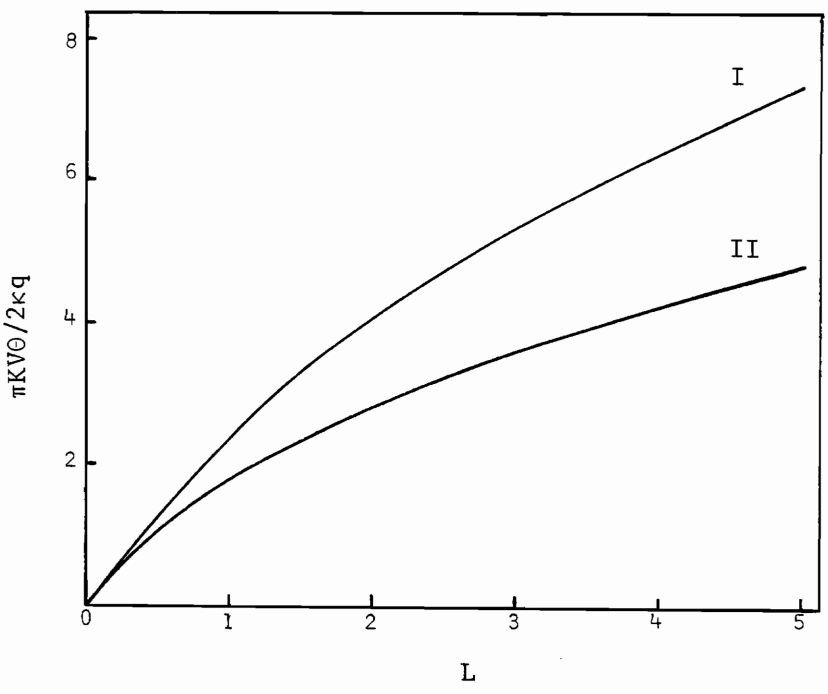

Figure 2   Graphical Method for Both Maximum (I) and Average (II) Temperature Calculation as Developed by Jaeger

where

$$y = (\pi K_1 V/2Aq\kappa_1)\Theta_m \qquad \{18\}$$

and is the ordinate of Fig. 2 for the abscissa L. Applying these values of A to the corresponding average temperature equations, the final equations were found for the three regimes of L. Thus,

$$\Theta_m = 0.946q\ell/(K_1 + K_2) \qquad (L < 0.1) \qquad \{19\}$$

$$\Theta_m = \frac{1.064q\ell\kappa_1^{\frac{1}{2}}}{1.125K_2\kappa_1^{\frac{1}{2}} + K_1(\ell V)^{\frac{1}{2}}} \qquad (L > 5) \qquad \{20\}$$

$$\Theta_m = \frac{0.946\ell\kappa_1 qy}{1.486\ell K_1 V + \kappa_1 K_2 y} \qquad (0.1 < L < 5) \qquad \{21\}$$

The theoretical work done by Blok and Jaeger is a fairly complete surface temperature analysis of a single sliding contact point on a plane surface. However, due to the mathematical complexities of these analyses, Archard (30) approached the problem of determining surface temperature by emphasizing the physical considerations upon which the calculations are based. The model used by Archard is shown in Fig. 3. A protuberance on the surface of body B forms a circular contacting region $A = \pi a^2$, which slides with a velocity V over the plane surface of body C. Thus, body B receives heat from a stationary heat source and body C receives heat from a moving heat source. The temperatures were calculated on the assumption that the heat is generated at the area of true contact and that heat is conducted into the bulk of the two bodies. For simplification, only a single contact point is used. To determine the area of contact, both elastic and plastic deformation theories were used and included within the temperature equations.

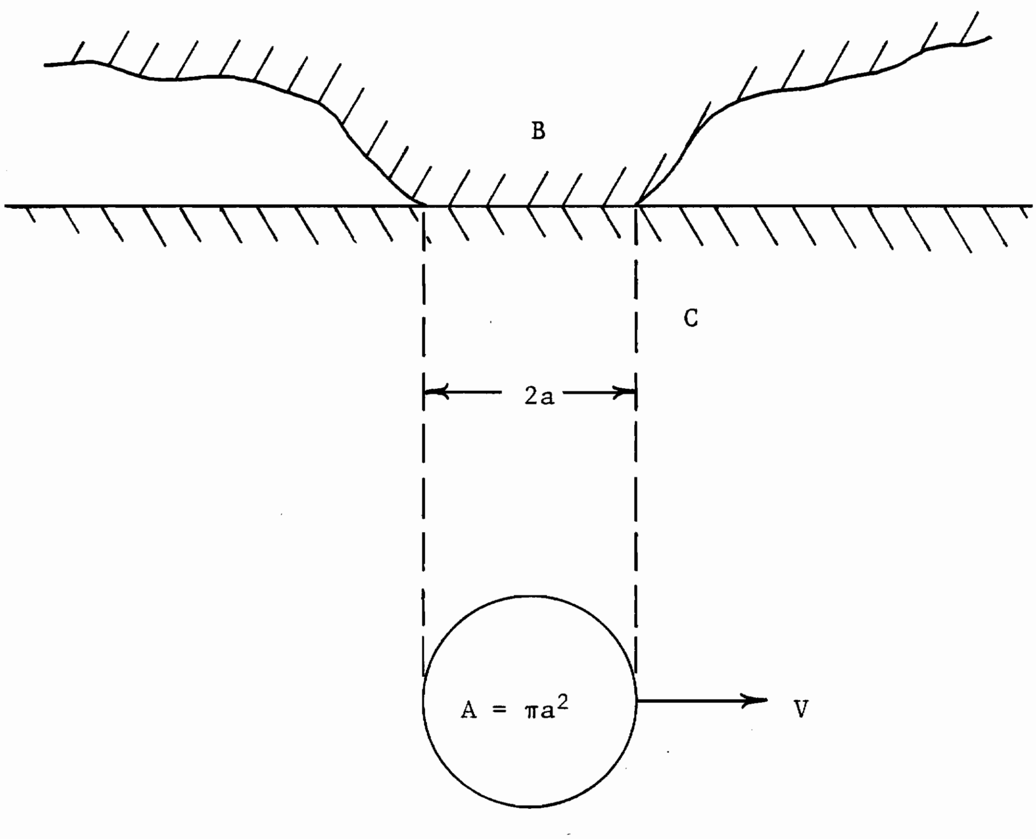

Figure 3 Archard's Model for Surface Temperature Calculations Between Rubbing Surfaces

Archard developed his theory by first deriving the equations for the flow of heat into each body. The surface temperatures were then expressed in terms of rate of heat supply, the size and speed of the heat source, and the thermal properties of the material. Finally, the proportion of heat entering into each body was determined. Like Jaeger (28), Archard used the Peclet number, *L*, where

$$L \equiv Va/2\kappa \tag{22}$$

as a speed criterion to determine which temperature equation applies for a given sliding condition. The stationary heat source problem was shown to result in a steady average temperature across the contact area as

$$\Theta_m = Q_B/(4aK_B) \tag{23}$$

The subscript, *B*, applies to body *B* since it will be, in all cases, subjected to a stationary heat source.

For the slow moving heat source as defined by $L < 0.1$, the average temperature was given to be the same as the stationary case since there will be sufficient time for the temperature distribution to be established in body *C*. Thus,

$$\Theta_m = Q_C/(4aK_C) \tag{24}$$

As the velocity increases to the point where $L > 5.0$, the heat penetrates into body *C* only into a very thin layer such that lateral flow of heat can be neglected. Thus, the high speed equation was determined as

$$\Theta_m = \frac{0.31Q_C}{K_C a} \cdot \left\{ \frac{\kappa_C}{Va} \right\}^{\frac{1}{2}} \tag{25}$$

For the intermediate range of velocities, i.e., $0.1 < L < 5.0$, Archard gave the following equation as an approximation

$$\Theta_m = 0.5\alpha NL \tag{26}$$

where $N = \pi q/\rho c V$, q being the rate of heat supply per unit area. The parameter α is a function of L which must be obtained using Jaeger's graphical method (see Fig. 2). Archard stated that α ranges from approximately *0.85* at $L = 0.1$ to about *0.35* at $L = 5.0$.

To determine the proportion of heat entering each body, Archard proposes a method which differs from both Blok's and Jaeger's. The method is to determine the flash temperature of each body on the assumption that all the heat is supplied to each separately. Thus, the stationary heat source equation should be used for body B, and the appropriate flash temperature equation based on the value of L should be used for body C. Then, the final average surface temperature between body B and body C will be given by

$$1/\Theta_m = 1/\Theta_B + 1/\Theta_C \tag{27}$$

Applying elastic and plastic deformation theories where both bodies are of the same material, Archard derives the following equations for low and high sliding speeds.

At low speed ($L < 0.1$) with plastic deformation,

$$\Theta_m = \frac{\mu(\pi p_m W)^{1/2} V}{8K} \tag{28}$$

At low speed ($L < 0.1$) with elastic deformation,

$$\Theta_m = \frac{\mu W^{2/3} V}{8.8K} \cdot (E/R)^{1/3} \tag{29}$$

For high sliding speeds (*L* > *100*) with plastic deformation,

$$\Theta_m = \frac{\mu(\pi p_m)^{3/4} W^{1/4} V^{1/2}}{3.25(K\rho c)^{1/2}} \qquad \{30\}$$

For high sliding speeds (*L* > *100*) with elastic deformation,

$$\Theta_m = \frac{\mu(WV)^{1/2}}{3.8} \cdot \left(\frac{E}{K\rho c R}\right)^{1/2} \qquad \{31\}$$

The above equations reveal how the mean surface temperature varies with load, speed, and material properties. It can be seen that the surface temperature rise will increase with velocity and load, where velocity has the greater effect in most cases.

The case of sub-dividing the contact region into a number of small contact areas was discussed briefly by Archard. It was noted that if the smaller contact areas were closely packed, the above derived equations may give a first approximation of the final average surface temperature since the heat conduction interaction between contact areas will be high. In the limit, the largest calculated temperature will result if the contact region is considered to be wholly in contact.

The early work by Blok, Jaeger, and Archard has been widely used to estimate flash temperatures in frictional processes. However, a number of investigators of relatively recent years have proposed interesting theories spurred by valid questions. The earlier work has been used as a foundation upon which various modifications have been made in order to provide a more accurate mathematical model of the basic sliding system and to give a better estimate of the temperatures generated between the two bodies.

The effect of multiple contacts on the calculated temperature rise has been reviewed in detail (31). To determine this effect, Archard's flash temperature theory was applied to an increasing number of contacts, each having equal area, while the total contact area remained constant. For any number of contacts existing within the general region of contact, the total area determined by plastic deformation is given by

$$A_r = n\pi a^2 = W/p_m \qquad \{32\}$$

where n is the number of circular contacts, each having a radius of a. Assuming an even distribution of heat, each individual contact will receive heat at the rate of Q/n. Interaction of heat flow on neighboring contact areas was neglected. Substituting equation {32} into equations {24} and {25}, the temperature rise of a contacting asperity becomes

$$\Theta_m = \frac{Q}{4K_C} \cdot \left(\frac{\pi p_m}{nW} \right)^{1/2} \qquad \{33\}$$

at low velocity, and

$$\Theta_m = \frac{0.31Q}{(K\rho cV)^{1/2}} \cdot \left(\frac{\pi p_m}{W} \right)^{3/4} \cdot \left(\frac{1}{n} \right)^{1/4} \qquad \{34\}$$

at high velocity.

From the above equations, the number of contacting areas will decrease the flash temperature by a factor of $(1/n)^{1/2}$ for low sliding speeds and by a factor of $(1/n)^{1/4}$ at high sliding speeds. A general example showing the flash temperature at low speeds as a function of the number of contacts is given in Fig. 4. The number of contact areas in the range of *1* to *100* has a significant effect on the calculated surface temperature. Therefore, to obtain a better estimate of the surface temperature likely to be obtained, the probable number of contacts must be assessed.

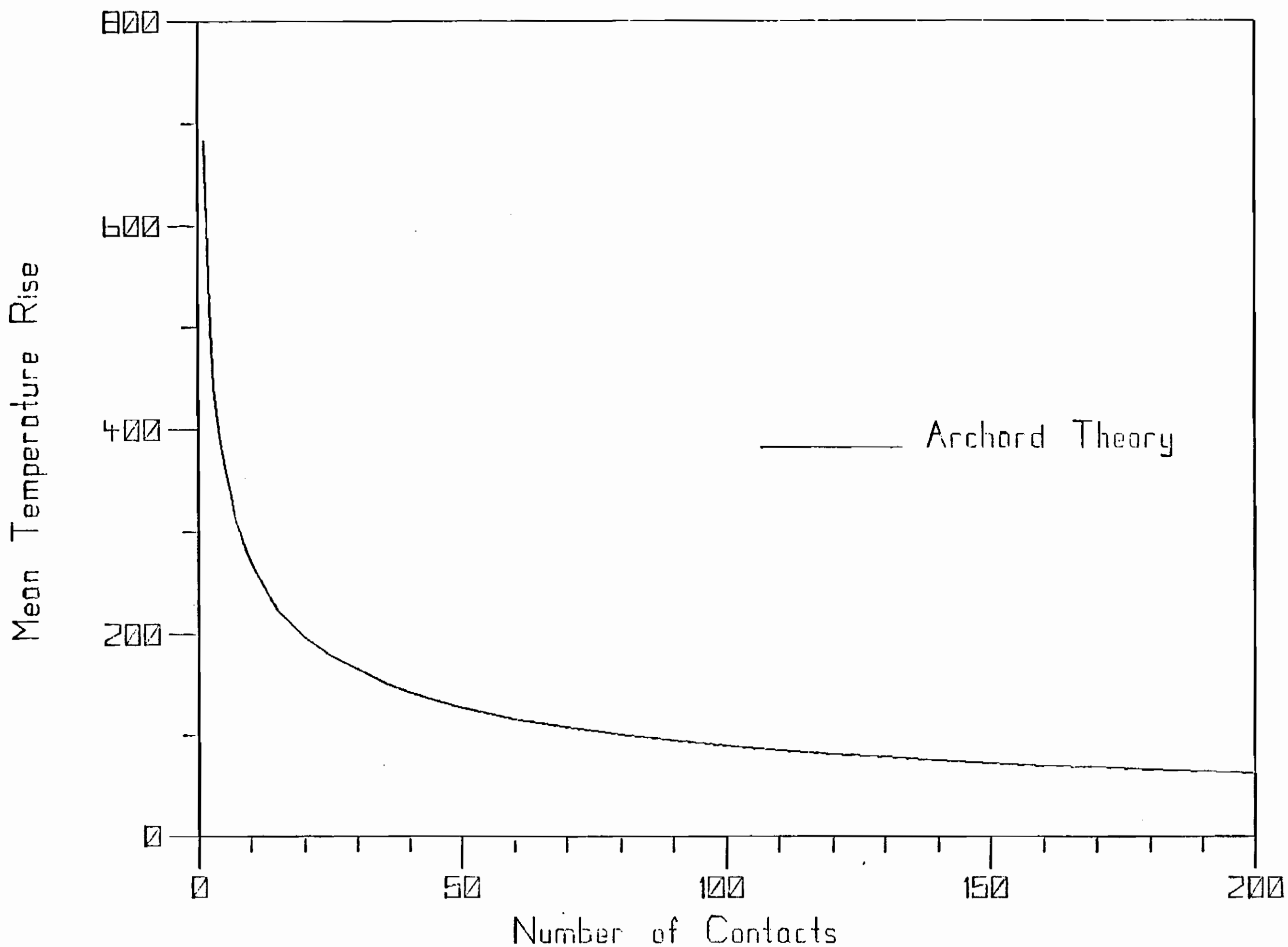

Figure 4   An Example Showing the Effect of Multiple Contacts on Surface Temperature Rise

The theoretical and experimental investigations by Ling, et al. have addressed some interesting questions. Ling and Pu (32) have developed a simple, stochastic model which allows the computation of surface temperture in a contact region within which the actual contact area changes with time and space. In this model, the simplifying assumptions are: all the heat enters a semi-infinite solid, no heat loss occurs over the surface, heat enters only at the common contact areas, and the real area of contact does not change with time. The model in Fig. 5 shows a square protrusion divided into $m \times m$ square areas, each being of the magnitude of the smallest microscopic contact area. From plastic deformation theory, only a certain percentage of the m^2 areas will be in contact for a given load and material yield strength. Thus, as time proceeds, a number of the basic squares may coalesce. The stochastic process is applied for each time interval $\Delta\tau$. From a histogram of surface temperature transients, it was found that a significant peak average occurred, having a magnitude of approximately five times the average temperature.

The existence of transient temperatures above the average surface temperature has been observed experimentally, i.e., that noted by Furey (21), who utilized the dynamic thermocouple principle in a ball-on-cylinder test machine for friction studies.

Ling and Rice (33) investigated the effect of temperature-dependent thermal properties on surface temperatures generated by a moving heat source along the surface of a semi-infinite body. The solution to this problem was given by Blok, Jaeger, and Archard assuming constant thermal properties. To provide for the temperature dependency of the thermal

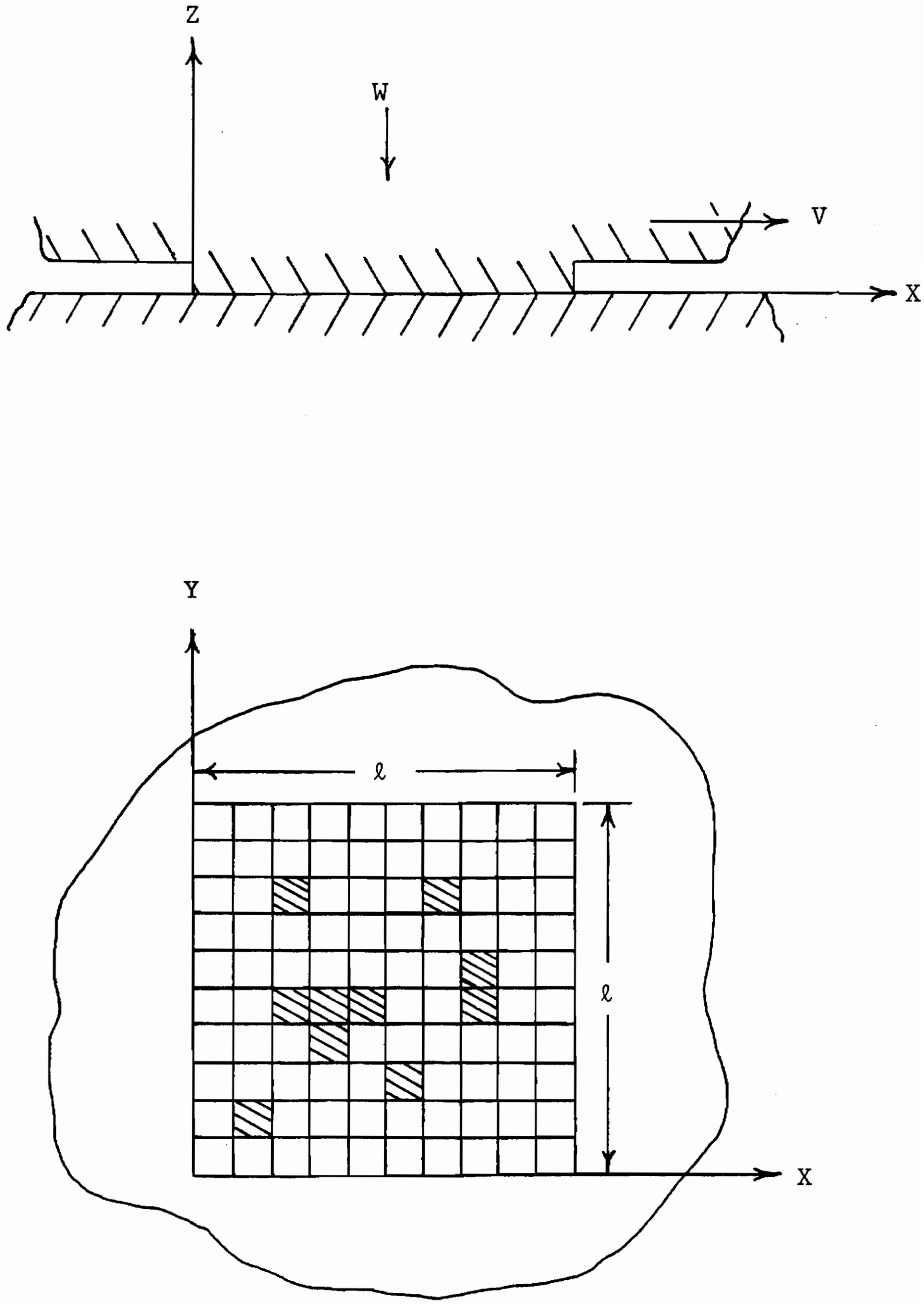

Figure 5 Stochastic Model for Calculating Surface Temperature Transients (from reference 32)

properties, the governing heat conduction equation becomes nonlinear. With no general method of solving nonlinear differential equations, an iterative method was developed. The function $(\rho' cK)^{-\frac{1}{2}}$ was used as a criterion to determine whether the temperature dependency of the relevant thermal properties should be considered.

The steady-state temperature distribution within a sliding Hertzian contact region was derived by Francis (34). An ellipsoidal distribution of the frictional power was used which arises from the pressure distribution of the elastically deformed surface. Also, the contacting bodies were not assumed semi-infinite, thus, a bulk temperature term for each body was included in the calculations. The resulting equation gives a maximum flash temperature *33-38* percent higher than that predicted by Blok (27).

The question of the effect of surface roughness has been investigated by Cook and Bhushan (35). Their analysis included the temperature rise at each pair of mating asperities and the interaction of the temperature rise on neighboring asperities. The average surface temperature between two bodies was given as

$$\Theta_m = \frac{\mu V}{K_1 + K_2} \cdot (0.44H\bar{d}_{max} + 0.35\sigma) \qquad \{35\}$$

where $\bar{d}_{max}$ is the area weighted average of maximum junction diameter, $\bar{\sigma}$ is the mean contact stress, and H is the material bulk hardness.

Malkin and Marmur (36) calculated surface temperatures by modeling the moving heat source as being distributed within a thin layer beneath the surface, in contrast to the classical plane heat source that moves on the surface. The temperature was expressed in dimensionless form.

However, due to the complexity of the temperature equation and the subsurface energy input distribution, integration was done by a digital computer. The numerical results were compared to those predicted by Jaeger, and it was found that the surface temperature can be significantly overpredicted by classical flash temperature theory. The deviation between the two theories was shown to become greater at higher Peclet numbers and at lower energy input gradients in the subsurface.

The problems of non-stationary heat exhange and heat mass transfer processes which can occur at the sliding interface were discussed by Balakin (37). To solve the heat conduction equation, proper boundary conditions must be chosen. A variety of thermophysical models of sliding contact was considered. Balakin stated that analysis of non-stationary heat generation and heat exhange in high-speed and heavily loaded sliding contacts can only be solved statistically, based upon experimental data on various factors, e.g., asperity interaction, material transfer, effect of surface films, possible changes of real contact area, and the thermophysical properties of the bodies.

In conclusion, it becomes clear that at some point, certain assumptions must be made in order to obtain an analytical solution for surface temperatures generated in tribological processes. These assumptions must be made in consideration of the particular system being analyzed and upon the degree of accuracy desired. To develop useful mathematical models, additional experimental work is necessary to broaden the present knowledge concerning the complex interactions at the sliding interface.

EXPERIMENTAL

A. Description of Apparatus

The focus of this experimental investigation of surface temperature was centered on the interface between an iron specimen having a hemispherical end in sliding contact with a rotating sapphire disk. The sliding system is shown in Fig. 6. The pin test specimen was constructed of Armco iron having a length and diameter of approximately $12.5\ mm$ and $3.2\ mm$, respectively. The pin, being held securely by two setscrews, was positioned to extend approximately $3.2\ mm$ above the holder. The machined hemispherical end ($diameter = 3.18\ mm$) provided convenient location of the initial contact area and microscope focusing. The geometry also simplified the application of elastic deformation theory necessary in using flash temperature theories. A copper-constantan thermocouple was used to measure the bulk temperature rise of the test specimen.

The specimen was loaded against a sapphire disk which was rotated at various constant rotational velocities. The disk has a diameter and thickness of $50.8\ mm$ and $1.0\ mm$, respectively. Sapphire was the material choice for several reasons. First, sapphire is highly transparent within the radiation bandwidth of the microscope's infrared detector ($\tau = 0.85$) and to the eye. Second, sapphire is much harder than many materials which prevents excessive wear of the disk's surface. Third, sapphire disks are readily available having optically flat surfaces. The material properties of both Armco iron and sapphire are given in Table 1.

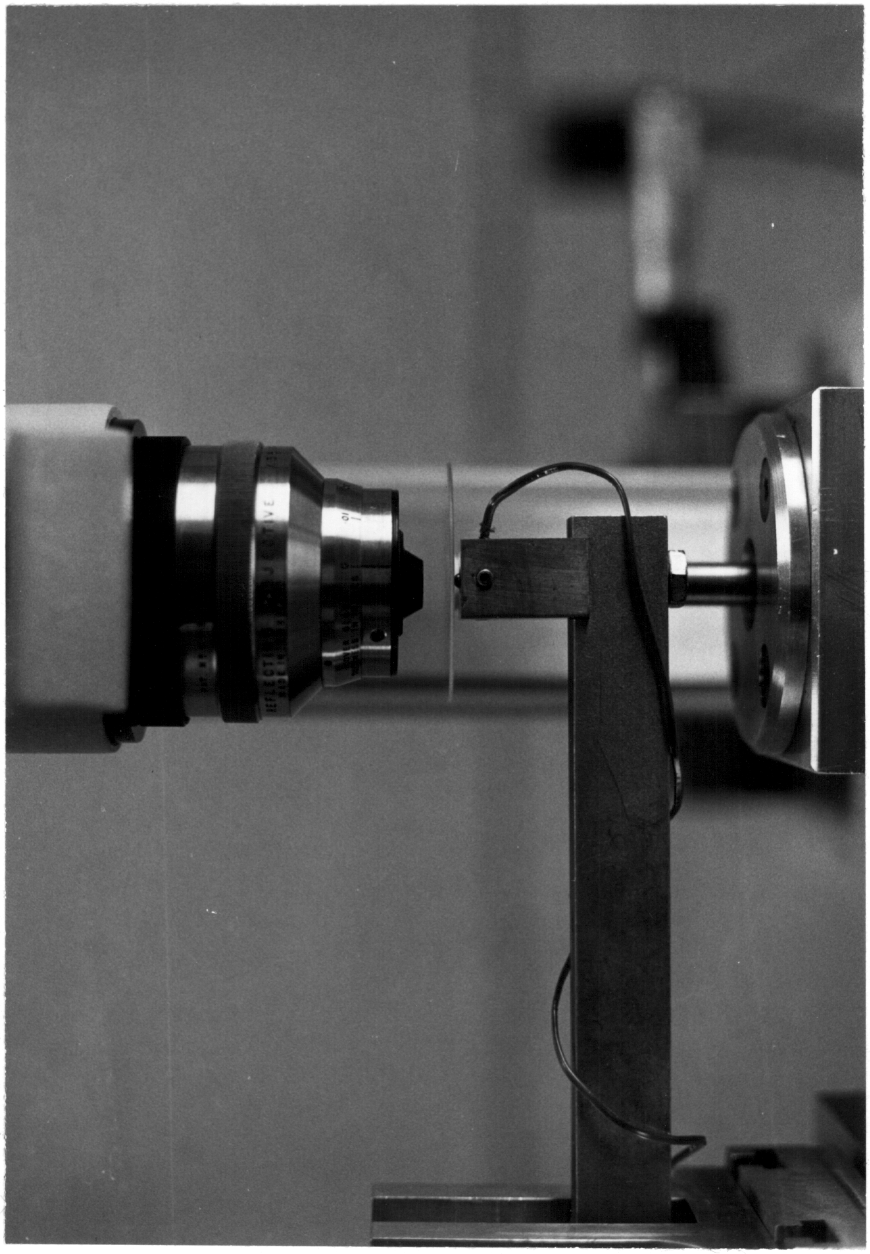

Figure 6 Basic Sliding System with Infrared Microscope

TABLE 1

THERMAL AND MECHANICAL PROPERTIES OF

ARMCO IRON AND SAPPHIRE

Material:	Armco Iron[1]	Sapphire[2]
Modulus of Elasticity (N/m^2)	2.09×10^{11}	3.65×10^{11}
Density (kg/m^3)	7.86×10^{3}	3.98×10^{3}
Specific Heat (J/kg-C)	4.52×10^{2}	4.20×10^{2}
Conductivity (J/s-m-C)	6.69×10^{1}	2.18×10^{1}
Hardness (N/m^2)	9.00×10^{8}	1.77×10^{10}
Melting Point (C)	1.54×10^{3}	2.31×10^{3}
Poissons Ratio	2.80×10^{-1}	2.00×10^{-1}

[1] Materials Handbook. Brady, 11th ed. New York: McGraw-Hill, 1977.

[2] General Ruby and Sapphire Corporation, 50 East 42nd Street, New York, New York 10017.

The temperature at the sliding contact was measured indirectly by a Barnes Infrared Radiometric Microscope Model RM-2A. The microscope responds to the emanating radiation from the surface without physical contact. Figure 7 shows the infrared microscope unit. The microscope has both a visual and infrared optical channel allowing simultaneous viewing and measurement from the target area. A resolution of 1.778×10^{-5} m is obtained by using a *36X* reflecting objective, resulting in a total visual magnification of *360X*. The *10X* eyepiece contains a crosshair reticle which enables precise location of the target area. The infrared channel contains a tuning-fork optical chopper which serves as an ambient background reference source having a *50%* duty cycle. A copper-constantan thermocouple was attached to the microscope body to detect any variation in ambient temperature. The liquid nitrogen-cooled (*77 K*) indium antimonide photovoltaic detector receives the radiation from both the specimen and the chopper, converting it to an AC electrical signal. The spectral response of the detector is shown in Fig. 8. The detector responds within the bandwidth of *1.8* to *5.5* microns. The microscope was calibrated following the procedure given in Appendix A.

The infrared microscope is attached to a precision *X-Y* table which allows the general area of contact to be scanned. The relative position was accurately measured by a linear variable differential transformer (LVDT) in both the radial and tangential directions. Figure 9 shows the precision *X-Y* table and the location of the LVDTs. Details concerning the calibration of the LVDTs are given in Appendix B.

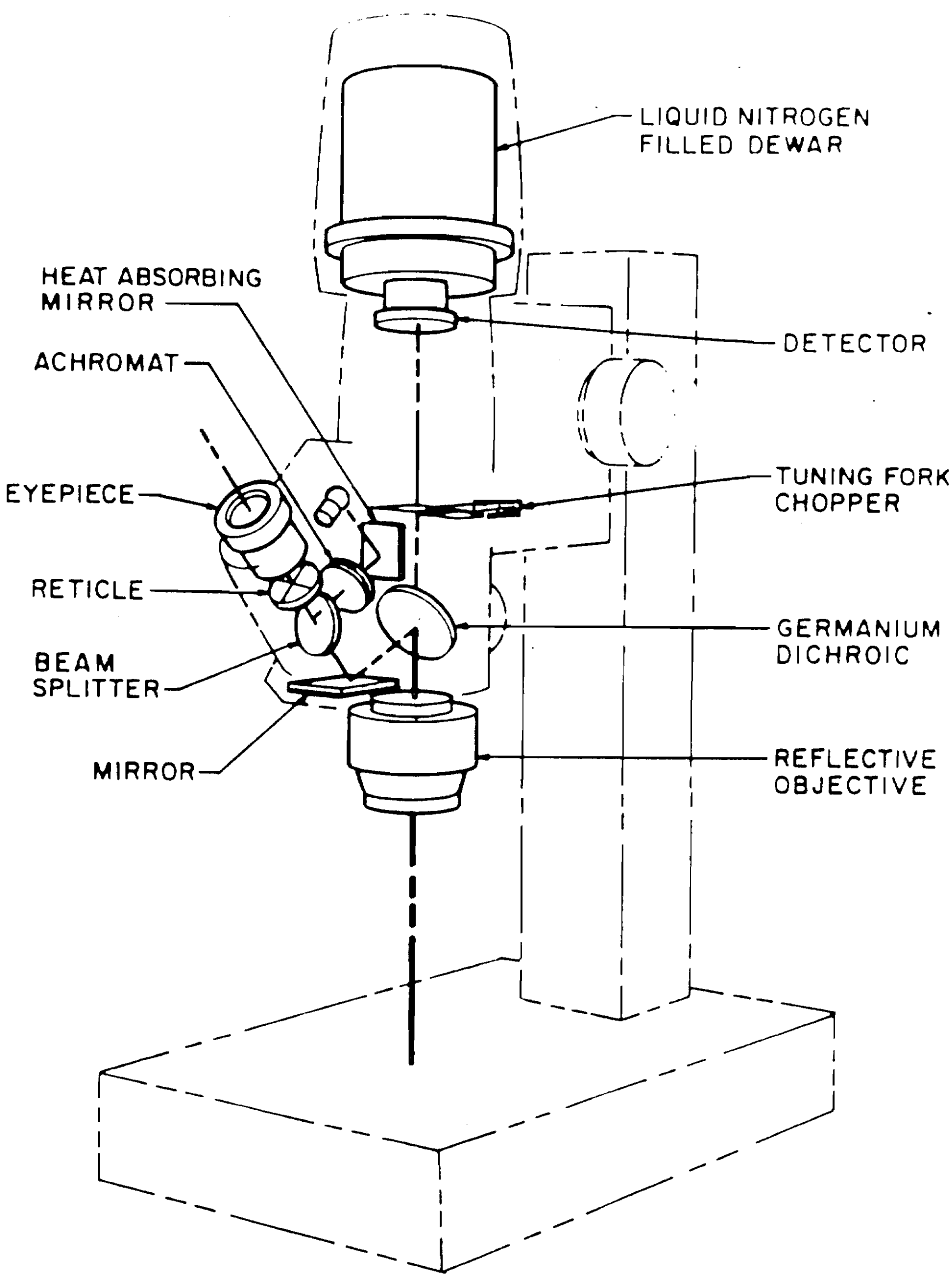

Figure 7 Schematic Diagram of Barnes Model RM-2A Infrared Microscope (from reference 38)

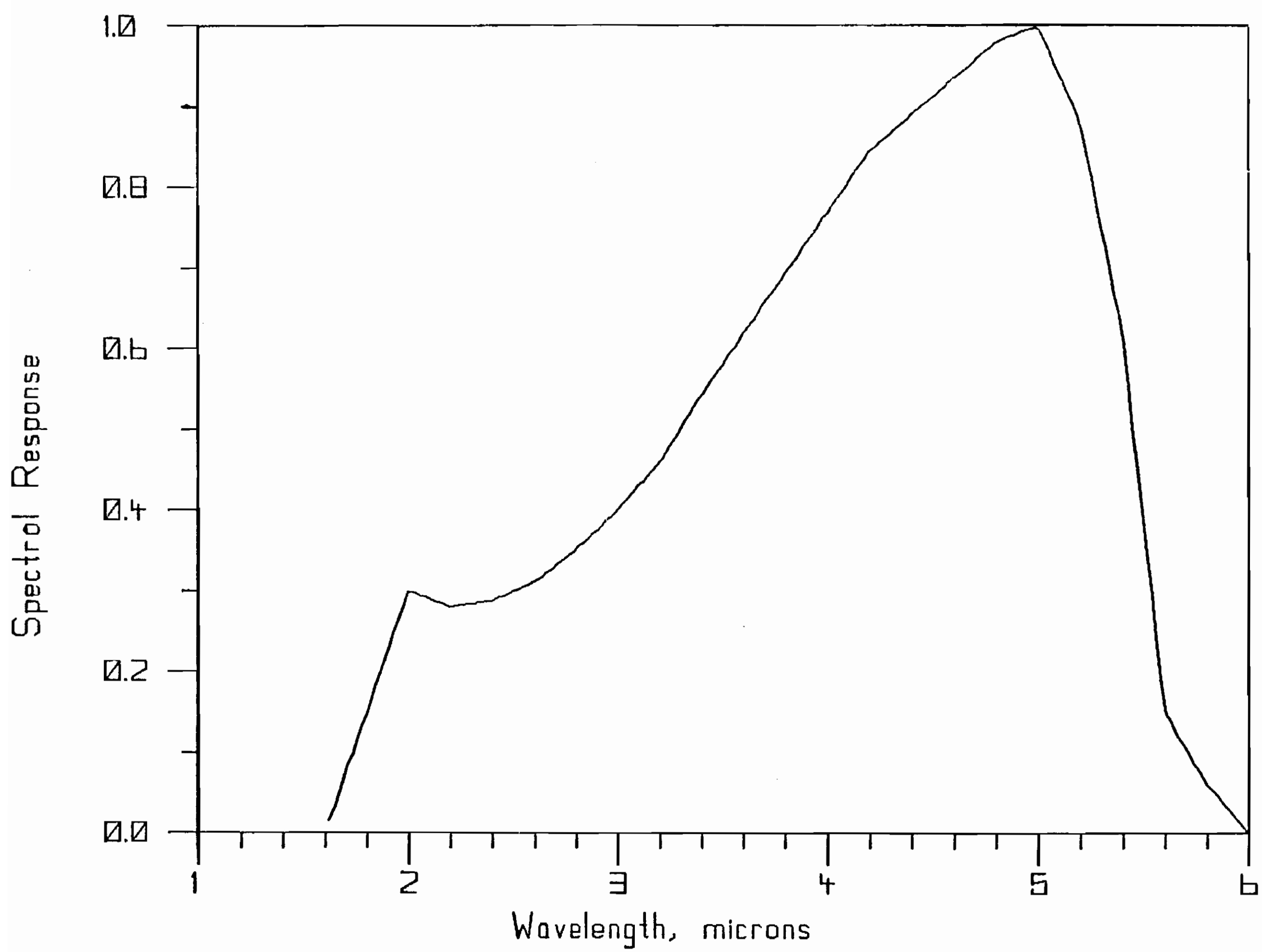

Figure 8 Normalized Spectral Response of Infrared Detector

(from reference 39)

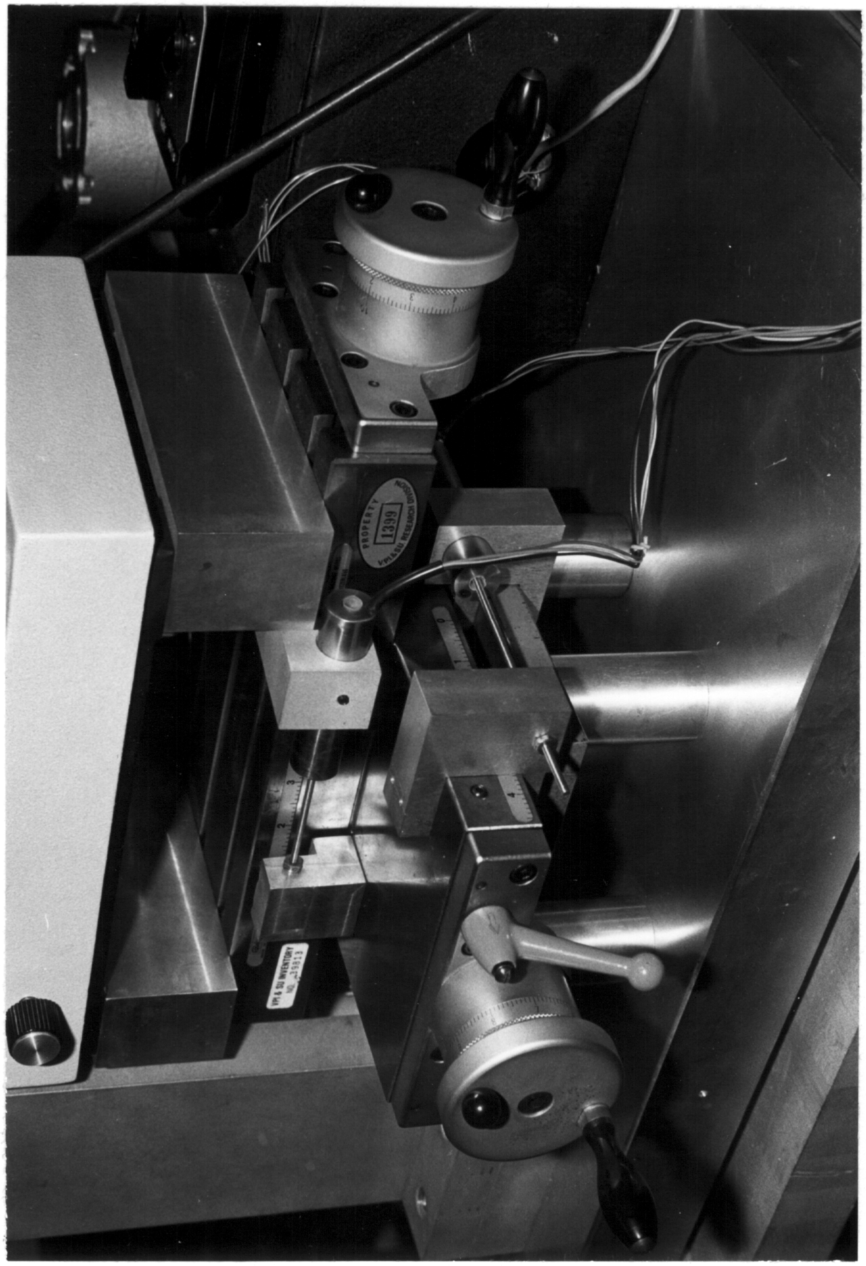

Figure 9 Precision X-Y Table and LVDTs

The coefficient of friction was determined by measuring the frictional resistance using the miniature torque transducer shown in Fig. 10. The calibration procedure and method of calculating the frictional coefficient are given in Appendix C and Appendix D, respectively. A magnetic speed sensor was attached to the torque transducer body to measure the rotational velocity.

The drive system is shown in Fig. 11. The arrangement of gears allows a variation of rotational velocities by interchanging drive belts. To maintain constant velocity, a hysteresis synchronous motor is used to drive the system. The radial position of the specimen determines the sliding velocity for a given disk angular velocity. The radial position is controlled and measured by the calibrated radial displacement slide arrangement shown in Fig. 12. The radial displacement slide supports the loading balance beam to which the specimen and a pan are attached at each end. Precision weights are added to the pan to produce the desired normal load at the interface.

Support instrumentation was added to complete the surface temperature measurements. All the desired outputs were recorded simultaneously on a seven-channel FM tape recorder and stored on magnetic tape. The camera setup in Fig. 13 was used to photograph the wear area through the visual channel of the microscope.

Figure 14 is a block diagram of the basic instrumentation system including the measured outputs.

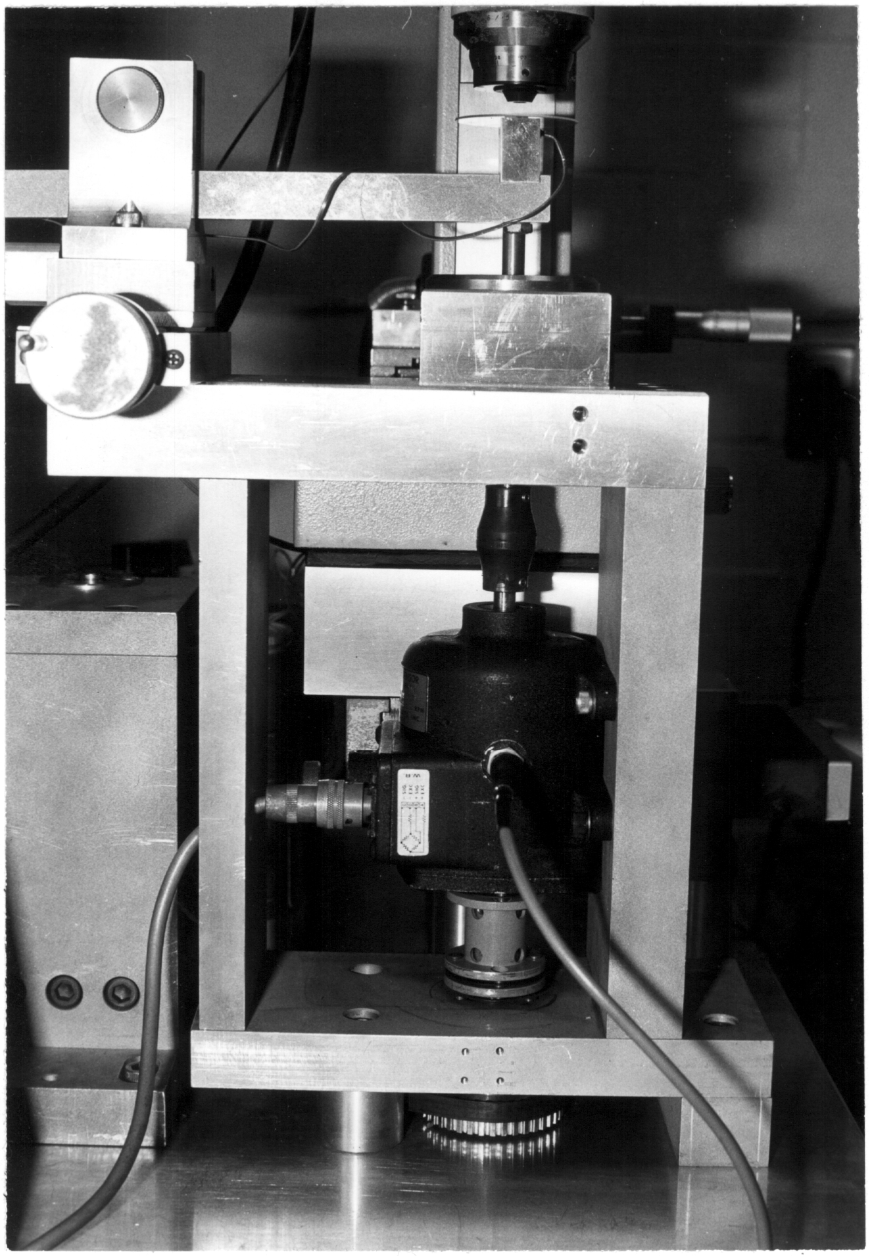

Figure 10 Miniature Torque Transducer Used to Measure Frictional Force

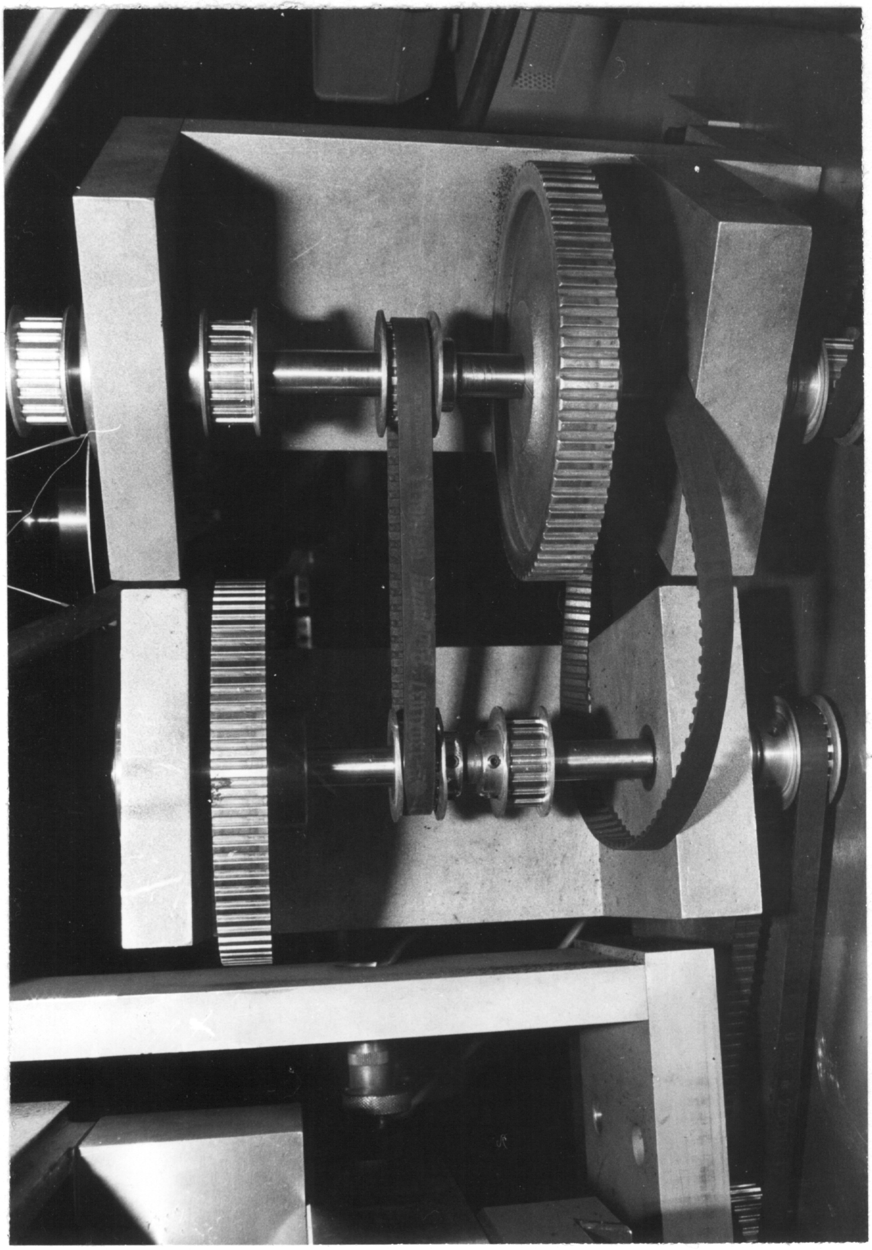

Figure 11 Drive System

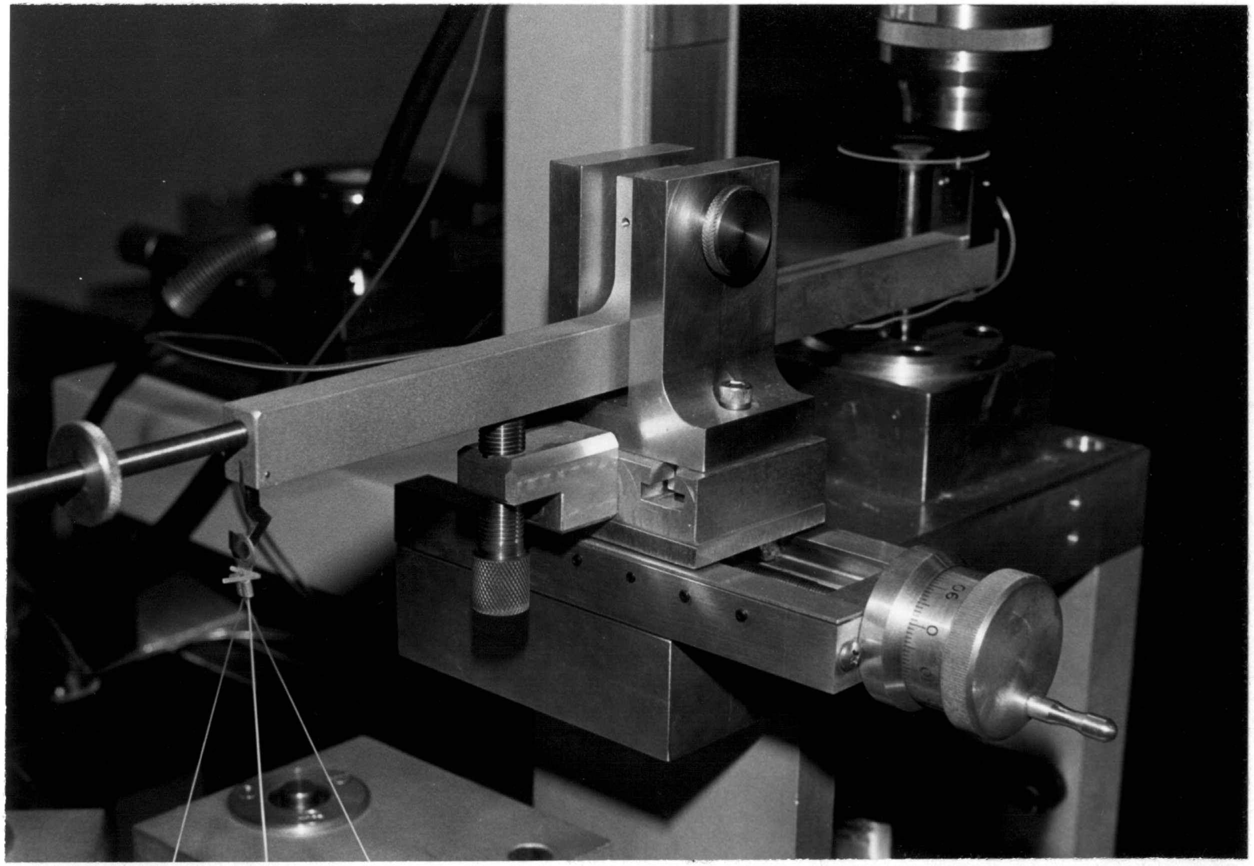

Figure 12 Radial Displacement Slide Arrangement for Positioning Specimen

Figure 13 Camera Arrangement for Photographing Wear Area

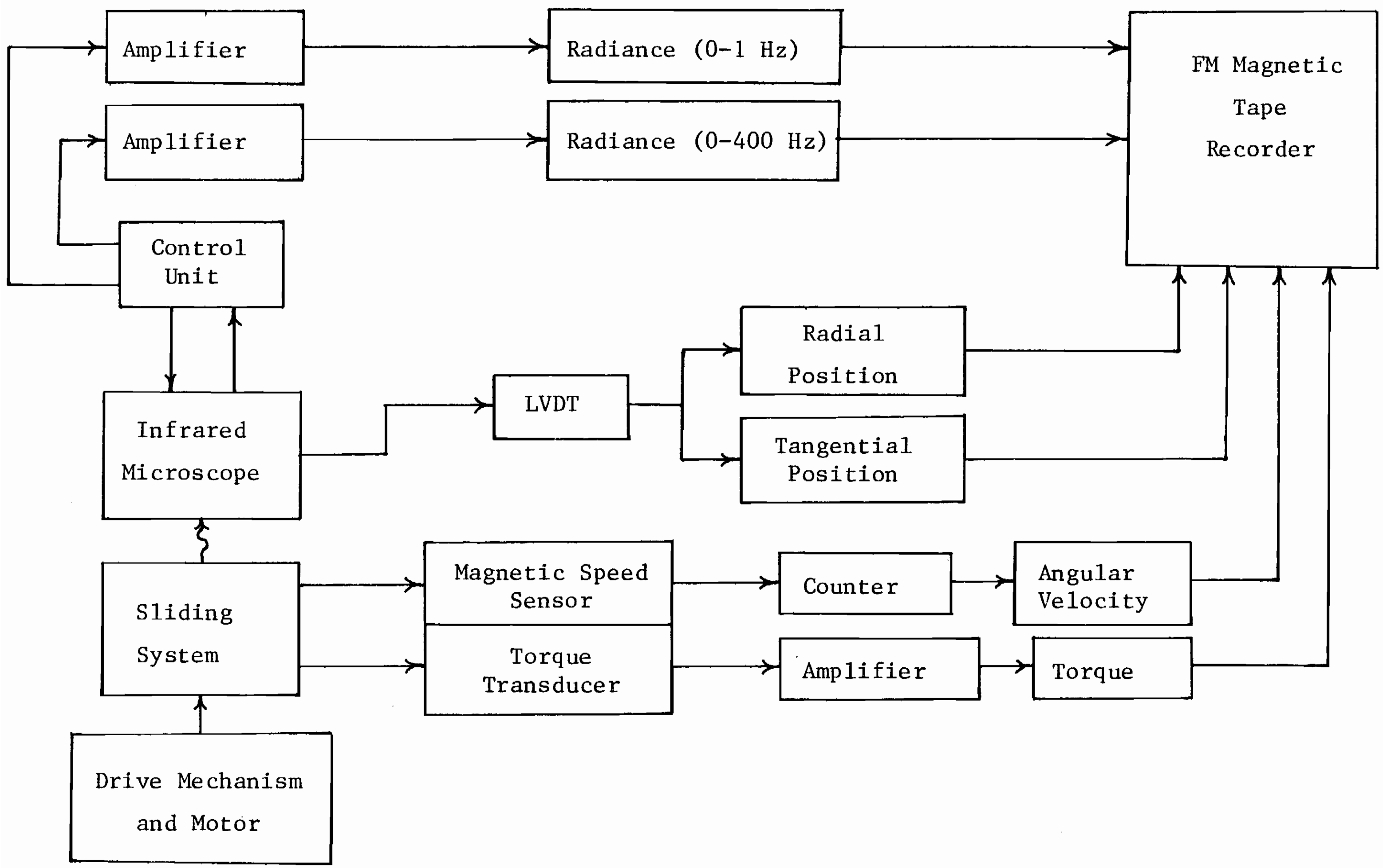

Figure 14 Block Diagram of Basic Instrumentation System

B. Operational Theory

The source of thermal radiation arises from the frictional interaction between the test specimen and rotating sapphire disk. The function of the infrared radiometric microscope is to measure radiance, the radiation intensity in milliwatts/steradians - cm^2. If the necessary radiative properties are known, the radiance data measured by the microscope can be converted to the temperatures generated at the sliding interface. However, the presence of the sapphire disk complicates the radiance to temperature conversion by its absorptive and reflective properties.

An infrared detector receives radiation from a body by two sources: (a) emitted radiation from the surface due to its temperature and (b) the radiation from the surroundings reflected from the body's surface. Assuming that the opaque body is gray, the relation between its ability to emit radiation in comparison to an ideal emitter and its reflective property is given by

$$\varepsilon + \rho = 1 \qquad \{36\}$$

Solving for the reflectivity results in

$$\rho = 1 - \varepsilon \qquad \{37\}$$

Thus, if N_{total} is the total radiation emitted by a gray body and received by the infrared detector, N_{total} is given by

$$N_{total} = \varepsilon N_{bbt} + (1 - \varepsilon)N_0 \qquad \{38\}$$

where N_{bbt} is the radiance emitted by a blackbody at the same temperature as the body, and N_0 is the radiance emitted by the ambient background.

Since the infrared microscope utilizes a chopper permitting the detector to observe the incoming radiation only one-half of the time, the electrical output of the detector is proportional to the difference between the incoming radiation and the ambient radiation from the chopper. The detector electrical output may be expressed as

$$E = K_0 R_d (N_{total} - N_0) \qquad \{39\}$$

where K_o is an optical contant and R_d is the detector responsivity.

Substituting equation {38} in equation {39}, results in

$$E = K_0 R_d \varepsilon (N_{bbt} - N_0) \qquad \{40\}$$

The proportionality constant $(K_o R_d)$ was determined empirically by using the calibration heat source and recording the electrical output of the microscope. Since the heat source was black, the value of ε is *1*. The radiance of the ambient background, N_0, was determined from the blackbody radiance versus temperature curve from the microscope instruction manual (see Appendix E). This procedure was identical to the calibration procedure in Appendix A. From the calibration data points, a best-fit line was determined by linear regression and the magnitude of the slope which is equal to $(K_o R_d)$ was derived.

Therefore, if the ambient background radiance and the target emissivity are known, the radiance emitted from the blackbody at the same temperature of the target can then be determined from the microscope's electrical output. The temperature of the target can then be found from the radiance versus temperature curves in Appendix E.

The derivations to convert the radiance to temperature become more complicated with the presence of the sapphire disk. The disk partially reflects and absorbs both the radiance emitted from the specimen and the radiance emitted from the ambient background. This problem can be handled by using a ray tracing technique. Figures 15 and 16 show the effect of internal transmissivity and the Fresnel reflections on the ambient radiation and the emitted radiation, respectively. The internal transmissivity is denoted by τ and the Fresnel reflection at the air/sapphire and iron/sapphire interfaces is denoted by ρ and ρ_s, respectively.

To determine the total radiation, N_{total}, reaching the detector, the fractions of radiation leaving the top surface of the sapphire disk must be summed and multiplied by the corresponding impinging radiance. Therefore, equation {38} becomes

$$N_{total} = \varepsilon T N_{bbt} + RN_0 \qquad \{41\}$$

where

$$T = \tau(1 - \rho) + \rho\rho_s\tau^3(1 - \rho) + \rho^2\rho_s^2\tau^5(1 - \rho) + \ldots \qquad \{42\}$$

$$R = \rho + \rho_s\tau^2(1 - \rho)^2 + \rho\rho_s^2\tau^4(1 - \rho)^2 + \ldots \qquad \{43\}$$

Substituting equation {39} into equation {41} and solving for N_{bbt} gives

$$N_{bbt} = \left(\frac{E}{K_0 R_d} + N_0(1 - R) \right) \cdot \frac{1}{\varepsilon T} \qquad \{44\}$$

Replacing R and T with the first three terms of each infinite series results in the following expression:

$$N_{bbt} = \frac{E/K_0R_d + N_0\{1 - (\rho + \rho_s\tau^2(1 - \rho)^2 + \rho\rho_s^2\tau^4(1 - \rho)^2)\}}{\varepsilon\{\tau(1 - \rho) + \rho\rho_s\tau^3(1 - \rho) + \rho^2\rho_s\tau^5(1 - \rho)\}} \qquad \{45\}$$

Once the value of N_{bbt} is obtained, the temperature may be found by using the curves in Appendix E. However, due to the unwieldy equation and necessary use of graphs, a computer program (in Appendix H) was developed by C. A. Rogers (39) to calculate both the radiance and target temperatures.

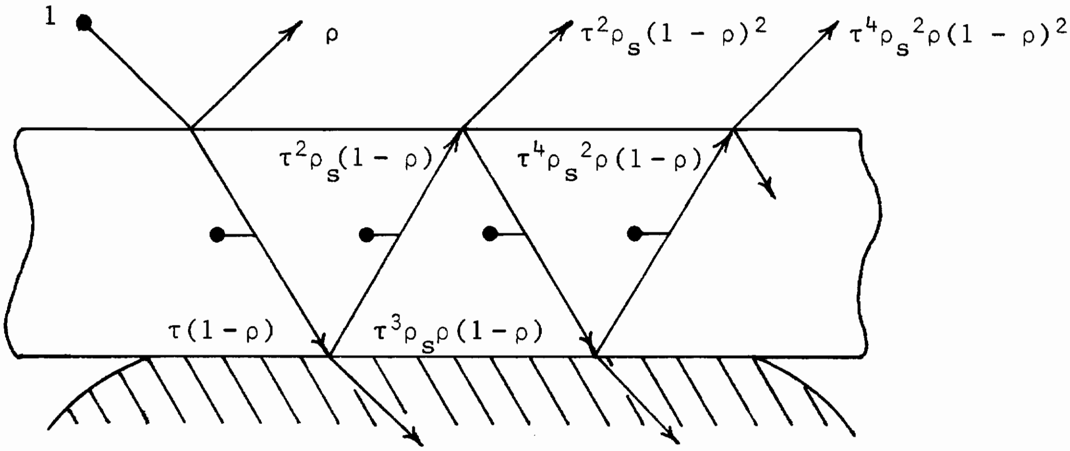

Figure 15 Ambient Radiation Ray Trace Through the Sapphire Disk

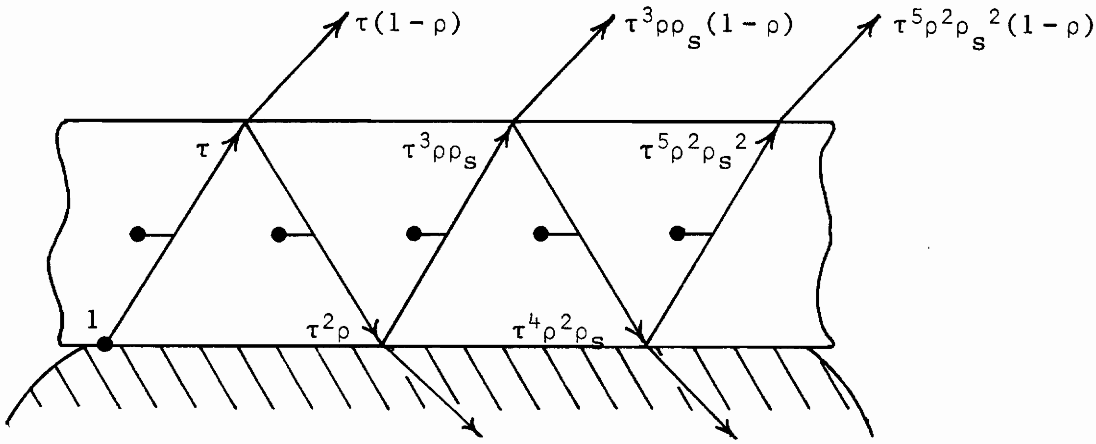

Figure 16 Emitted Radiation Ray Trace Through the Sapphire Disk

C. Experimental Conditions

The conditions of the experimental study allowed the effects of load, velocity, and environment to be observed from which a statistical analysis was performed, establishing the relative magnitude of these effects.

The normal loads and sliding velocities were particularly chosen to study their effects on surface temperature, friction, and wear. The loads ranged from $0.5\ N$ to $2.5\ N$ by increments of $0.5\ N$. Three sliding velocities were chosen, namely $2.0\ m/s$, $4.0\ m/s$, and $8.0\ m/s$. The velocities were determined by both the radial position of the test specimen and the angular velocity of the sapphire disk.

The tests were performed in two distinct environments -- air and nitrogen. Experimental studies in nitrogen allowed radiance measurements to be taken from a relatively oxide-free surface. Therefore, the effects of oxide formation in tests run in an air environment may be observed.

Table 2 summarizes the loads and velocities used in both air and nitrogen environments. The test conditions used in the analysis of variance study are designated. One repeat run was made for each test case.

The laboratory environmental conditions were controlled and monitored to avoid additional variables entering the experimental study. The observed range and mean values of ambient temperature and relative humidity during this study are presented in Table 3.

TABLE 2

SUMMARY OF

EXPERIMENTAL CONDITIONS

Environment		Normal Load				
		0.50 N	1.00 N	1.50 N	2.00 N	2.50 N
	Air	*2.0 m/s**	*2.0 m/s*	*2.0 m/s*	*2.0 m/s*	*2.0 m/s**
		4.0 m/s	*4.0 m/s*	*4.0 m/s*	*4.0 m/s*	*4.0 m/s*
		*8.0 m/s**	*8.0 m/s*	*8.0 m/s*	*8.0 m/s*	*8.0 m/s**
	Nitrogen	*2.0 m/s**	- - -	- - -	- - -	*2.0 m/s**
		4.0 m/s	*4.0 m/s*	*4.0 m/s*	*4.0 m/s*	*4.0 m/s*
		*8.0 m/s**	- - -	- - -	- - -	*8.0 m/s**

** Test conditions used in the analysis of variance study.*

TABLE 3

LABORATORY ENVIRONMENTAL CONDITIONS

	Ambient Temperature (C)	Relative Humidity (%)
Minimum	22	38
Maximum	26	62
Mean	25	52

D. Experimental Procedure

To obtain accurate radiance, torque, and position measurements, careful use and supervision of proper instrumentation operation was necessary to minimize experimental error. A listing of over thirty probable errors that may occur with the system being used is given in reference 26. The necessary measurements were made using the following procedure.

Various preliminary procedures necessary prior to a test run were as follows: 1) both the test specimen and sapphire disk were cleaned as described in Appendix F and the specimen was weighed; 2) an instrumentation warm-up period of approximately 30 minutes was allowed to insure stability; 3) the vibrational-induced noise of the torque transducer output was minimized by viewing the output signal on an oscilloscope and adjusting the drive belt tension (this procedure was repeated whenever the drive system had to be altered, i.e., for velocity changes); and 4) the proper operation of the instrumentation was checked by following the calibration procedures in Appendices A, B, and C.

When the above preliminaries were completed, the sapphire disk and test specimen were installed, including the thermocouple for measuring the bulk temperature. With the specimen at the proper radial position, the loading beam was balanced, and the proper weights were placed in the pan. After the infrared microscope was zeroed using the black calibration heat source at ambient temperature, it was focused on the center of the contacting area. At this position, both linear variable differential transformers (LVDTs) were adjusted to *0.000* volt output. The instrumentation output cables were connected to the FM magnetic tape recorder in the following order: 1) 0-1 *Hz* radiance, 2) 0-400 *Hz* radiance, 3) torque, 4) tangential LVDT, 5) radial LVDT, and 6) magnetic speed sensor.

After a 30 second initialization period at ambient temperature, the drive motor was started with the specimen in contact and run for approximately 3.5 minutes. Scanning of the general contact region to measure the maximum level of radiance was attempted. When the radiance data collection was completed, the final bulk temperature was recorded and the drive motor turned off. After 30 seconds to record the cooling response, the tape recorder was stopped. The diameter of the final wear area was determined by viewing through the microscope and recording the LVDT outputs at the wear area edges. After the necessary photographs were taken, the specimen was weighed.

All test specimens were handled by forceps, placed in individual vials, and stored in a desiccator.

The tests performed in nitrogen followed the above procedure with the exception of the nitrogen chamber attachment shown in Fig. 17. Prior to the test run, air was purged by allowing nitrogen to flow slowly into the chamber for approximately five minutes. The nitrogen was allowed to flow throughout the experiment.

The emissivity of the specimen was measured using a specially designed heater shown schematically in Fig. 18. The detailed procedure for determining the emissivity within the general contact area is given in Appendix G.

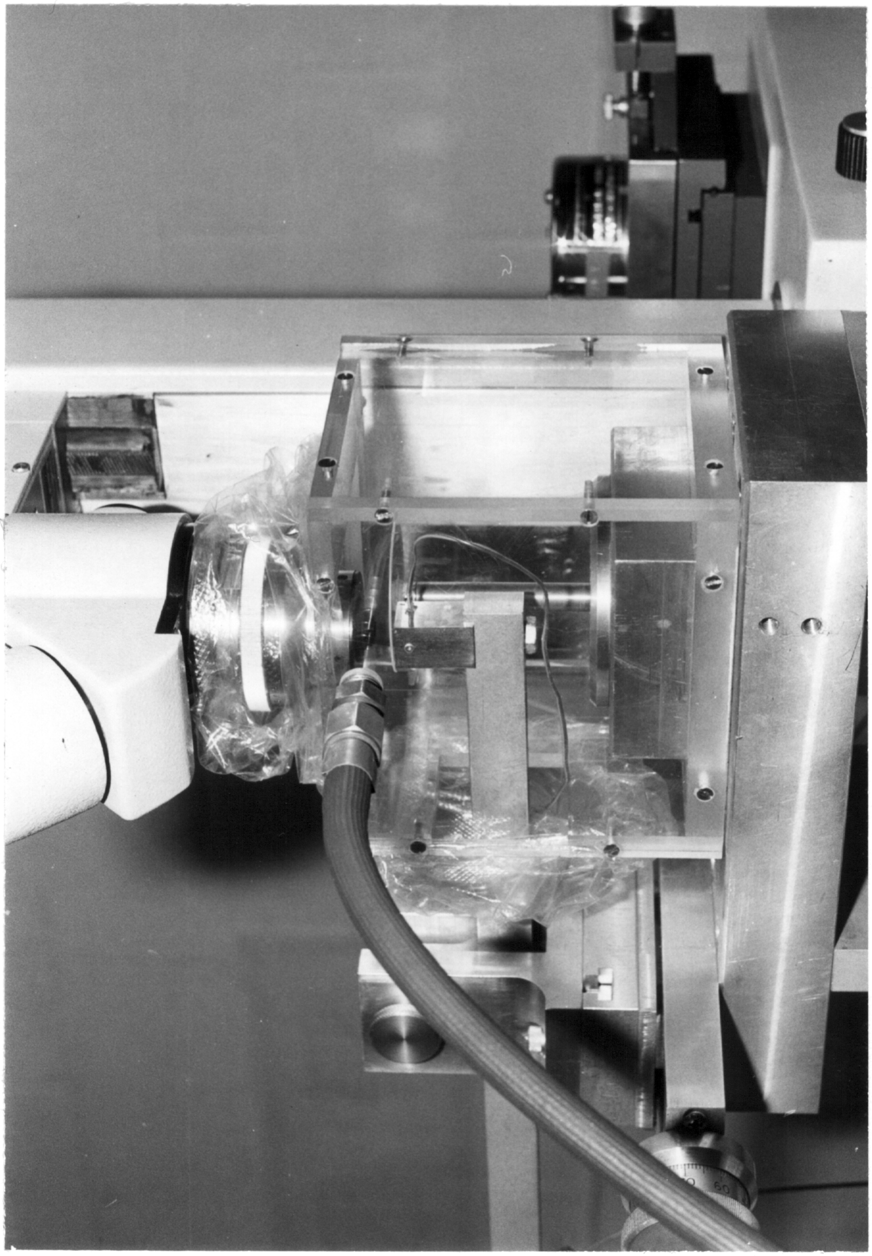

Figure 17 Nitrogen Test Chamber

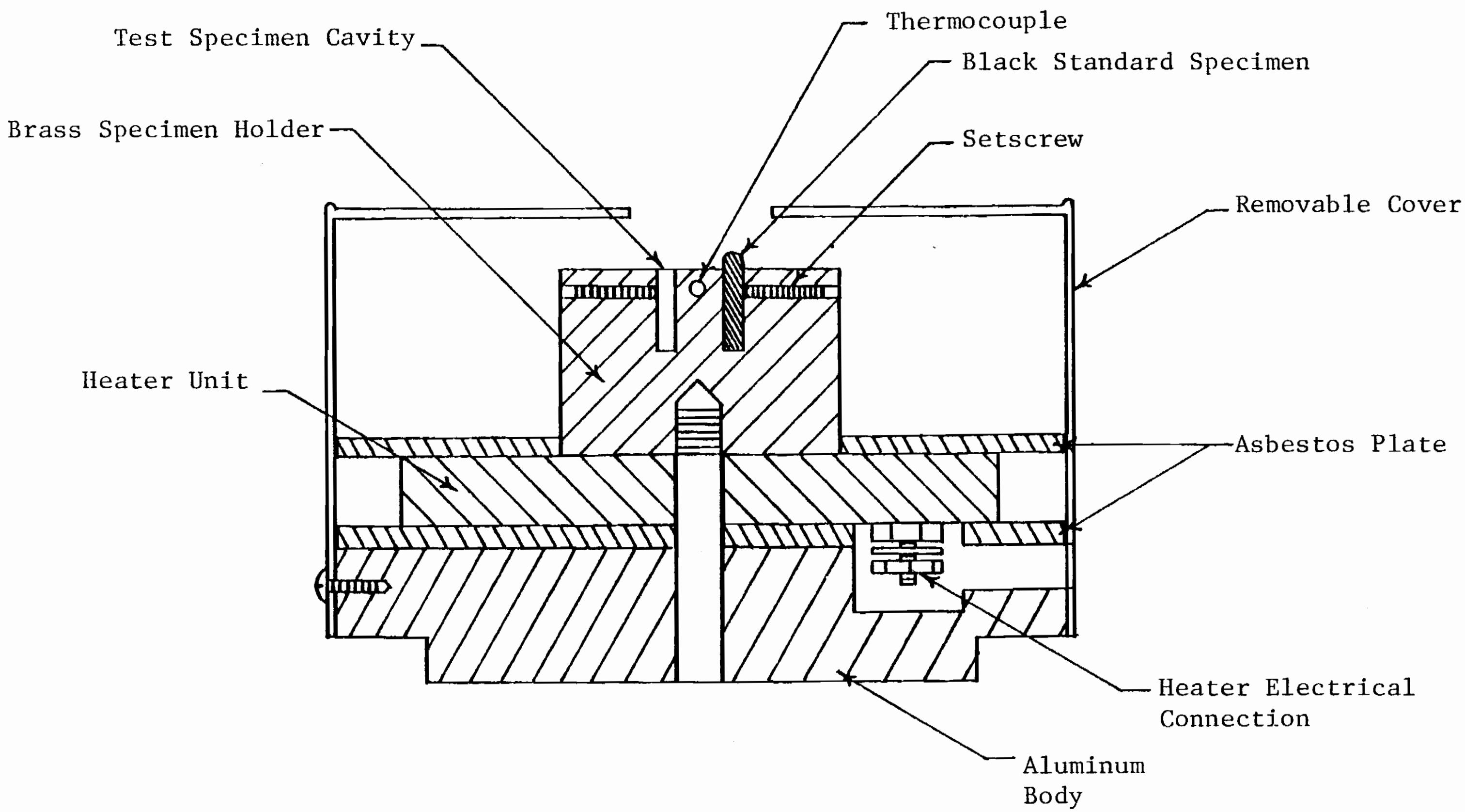

Figure 18 Special Heater for Emissivity Measurements

RESULTS

A. Radiance, Emissivity, and Temperature

The principal objective of this research was to measure the temperature rise due to frictional losses at the sliding interface. Since an infrared technique was used to measure this temperature rise indirectly, the handling of the radiance and emissivity data, which are necessary to obtain the surface temperature, must be done carefully to produce reasonable and accurate results.

Typical radiance traces from tests conducted in both air and nitrogen under identical test conditions, i.e., load and velocity, are shown in Figures 19 and 20, respectively, Both traces include stationary radiance measurements at the center of contact (first four minutes) followed by scanning radiance measurements through the center of contact, parallel to the sliding direction. In each case, a quasi-steady state condition was reached after approximately two minutes. It can also be seen from the traces recorded while scanning the wear area that radiance is a strong function of position for tests performed in air but much less for tests performed in nitrogen.

The appearance of sharp radiance rises may be an effect due to rapid changes in emissivity, temperature, or a combination of both emissivity and temperature. To be able to determine the surface temperature accurately, the effect of emissivity must be isolated.

Measurements of emissivity were made at the end of the test following the procedure in Appendix G. The number of sample points was sufficient to obtain an accurate emissivity contour plot of the wear area. Only

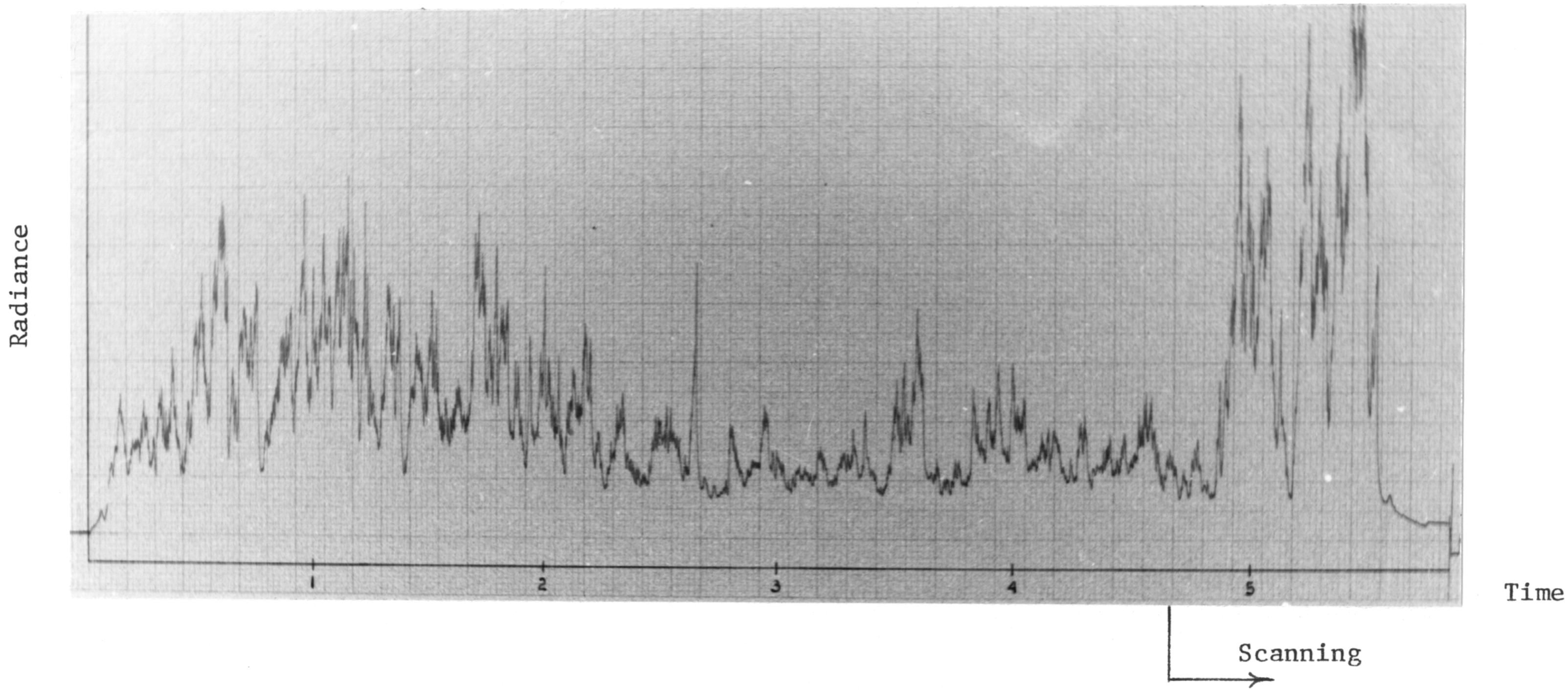

Figure 19 Typical Radiance Trace for Test Performed in Air as a Function of Time (Min) and Position

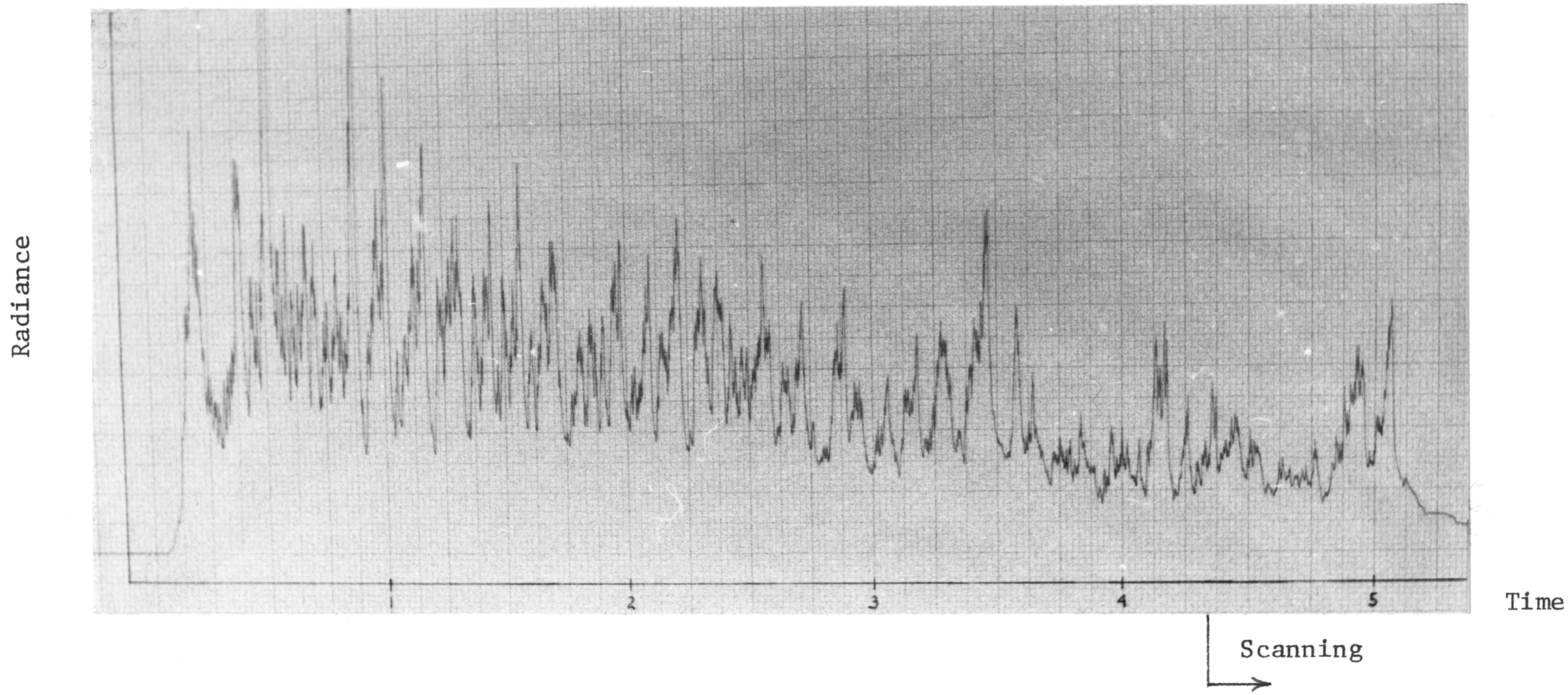

Figure 20 Typical Radiance Trace for Test Performed in Nitrogen as a Function of Time (Min) and Position

one sampling of emissivities was taken for each load and velocity case. Examples of these plots are given with their corresponding scanning electron microscope (SEM) photographs in Figures 21 through 32. From these figures, it can be observed that the presence of oxide formation becomes less pronounced with increasing load. Regions of increased emissivity correlate well with the presence of oxide debris on the wear area.

It was assumed that the data taken at the end of the test was indicative of the emissivity during the radiance measurements, once a steady condition was reached. Thus, an estimation of the expected emissivity was made possible by using a statistical treatment, multiple linear regression.

Each measured emissivity value was assigned an appropriate load and velocity as defined by the imposed test conditions and a position within the wear area. (See Appendix J for description.) Multiple linear regression was used to:

1. analyze the relationship between the dependent variable, emissivity, and the independent variables, load and velocity,
2. establish the significance of the above relationships, and
3. develop a prediction equation by which an estimated mean emissivity and confidence interval may be determined. This mathematical model is not only applicable for the specific tests from which the emissivities were measured, but for any future tests at any given load and velocity within the initial test condition limits.

The above method was applied for both air and nitrogen environments.

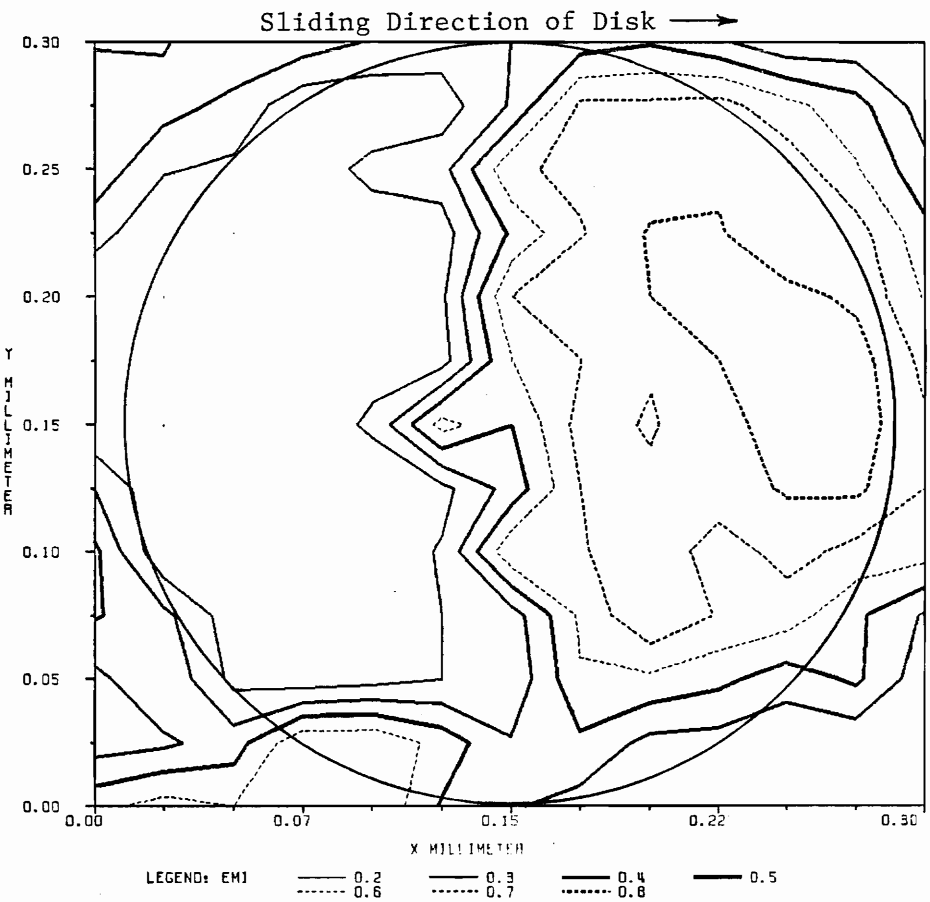

Figure 21 Emissivity Contour Plot of an Armco Iron Specimen Slid in Air at *4.0 m/s* with a *0.5 N* Load

Sliding Direction of Disk ⟶

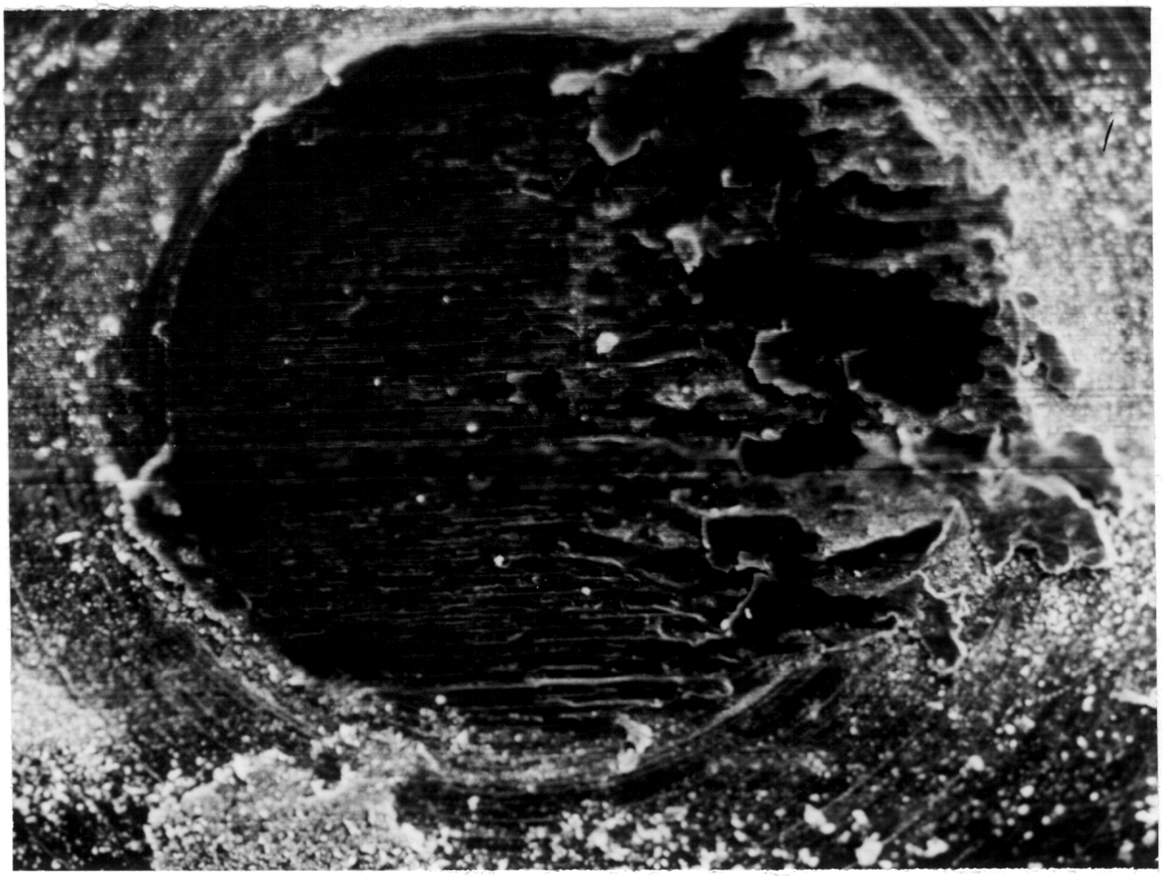

Figure 22 SEM Photograph of Wear Area in Fig. 21 at 280X

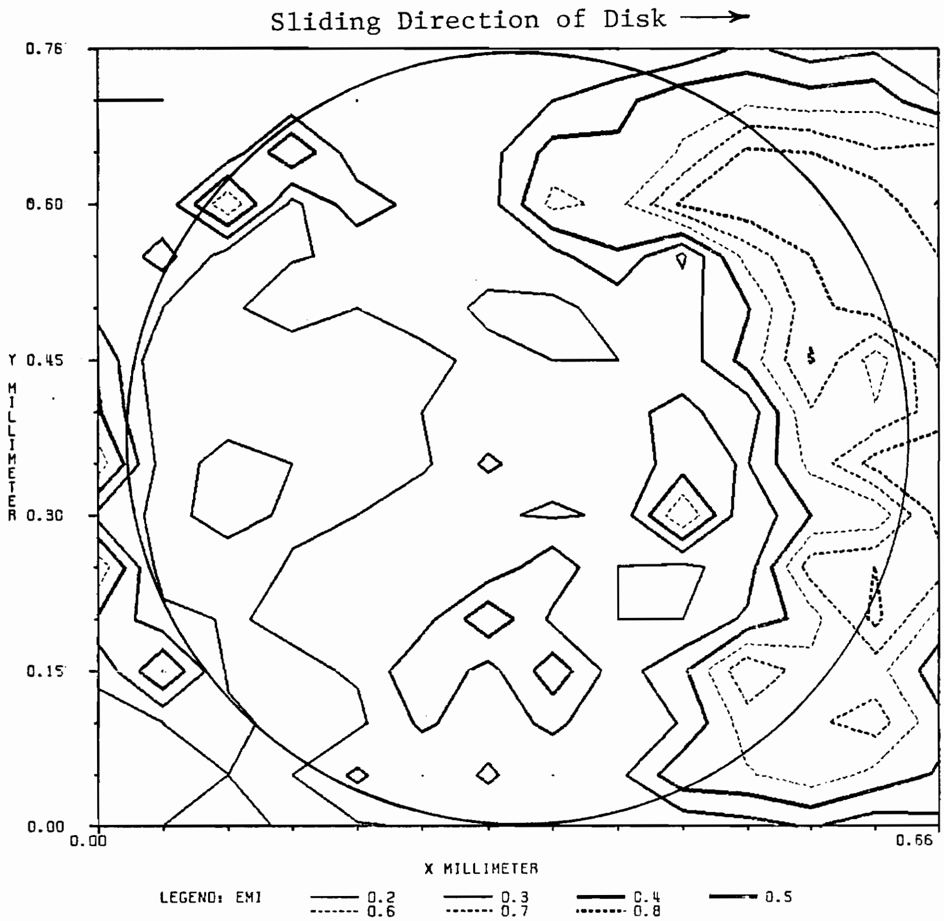

Figure 23 Emissivity Contour Plot of an Armco Iron Specimen Slid in Air at *4.0 m/s* with a *1.5 N* Load

Sliding Direction of Disk →

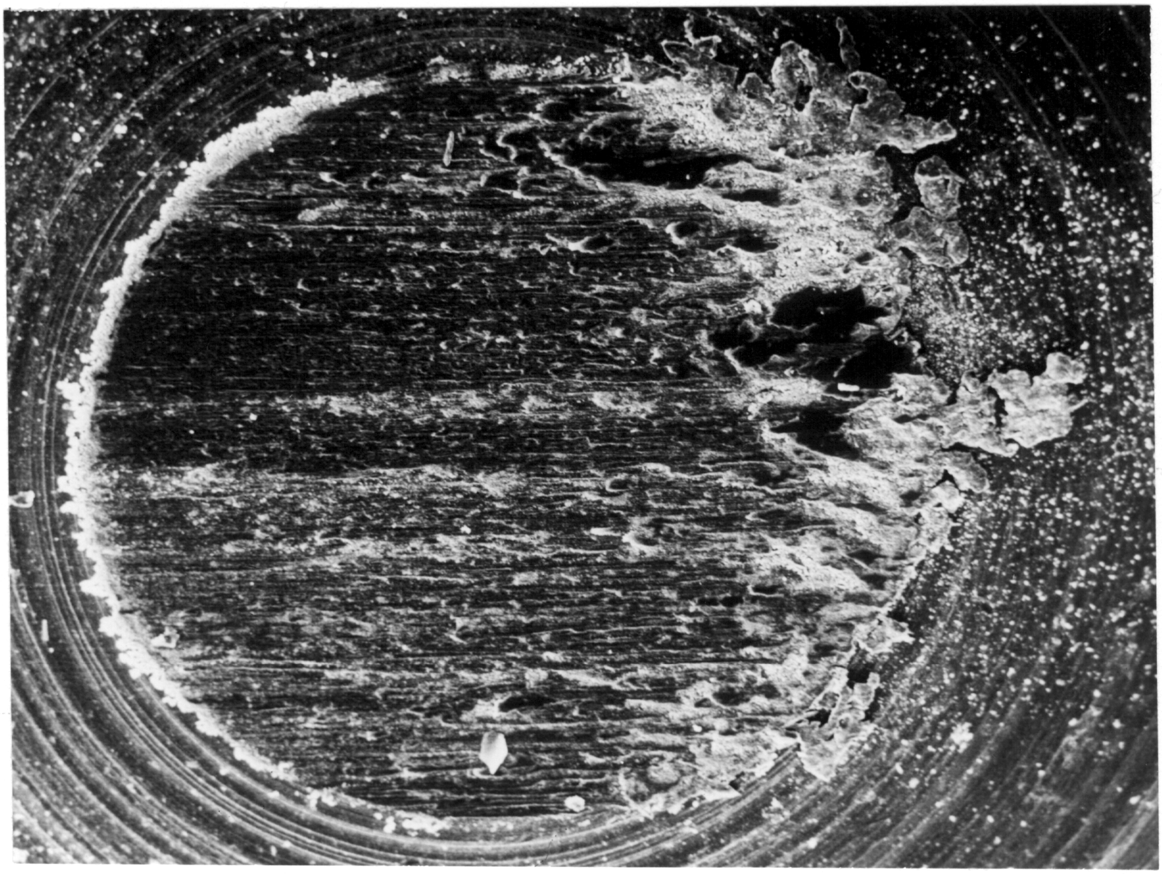

Figure 24 SEM Photograph of Wear Area in

Fig. 23 at 133X

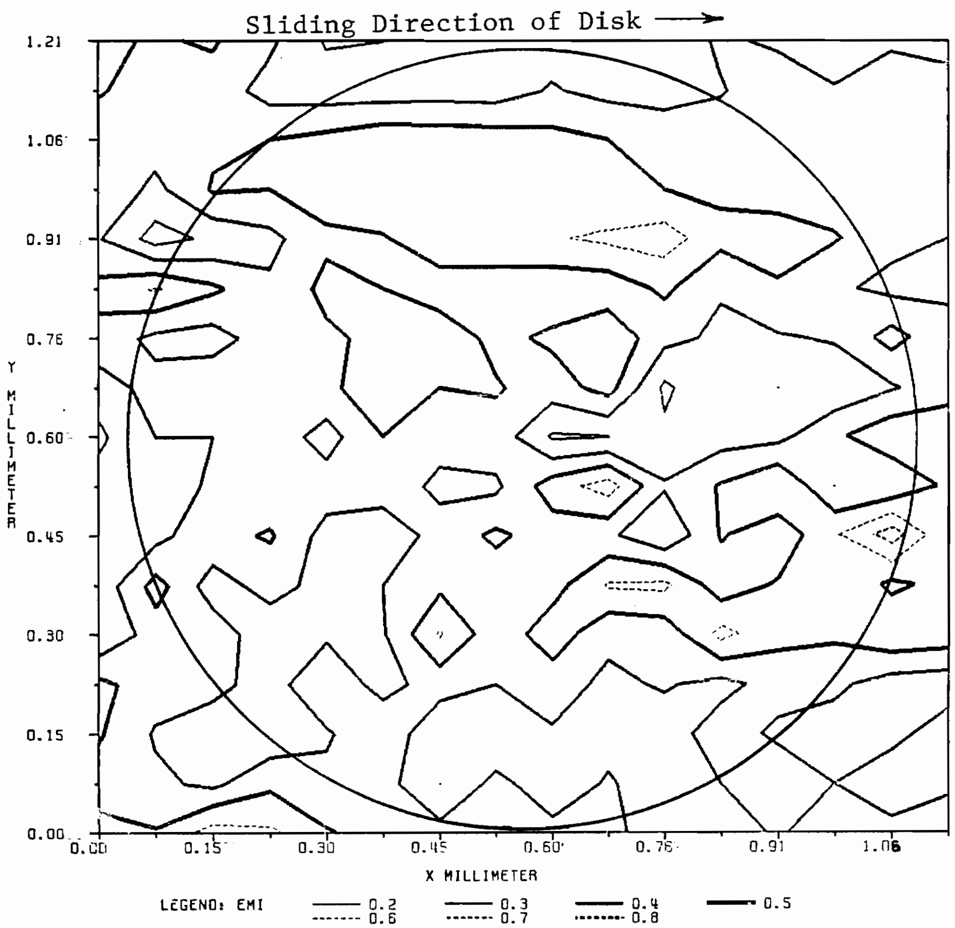

Figure 25 Emissivity Contour Plot of an Armco Iron Specimen Slid in Air at *4.0 m/s* with a *2.5 N* Load

Sliding Direction of Disk ⟶

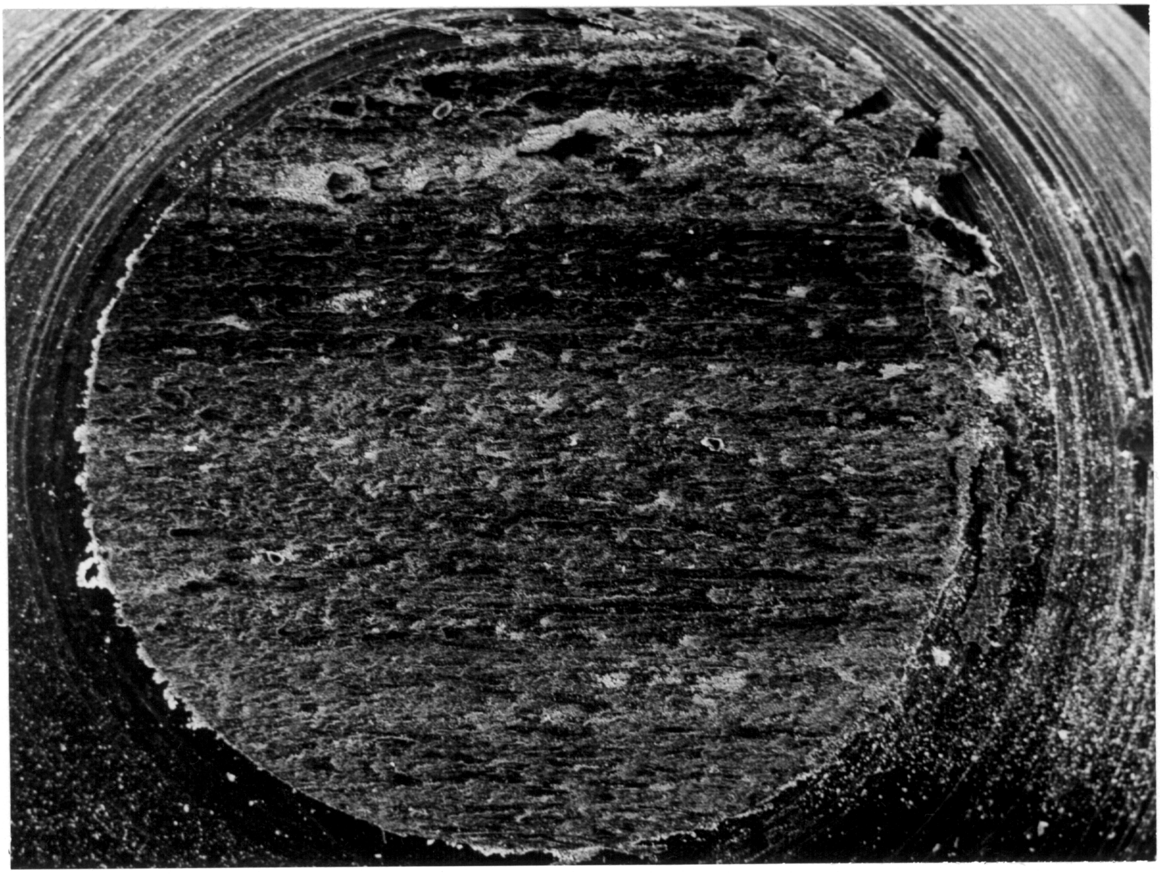

Figure 26 SEM Photograph of Wear Area in

Fig. 25 at 108X

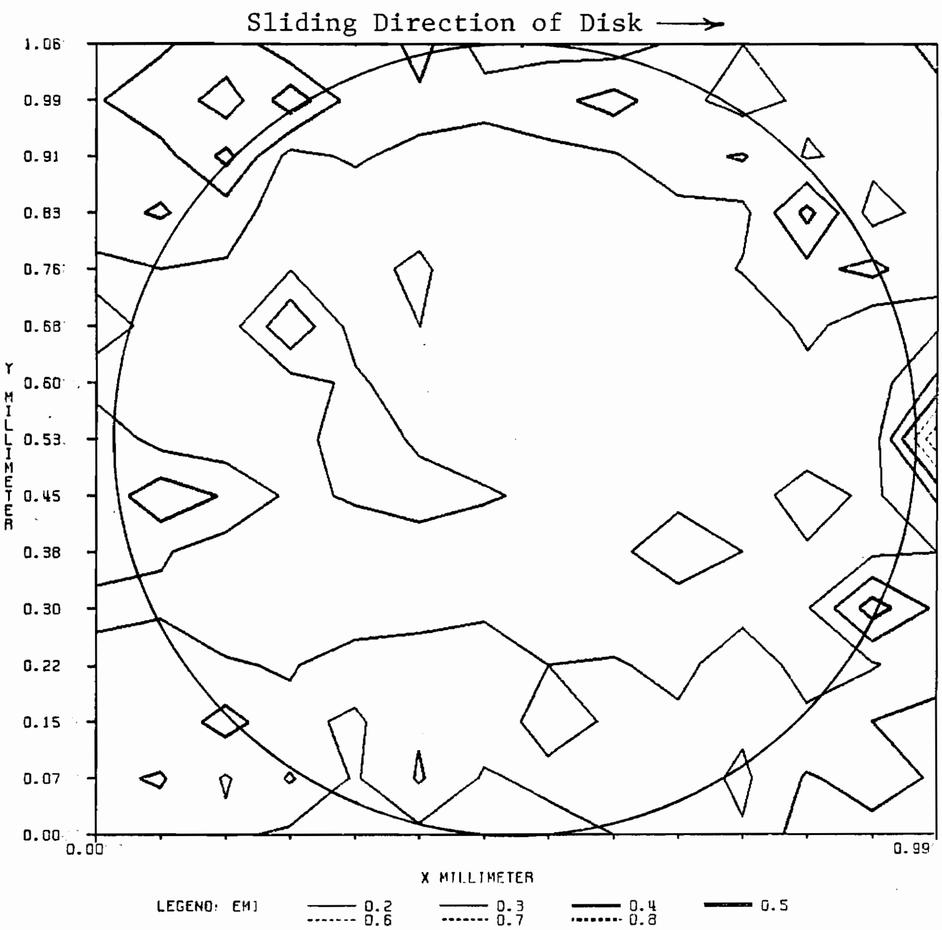

Figure 27 Emissivity Contour Plot of an Armco Iron Specimen Slid in Nitrogen at *4.0 m/s* with a *0.5 N* Load

Sliding Direction Of Disk →

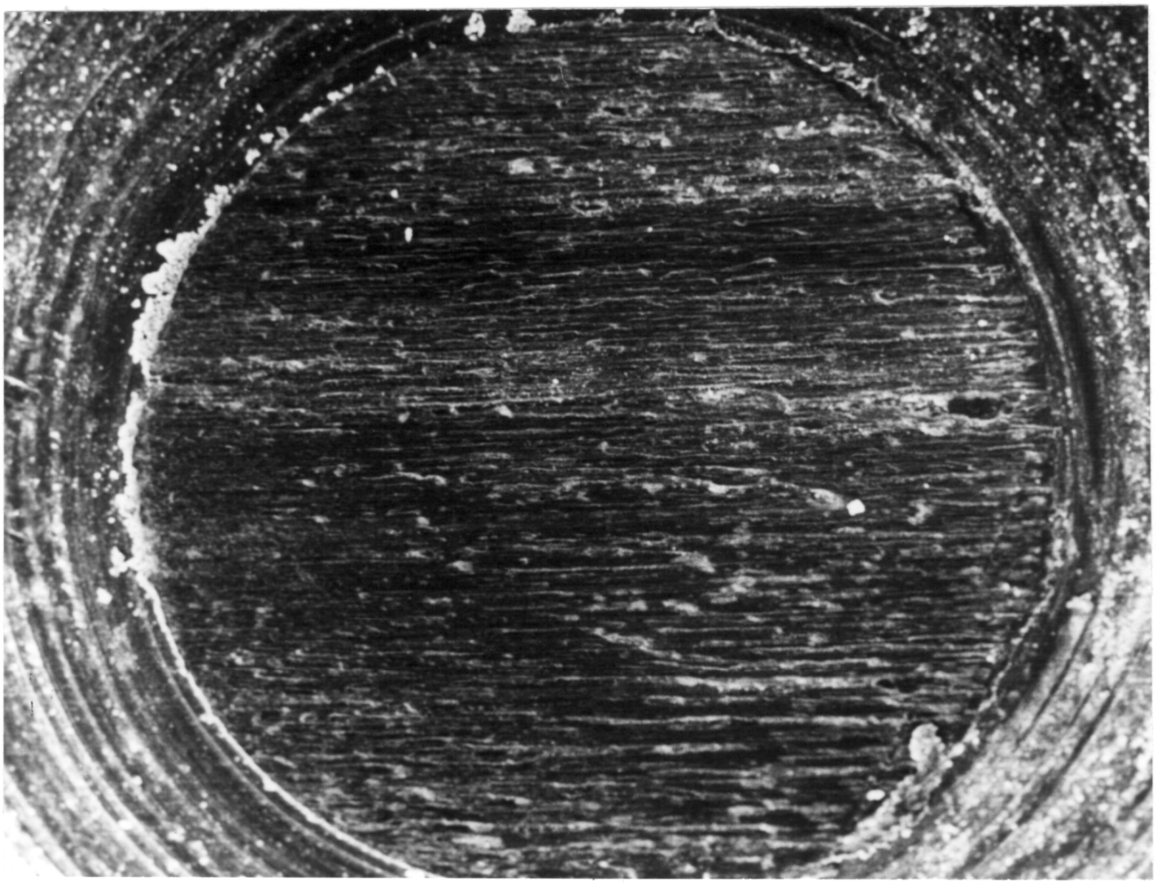

Figure 28 SEM Photograph of Wear Area in Fig. 27 at 121X

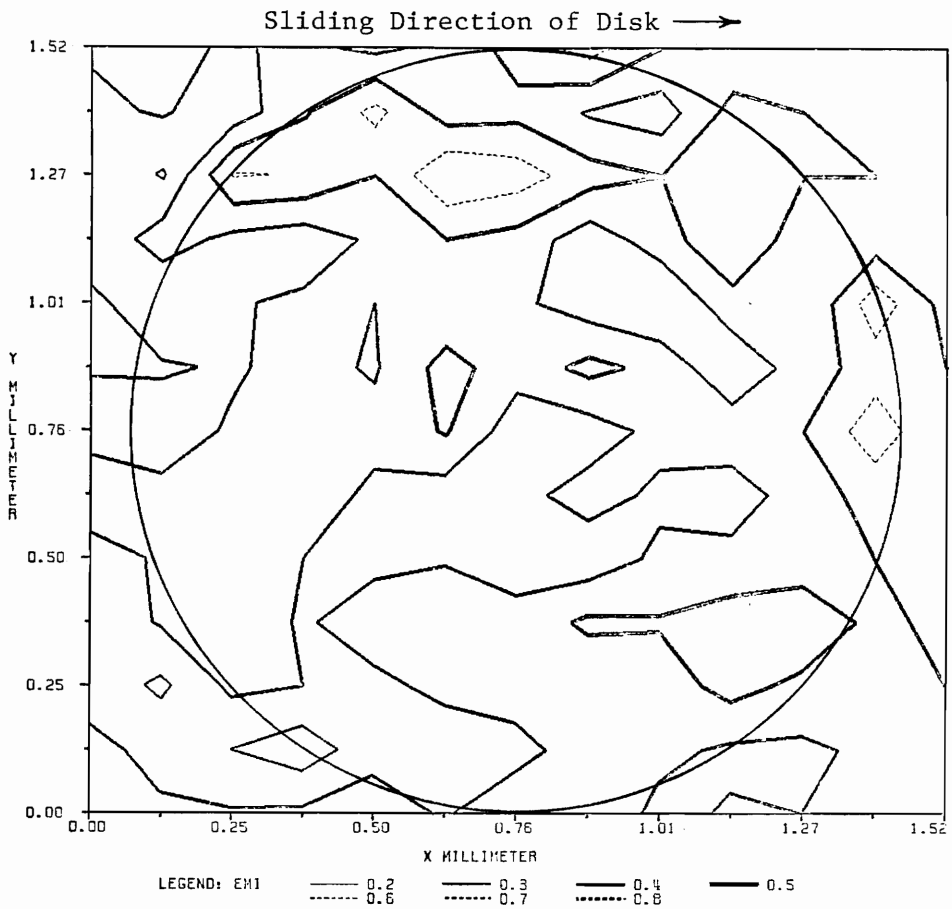

Figure 29 Emissivity Contour Plot of an Armco Iron Specimen Slid in Nitrogen at *4.0 m/s* with a *1.5 N* Load

Sliding Direction of Disk ⟶

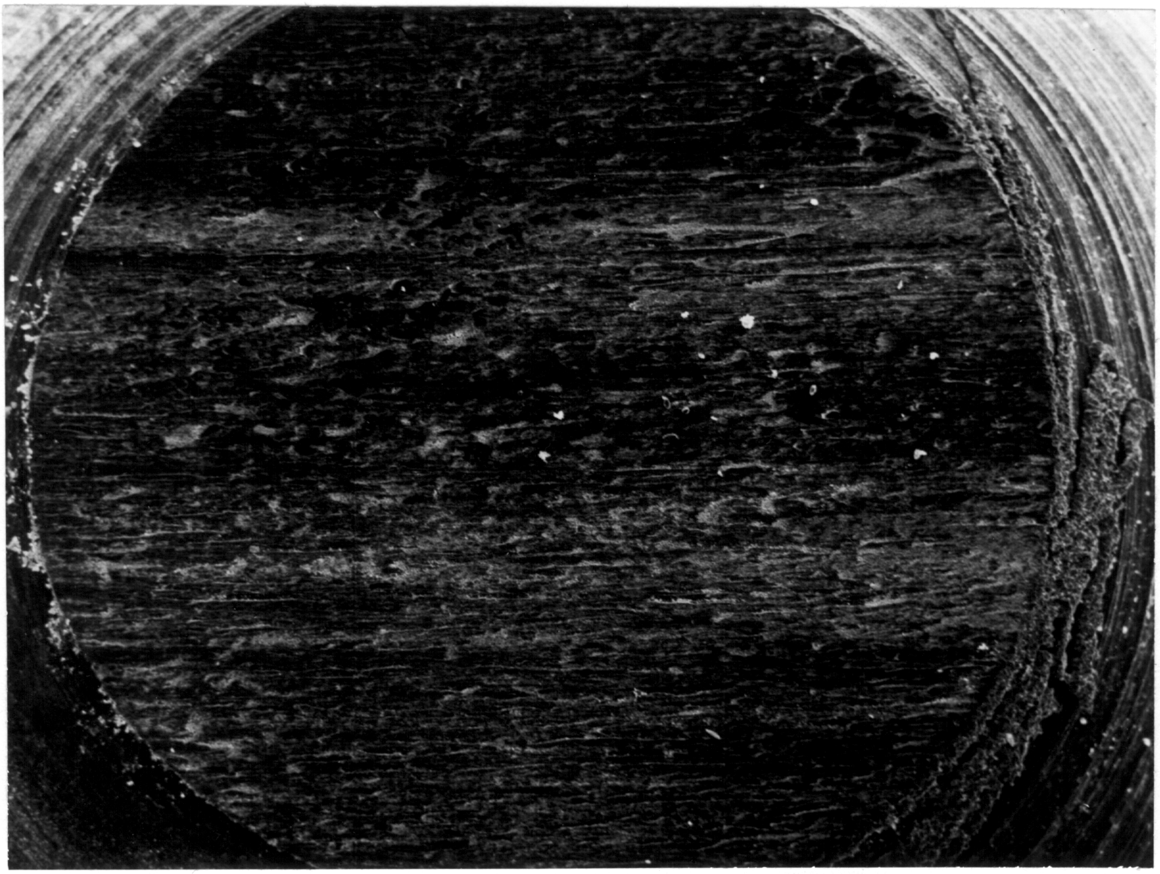

Figure 30 SEM Photograph of Wear Area in Fig. 29 at 85X

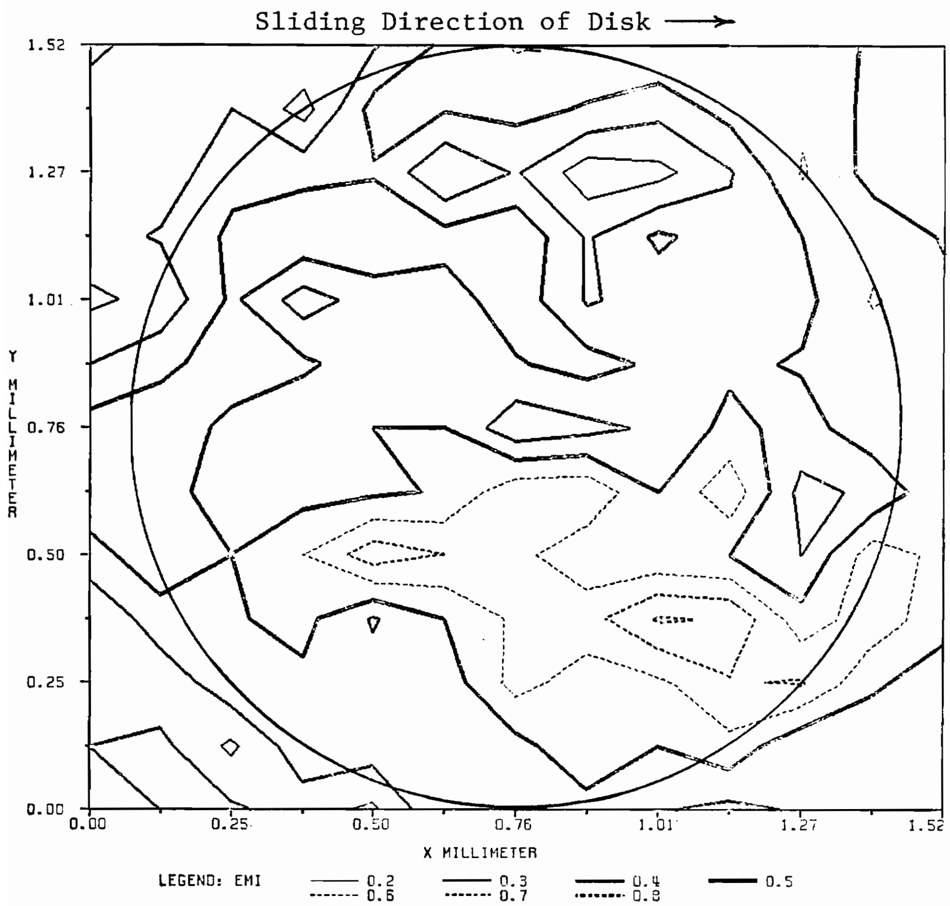

Figure 31 Emissivity Contour Plot of an Armco Iron Specimen Slid in Nitrogen at *4.0 m/s* with a *2.5 N* Load

Sliding Direction of Disk ⟶

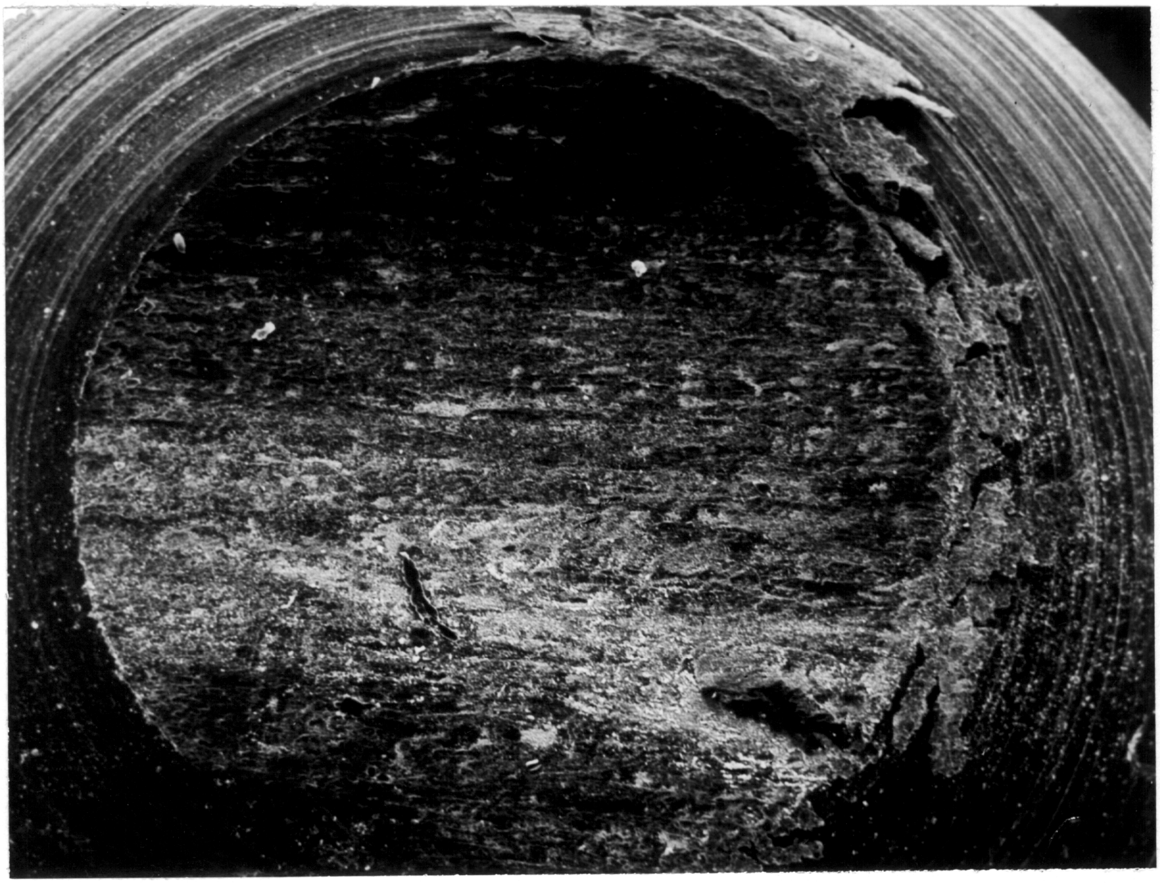

Figure 32 Sem Photograph of Wear Area in Fig. 31 at 92X

The final models derived are given below.

For tests conducted in air,

$$\bar{\varepsilon}_{est} = 0.74293 - 0.31353*LOAD - 0.03395*VEL + 0.02106*LOAD*VEL + 0.08433*LOAD*LOAD + \left\{\begin{array}{ll} & Position \\ -\ 0.16442 & 1 \\ -\ 0.14639 & 2 \\ -\ 0.07397 & 3 \\ \ \ 0 & 4 \end{array}\right\} \qquad \{46\}$$

Each independent variable was deemed highly significant (99% confident), with the model accounting for approximately *29%* of the total measured variation of emissivity.

For tests conducted in nitrogen,

$$\bar{\varepsilon}_{est} = 0.38311 + 0.22976*LOAD - 0.08300*VEL - 0.01137*LOAD*VEL - 0.02587*LOAD*LOAD \qquad \{47\}$$

Note that position is not a variable in this model for its significance was determined to be approximately *25%* confident. Again, each parameter in the equation was found to be significant (99% confident), with the model accounting for approximately *53%* of the total variation of emissivity.

From the above derived models, the maximum *95%* confidence interval about the estimated mean emissivity for both environments was determined to be ± *0.04*.

To obtain the range of surface temperatures measured within the contact region for each test run, the predominant maximum, minimum, and

[1]See Appendix J for definition.

average radiance levels were visually determined with a straight edge from the chart recordings after the quasi-steady state condition was reached. An example presenting these three radiance levels is shown in Fig. 33.

The estimated mean emissivity was used to calculate the surface temperature for each corresponding maximum, minimum, and average radiance value. The computer program in Appendix H was used to perform the radiance to temperature conversion. The measured bulk temperature was subtracted from the calculated total temperature to obtain the temperature rise. Appendix K contains the numerical data of radiance, emissivity, and temperature for each test. Using the computer program in Appendix I, the theoretical mean temperature rise as a function of both load and velocity was plotted. The range of temperature rises measured for each test case was also plotted to allow comparison with theory. Note that the temperatures were normalized to a coefficient of friction of one (*1.00*). This was accomplished by dividing the calculated temperature rise by its corresponding average friction coefficient. These plots are shown in Fig. 34 through 41. The numerical data for the measured temperature rises as determined by Archard and Jaeger theories are presented in Table 7.

B. Friction

A typical torque trace for both environments is shown in Fig. 42. The average torque was measured for each test run and the coefficient of friction was calculated following the procedure in Appendix D. The numerical data is given in Appendix L. It was found, in general, that .

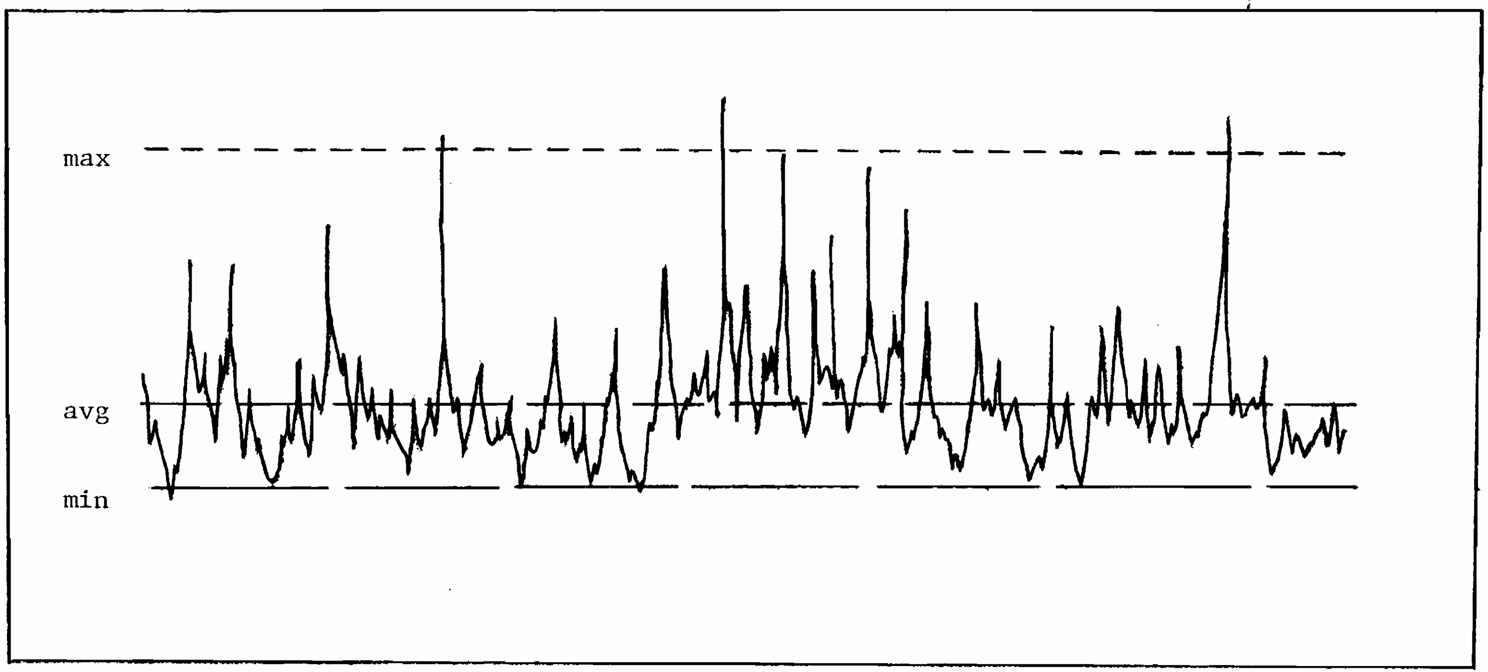

Figure 33 Example Revealing Predominant Maximum, Average, and Minimum Radiance Levels

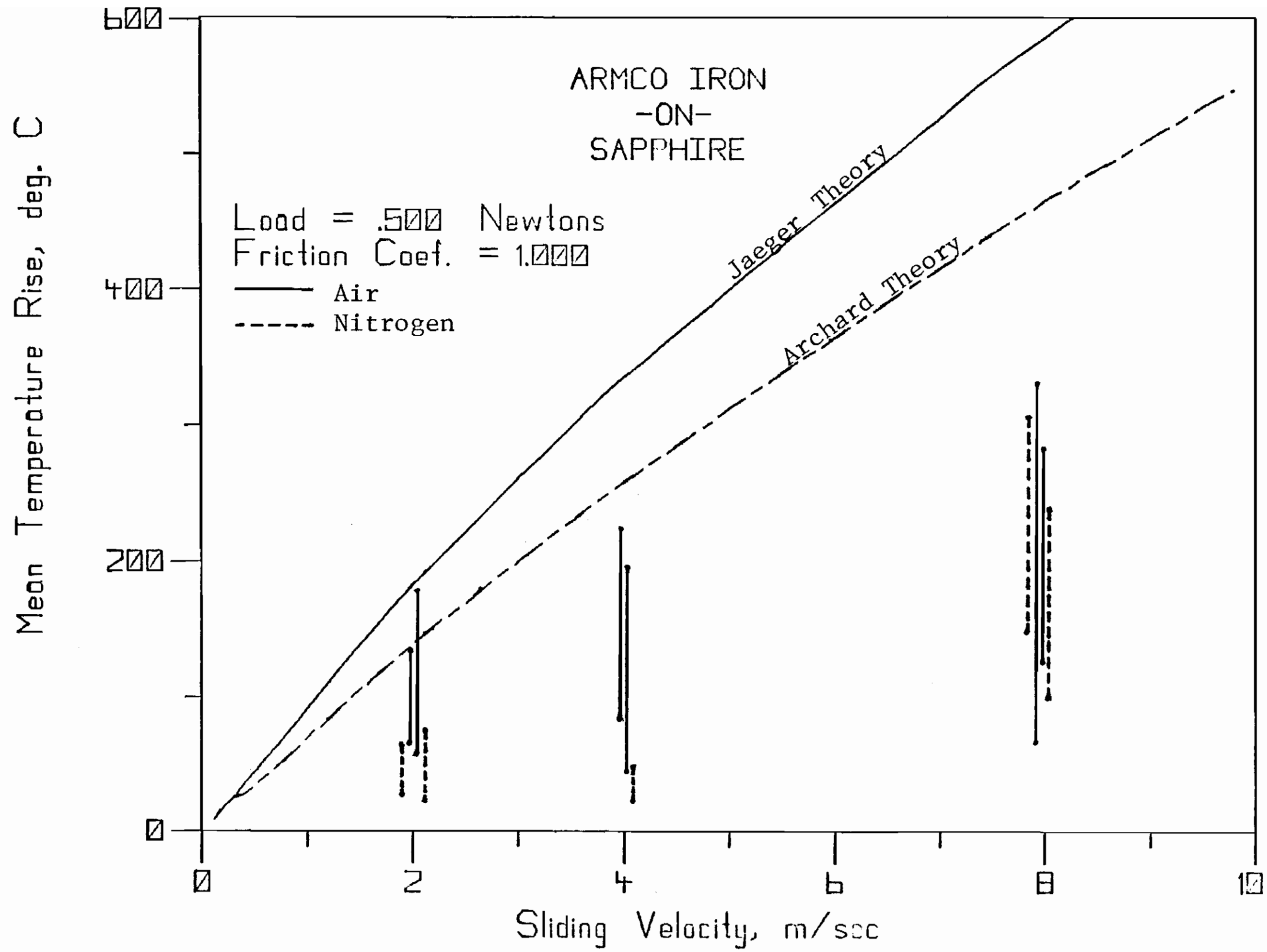

Figure 34 Comparison of Normalized Measured Temperature Rises to Theoretical Temperature Rise at 0.5 N Load

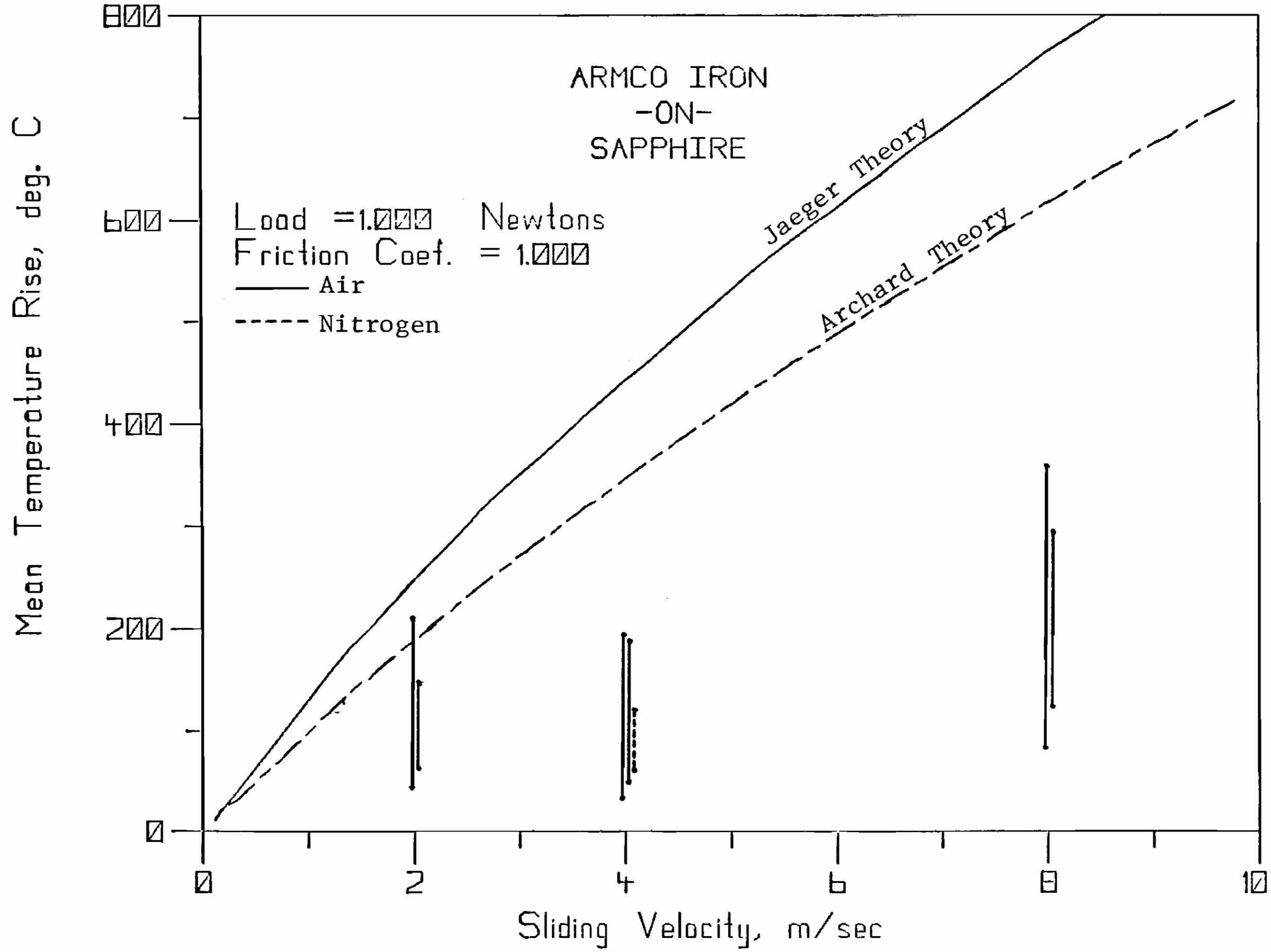

Figure 35 Comparison of Normalized Measured Temperature Rises to Theoretical Temperature Rise at 1.0 N Load

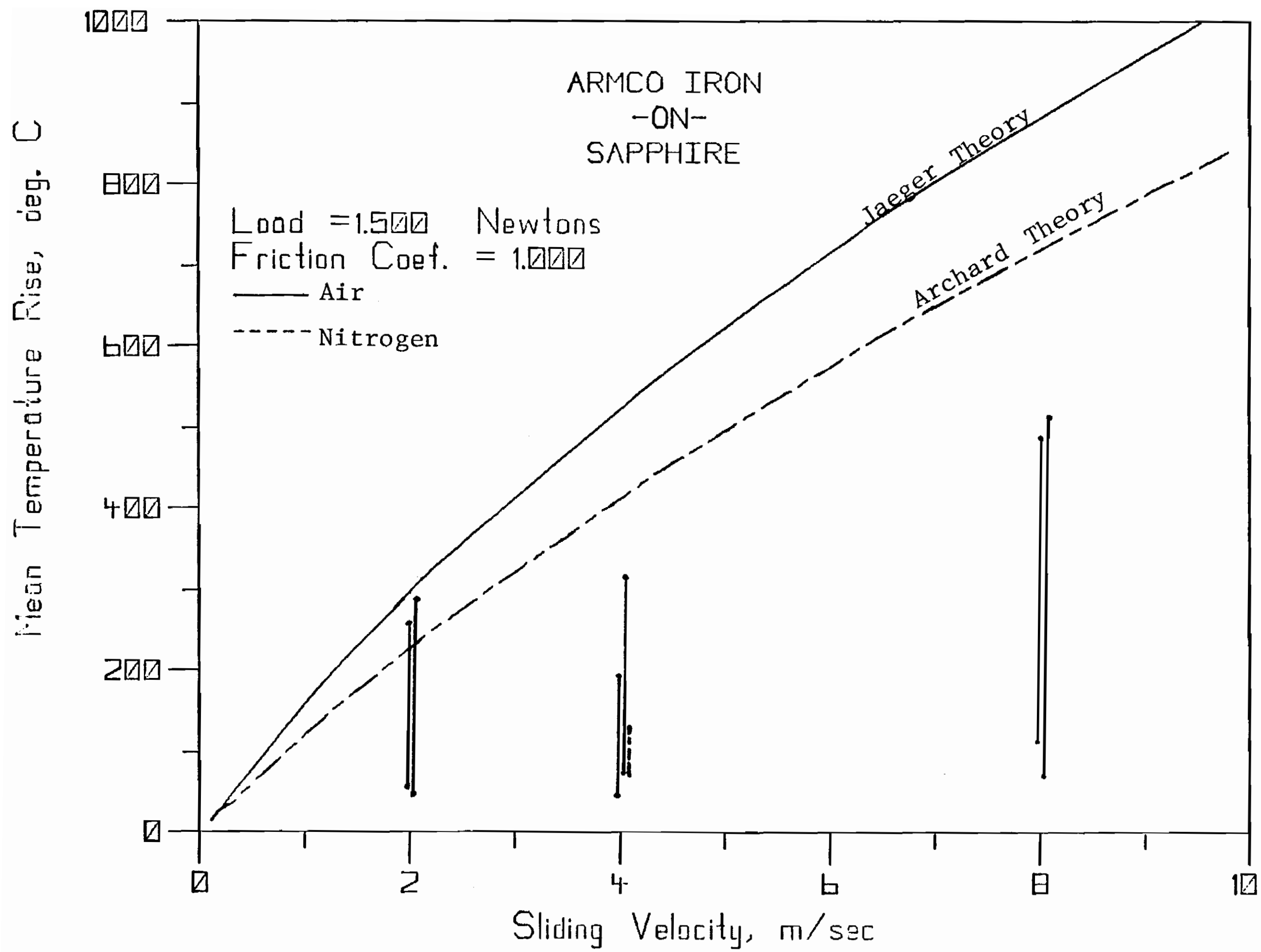

Figure 36 Comparison of Normalized Measured Temperature Rises to Theoretical Temperature Rise at 1.5 Load

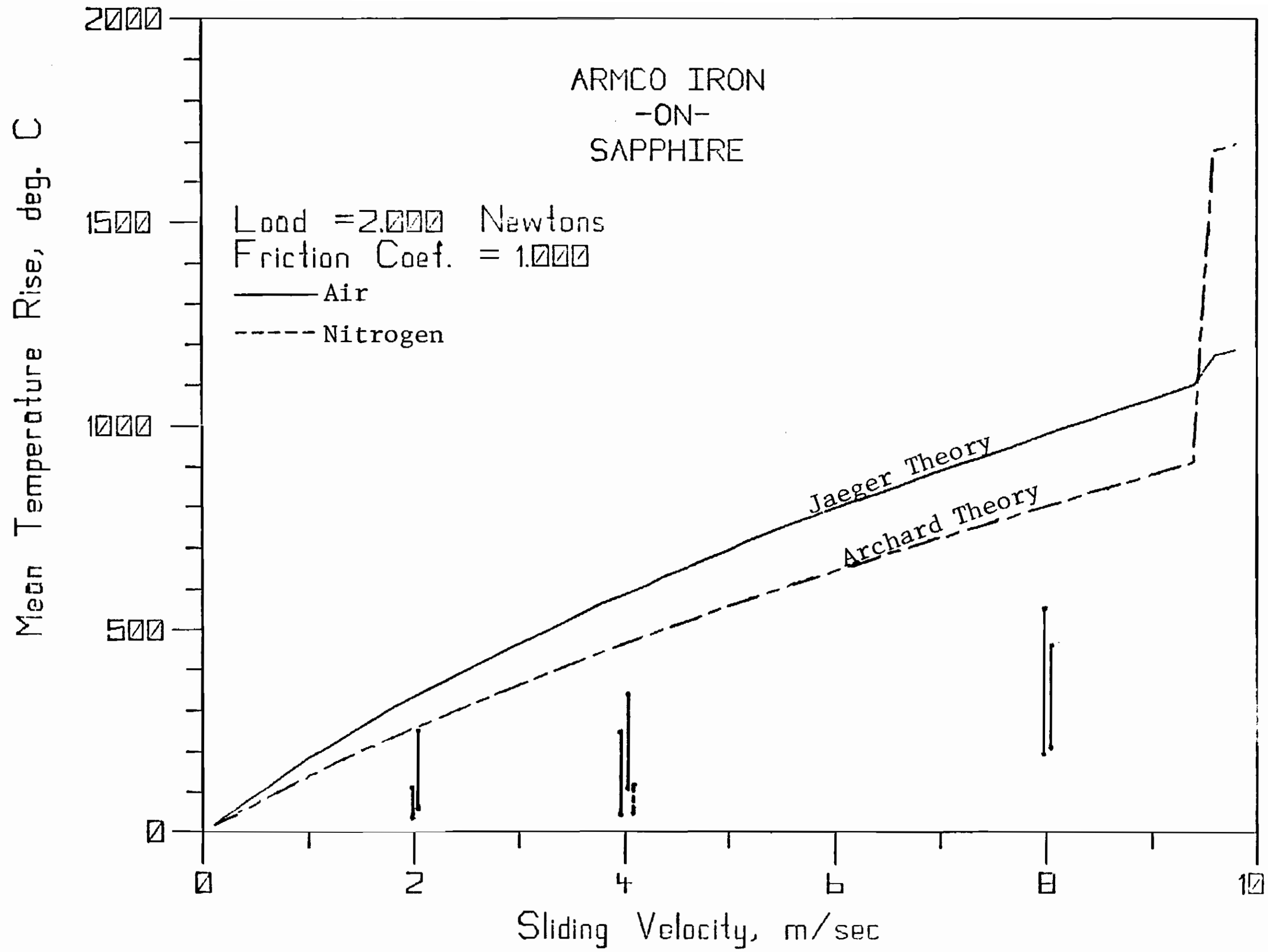

Figure 37 Comparison of Normalized Measured Temperature Rises to Theoretical Temperature Rise at 2.0 N Load

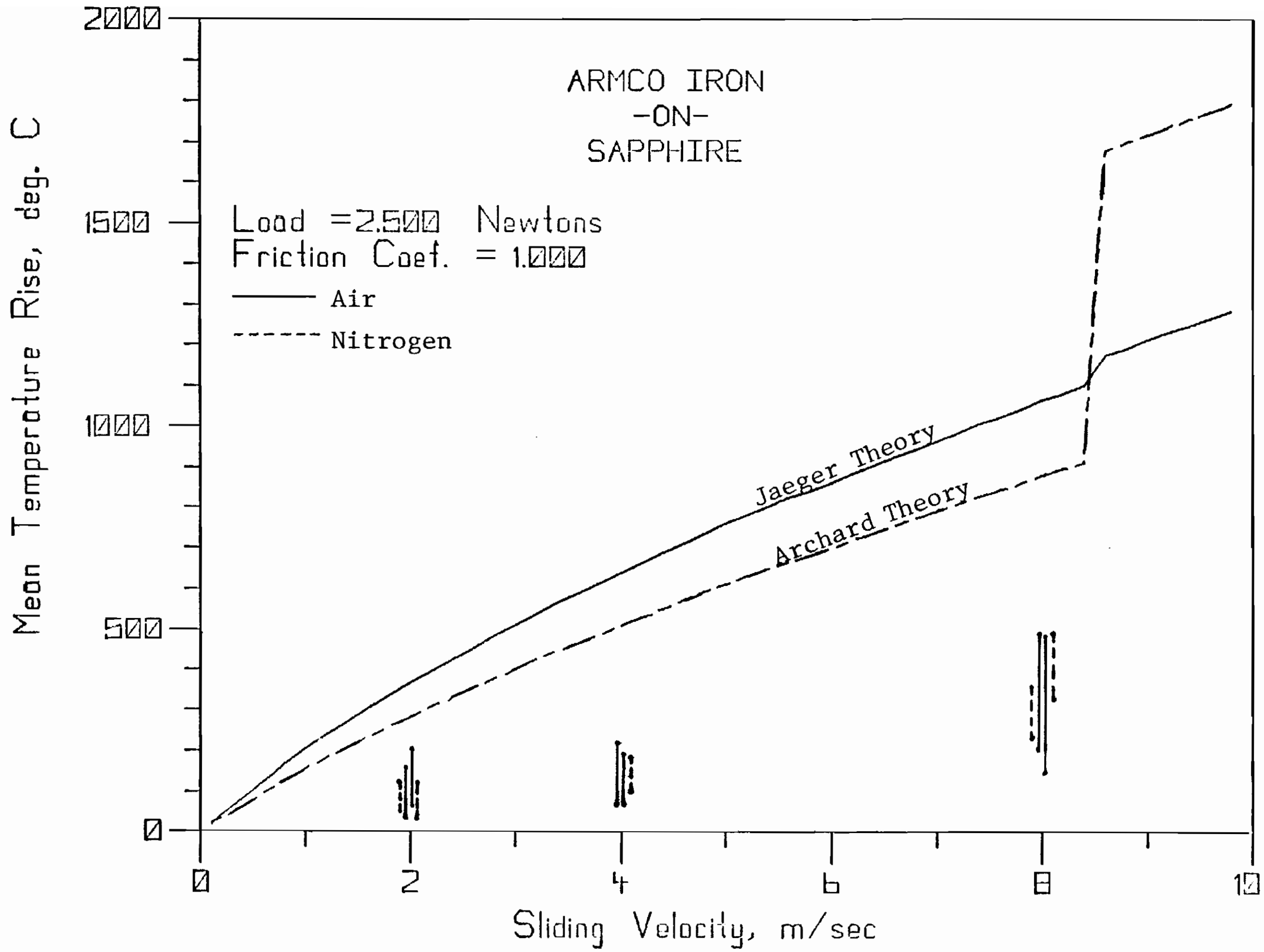

Figure 38 Comparison of Normalized Measured Temperature Rises to Theoretical Temperature Rise at 2.5 N Load

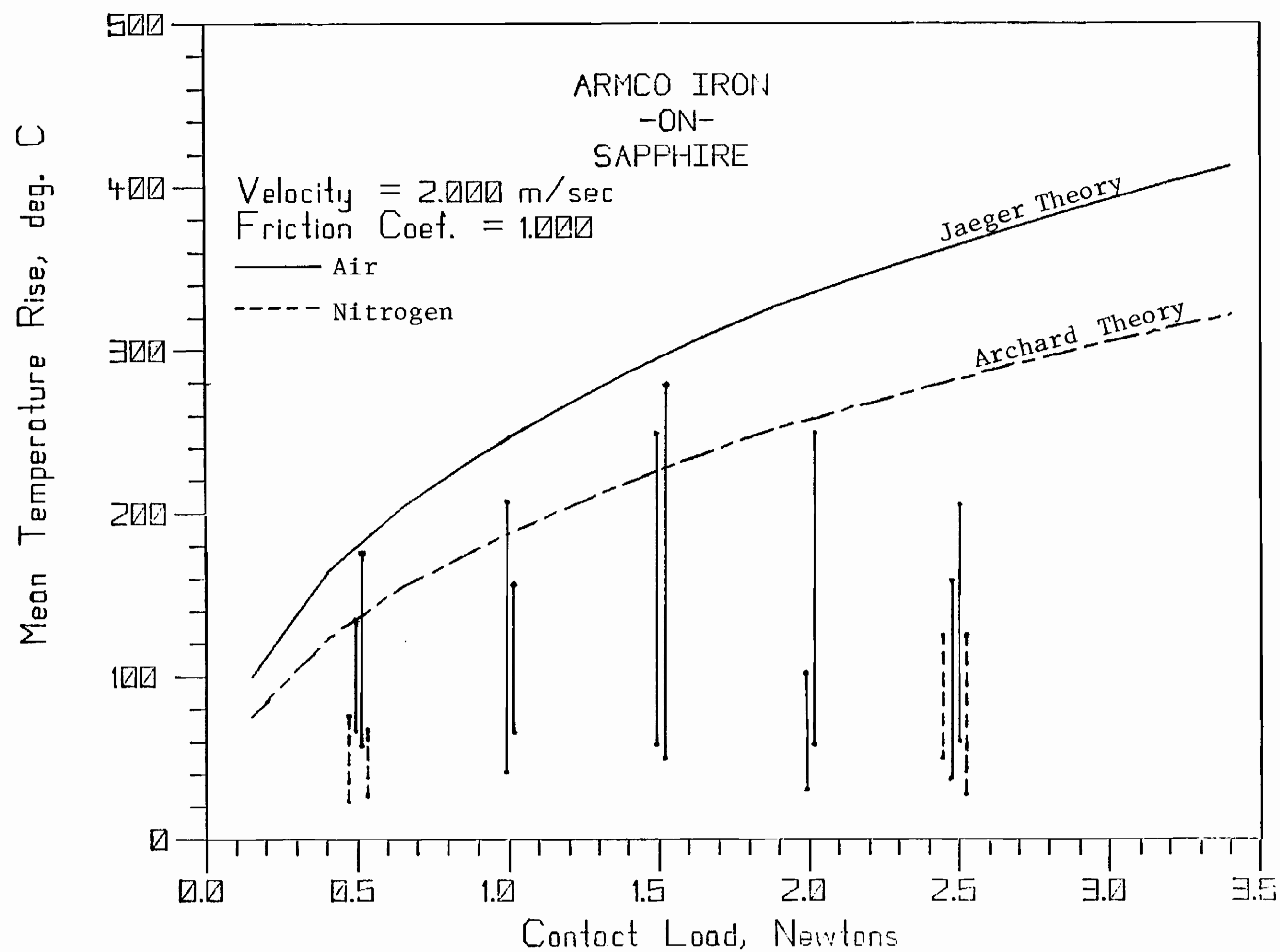

Figure 39 Comparison of Normalized Measured Temperature Rises to Theoretical Temperature Rise at 2.0 m/s Velocity

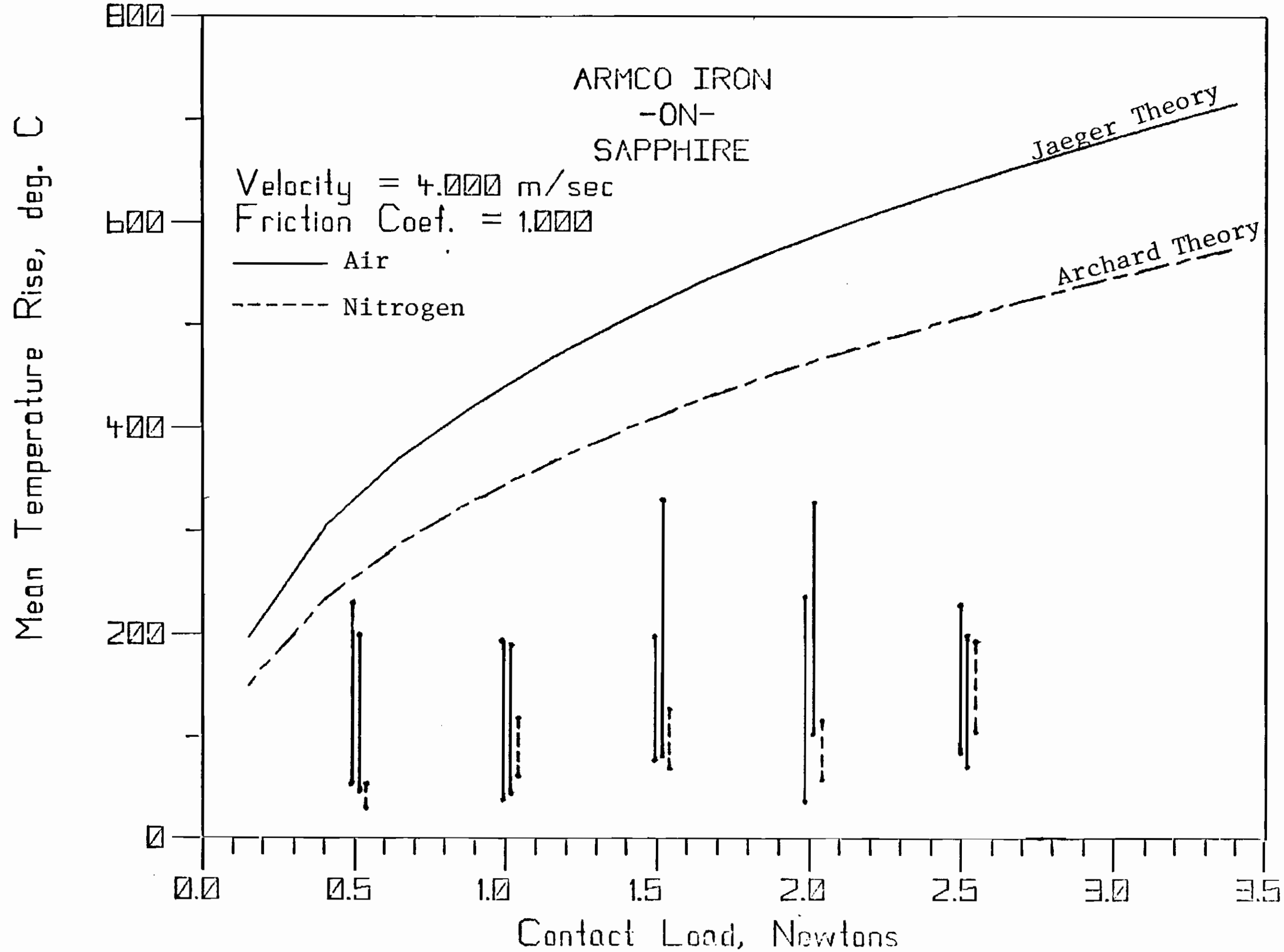

Figure 40 Comparison of Normalized Measured Temperature Rises to Theoretical Temperature Rise at 4.0 m/s Velocity

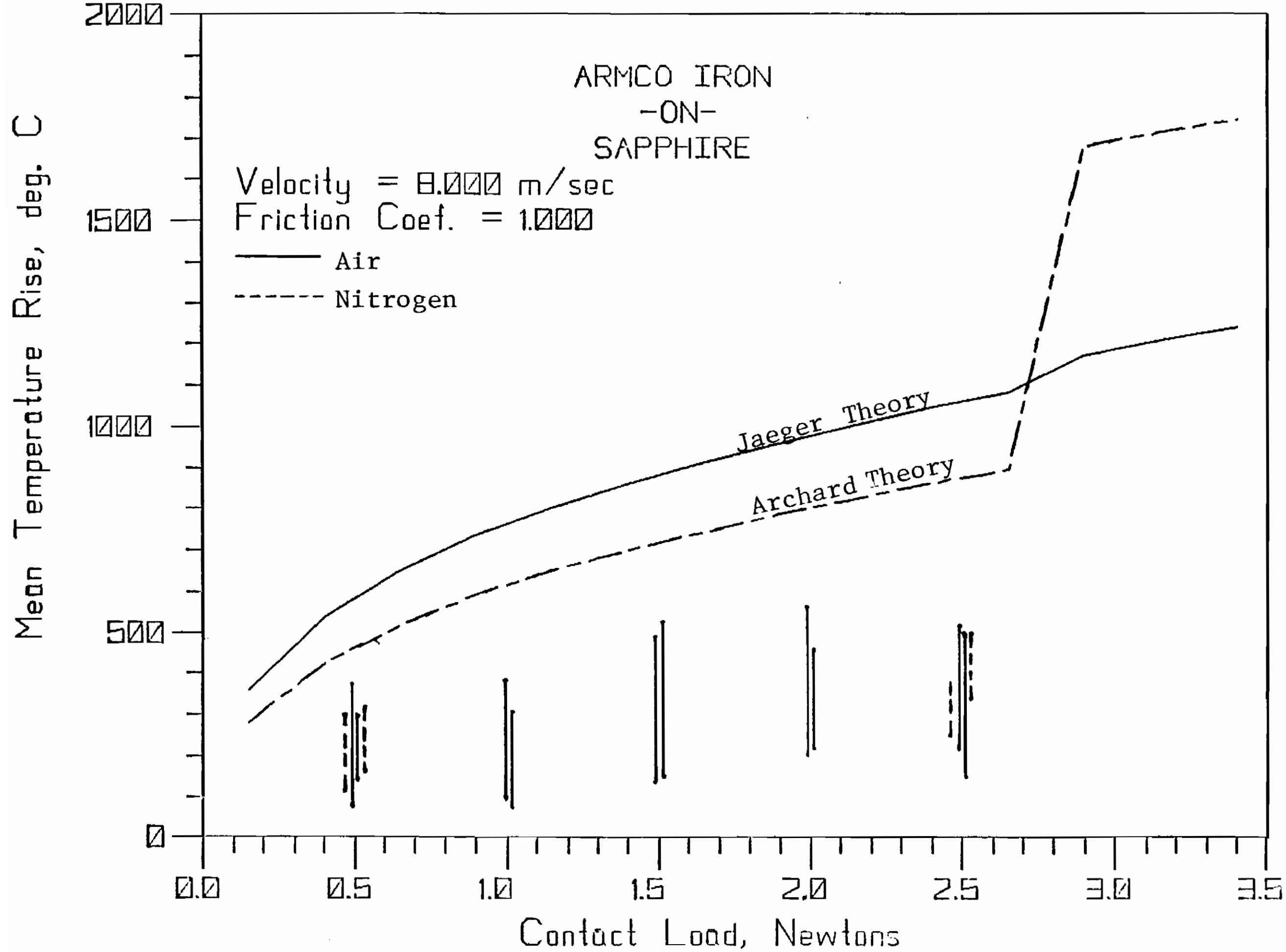

Figure 41 Comparison of Normalized Measured Temperature Rises to Theoretical Temperature Rise at 8.0 m/s Velocity

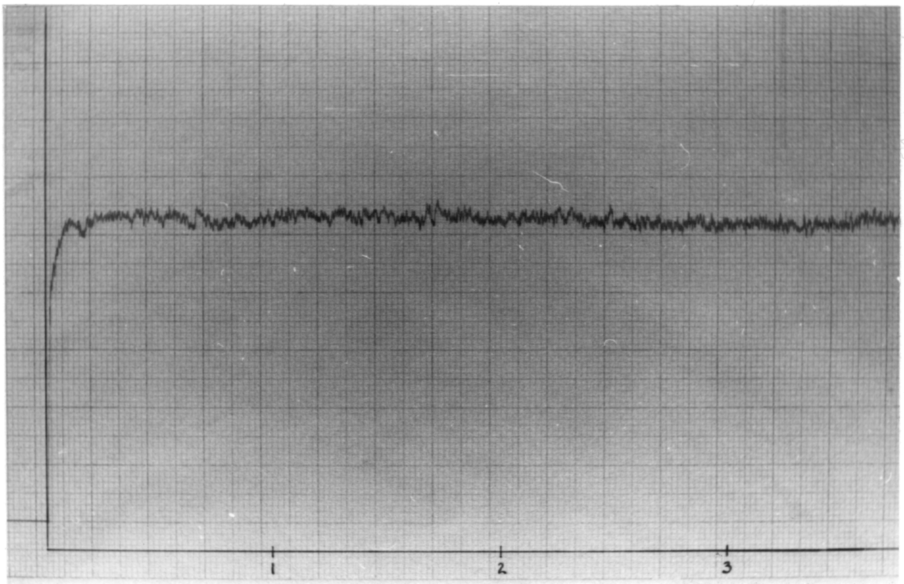

Figure 42 Typical Torque Output as a Function of Time in Minutes For Both Environments

the coefficient of friction was higher in nitrogen than in air, under the same load and velocity conditions. The numerical value of the coefficient of friction (μ) for each test case is given in Table 7.

C. Wear

The amount of wear for each test was determined from the calculated weight loss, the difference between the specimen's weight before and after a test run. The wear volume per sliding distance was calculated by dividing the change in weight (*mg*) by the density of Armco iron and the total sliding distance. Archard's wear "law" states that

$$\frac{V}{L} = K \cdot \frac{W}{H} \qquad \{48\}$$

V = wear volume
L = sliding distance
W = normal load
H = material hardness
K = coefficient of wear

All of the above variables were known for any given test run except for the coefficient of wear, *K*, thus, it was claculated for each test. Appendix M contains the numerical wear data. In general, the wear rate was higher in nitrogen than in air under identical load and velocity conditions, increased relatively linearly with load, and decreased with velocity. The numerical wear data is given in Table 7 in terms of V/L for each test case.

D. Analysis of Variance

A statistical treatment, the analysis of variance, was performed to determine the significance of the effects of load, velocity, environment (air and nitrogen), and their interactions on the measured values of surface temperature, friction, and wear. Table 4-6 summarizes the statistical results. The R-Square value is the proportion of variation explained by the main effects and their interactions.

E. Summary

The results of the measurements of temperature rise, coefficient of friction, and wear are summarized in Table 7. The relative trends of these parameters as a function of load, velocity, and environment are graphically presented in Figs. 43 through 47.

TABLE 4

ANALYSIS OF VARIANCE OF TEMPERATURE

Parameter	Degree of Freedom	Sum of Squares	Mean Square	F Value	Significance
LOAD	*1*	*3393.06*	*3393.06*	*40.98*	*99%*
VEL	*1*	*10660.56*	*10660.56*	*128.77*	*99%*
ENVIR	*1*	*370.56*	*370.56*	*4.48*	*90%*
LOAD*VEL	*1*	*855.56*	*855.56*	*10.33*	*99%*
RESIDUAL	*11*	*910.69*	*82.79*		

R-SQUARE = *0.9438*

TABLE 5

ANALYSIS OF VARIANCE OF COEFFICIENT OF FRICTION

Parameter	Degree of Freedom	Sum of Squares	Mean Square	F Value	Significance
VEL	1	0.03240	0.03240	70.05	99%
ENVIR	1	0.01440	0.01440	31.74	99%
VEL*ENVIR	1	0.01103	0.01103	23.84	99%
RESIDUAL	12	0.00555	0.00046		

R-SQUARE = 0.9124

TABLE 6

ANALYSIS OF VARIANCE OF WEAR

Parameter	Degree of Freedom	Sum of Squares	Mean Square	F Value	Significance
LOAD	1	151.7762	151.7762	237.60	99%
VEL	1	160.2693	160.2693	250.89	99%
ENVIR	1	81.5454	81.5454	127.66	99%
LOAD*VEL	1	65.4521	65.4521	102.46	99%
LOAD*ENVIR	1	32.8300	32.8300	51.39	99%
VEL*ENVIR	1	89.2978	89.2978	139.79	99%
LOAD*VEL*ENVIR	1	34.6950	34.6950	54.31	99%
RESIDUAL	8	5.1104	0.6388		

R-SQUARE = 0.9918

TABLE 7

SUMMARY OF NUMERICAL DATA

[1]Test No.	Range of Measured Temperature Rises (*C*)	[2]Theoretical Mean Temp. Rise (*C*) Archard	Jaeger	μ	Wear, V/L ($\times 10^{-14} m^2$)	$K (\times 10^{-5})$
A-2-50-1	*14 - 44*	*34*	*45*	*0.25*	*1.4*	*2.49*
A-2-50-2	*18 - 37*	*37*	*49*	*0.27*	*1.95*	*1.75*
A-2-100-1	*21 - 50*	*60*	*79*	*0.32*	- -	- -
A-2-100-2	*14 - 67*	*60*	*79*	*0.32*	*2.37*	*2.13*
A-2-150-1	*13 - 73*	*59*	*77*	*0.26*	*5.51*	*3.30*
A-2-150-2	*19 - 83*	*75*	*97*	*0.33*	*1.4*	*0.83*
A-2-200-1	*20 - 85*	*87*	*113*	*0.34*	*2.81*	*1.27*
A-2-200-2	*10 - 34*	*85*	*110*	*0.33*	*2.78*	*1.25*
A-2-250-1	*17 - 55*	*76*	*98*	*0.27*	*7.04*	*2.53*
A-2-250-2	*12 - 50*	*88*	*113*	*0.31*	*5.08*	*1.83*
A-4-50-1	*14 - 60*	*77*	*100*	*0.30*	*1.46*	*2.62*
A-4-50-2	*16 - 63*	*69*	*90*	*0.27*	*1.61*	*2.90*
A-4-100-1	*11 - 50*	*90*	*114*	*0.26*	- -	- -
A-4-100-2	*9 - 47*	*83*	*106*	*0.24*	*0.98*	*0.89*
A-4-150-1	*19 - 80*	*99*	*125*	*0.24*	- -	- -

[1]See Appendix J for key.

[2]Area of contact calculated from plastic deformation theory.

TABLE 7 CONT.

Test No.	Range of Measured Temperature Rises (C)	Theoretical Mean Temp. Rise (C) Archard	Jaeger	μ	Wear, V/L ($\times 10^{-14} m^2$)	$K(\times 10^{-5})$
A-4-150-2	15 - 56	115	146	0.28	3.92	2.35
A-4-200-1	32 - 99	139	175	0.30	- -	- -
A-4-200-2	12 - 79	153	193	0.33	1.84	0.83
A-4-250-1	25 - 70	178	223	0.35	3.64	1.31
A-4-250-2	26 - 74	163	204	0.32	4.33	1.56
A-8-50-1	29 - 65	102	129	0.22	1.33	2.39
A-8-50-2	18 - 92	116	146	0.25	0.99	1.78
A-8-100-1	25 - 102	209	260	0.34	1.14	1.03
A-8-100-2	29 - 121	203	252	0.33	1.50	1.35
A-8-150-1	35 - 150	208	255	0.29	1.96	1.17
A-8-150-2	37 - 142	208	255	0.29	1.92	1.15
A-8-200-1	57 - 122	217	264	0.27	3.61	1.63
A-8-200-2	48 - 135	193	234	0.24	- -	- -
A-8-250-1	41 - 127	228	275	0.26	2.79	1.01
A-8-250-2	47 - 111	193	233	0.22	3.92	1.41
N-2-50-1	11 - 27	55	73	0.40	4.63	8.34
N-2-50-2	10 - 31	55	73	0.40	5.56	10.0
N-2-250-1	10 - 46	102	131	0.36	20.2	7.25
N-2-250-2	19 - 46	110	142	0.39	22.1	7.95

TABLE 7 CONT.

Test No.	Range of Measured Temperature Rises (C)	Theoretical Mean Temp. Rise (C)		μ	Wear, V/L ($\times 10^{-14} m^2$)	$K (\times 10^{-5})$
		Archard	Jaeger			
N-4-50-1	13 - 20	95	123	0.37	- -	- -
N-4-100-1	23 - 44	124	159	0.36	- -	- -
N-4-150-1	26 - 46	148	187	0.36	- -	- -
N-4-200-1	21 - 43	167	210	0.36	- -	- -
N-4-250-1	35 - 63	168	210	0.33	- -	- -
N-8-50-1	34 - 70	102	129	0.22	1.01	1.82
N-8-50-2	26 - 60	111	140	0.24	1.05	1.88
N-8-250-1	83 - 124	219	265	0.25	3.23	1.16
N-8-250-2	65 - 100	236	286	0.27	3.90	1.40

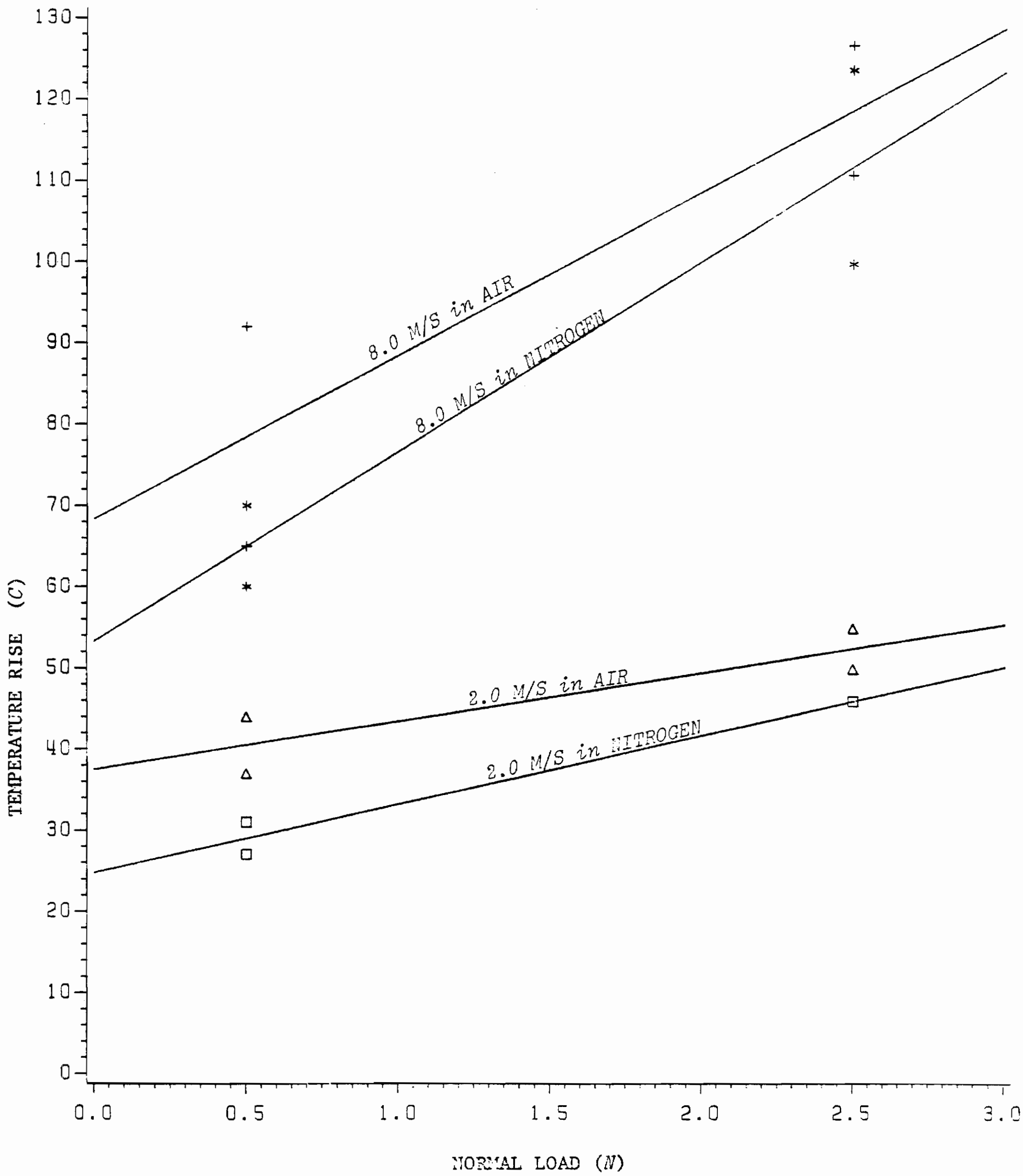

Figure 43 Trend of Measured Surface Temperature Rise as a Function of Normal Load in Both Air and Nitrogen

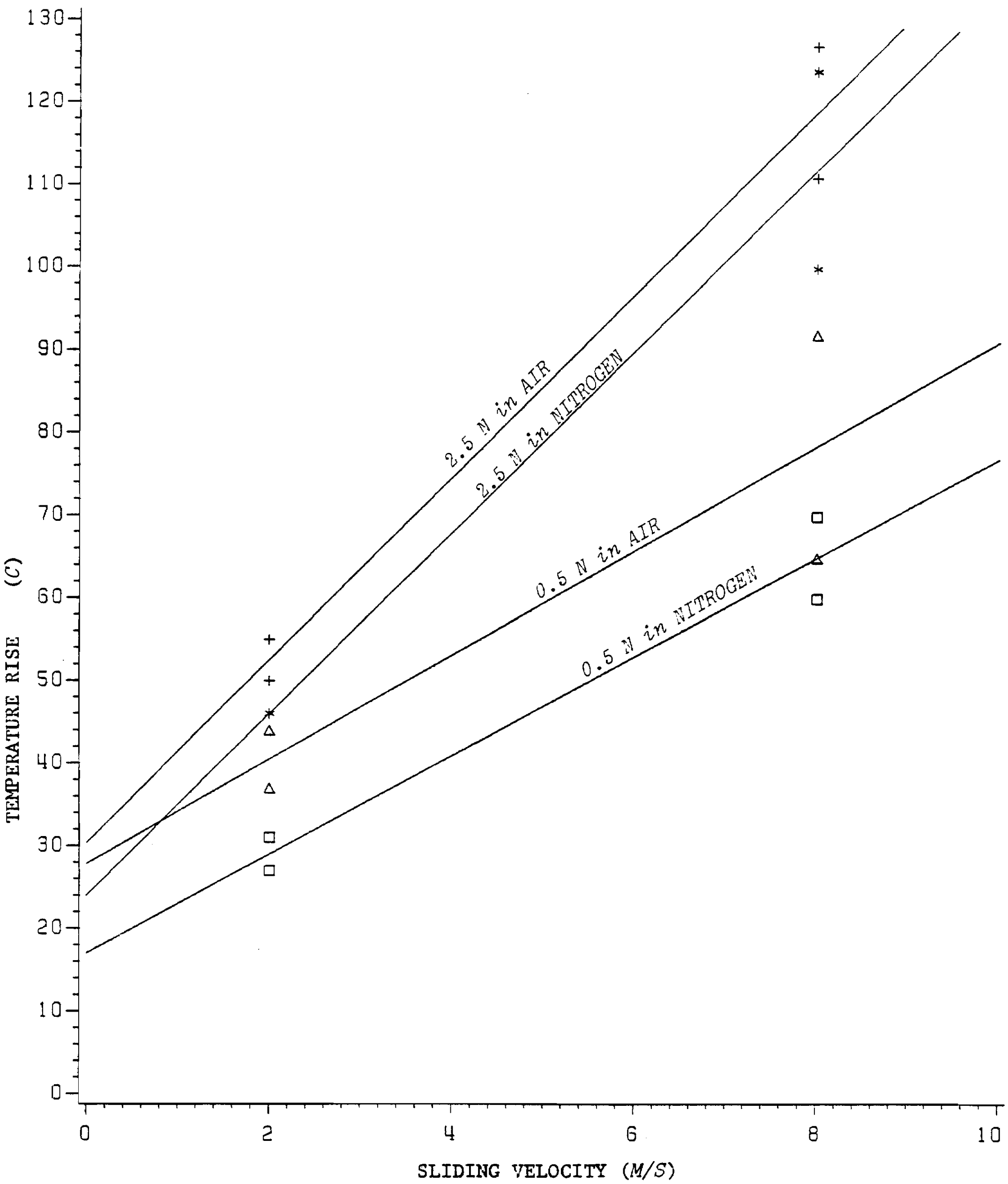

Figure 44 Trend of Measured Surface Temperature Rise as a Function of Sliding Velocity in Both Air and Nitrogen

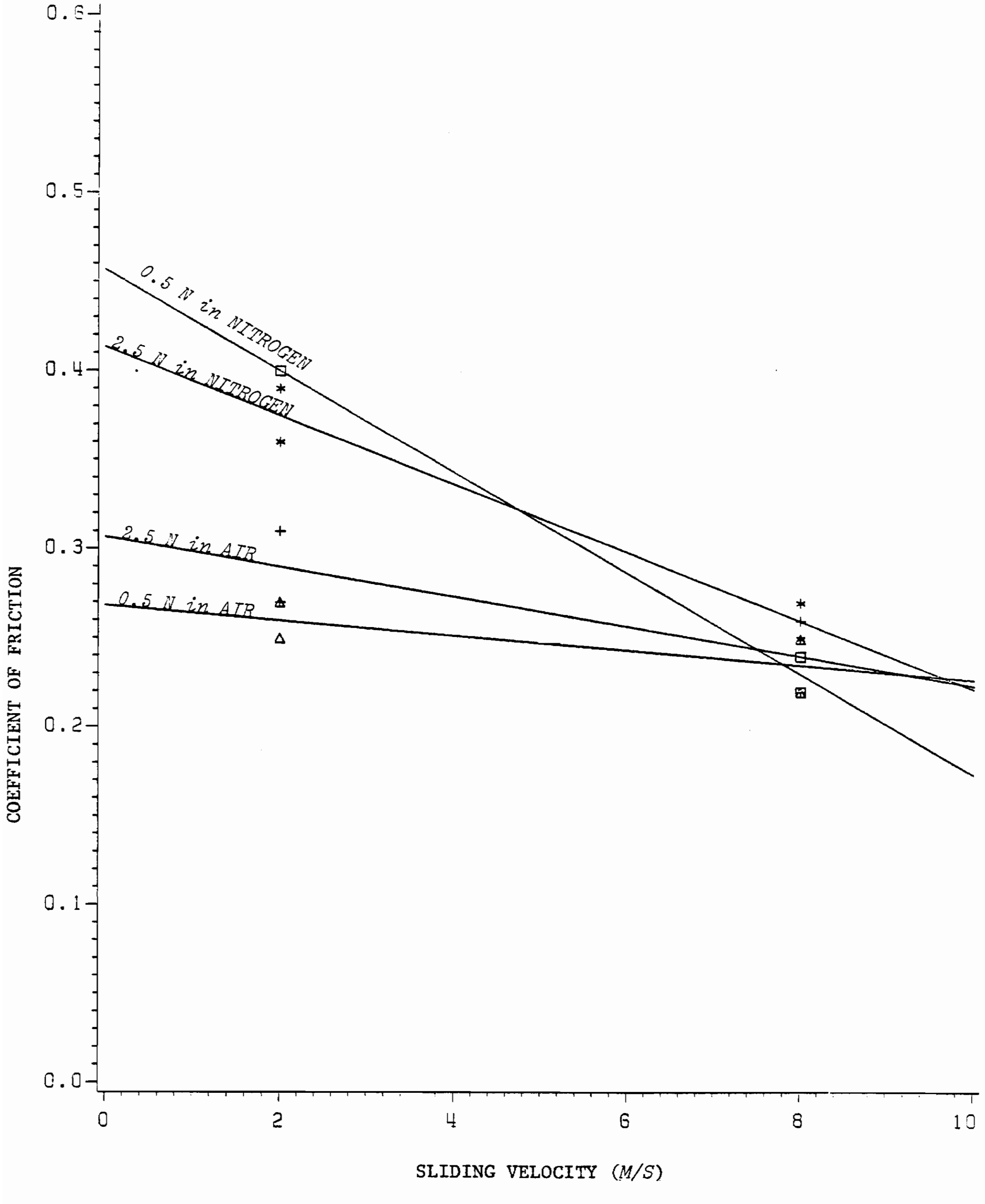

Figure 45 Trend of Coefficient of Friction as a Function of Sliding Velocity in Air and Nitrogen Environments

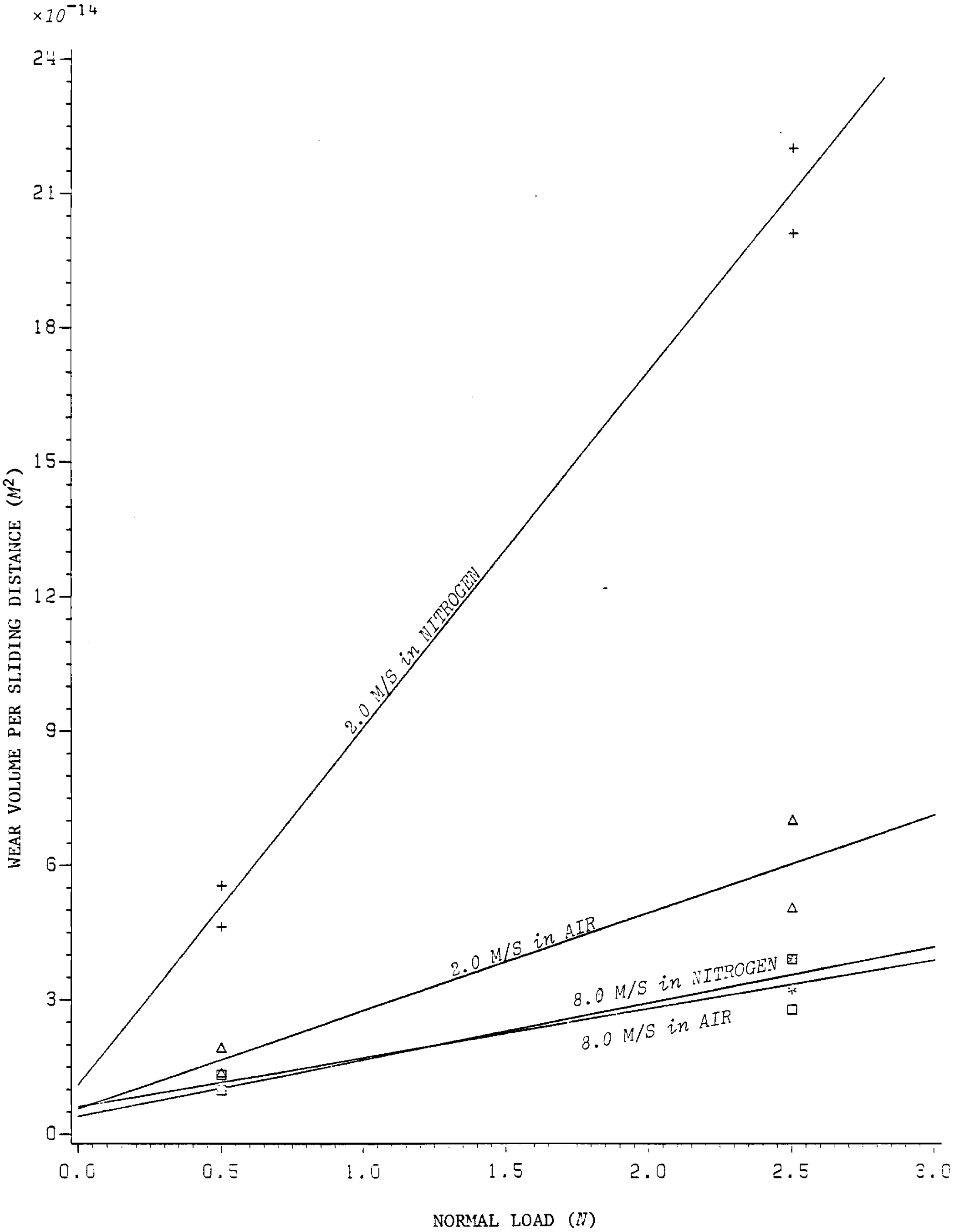

Figure 46 Trend of Wear Volume Per Sliding Distance Versus Normal Load in Both Air and Nitrogen

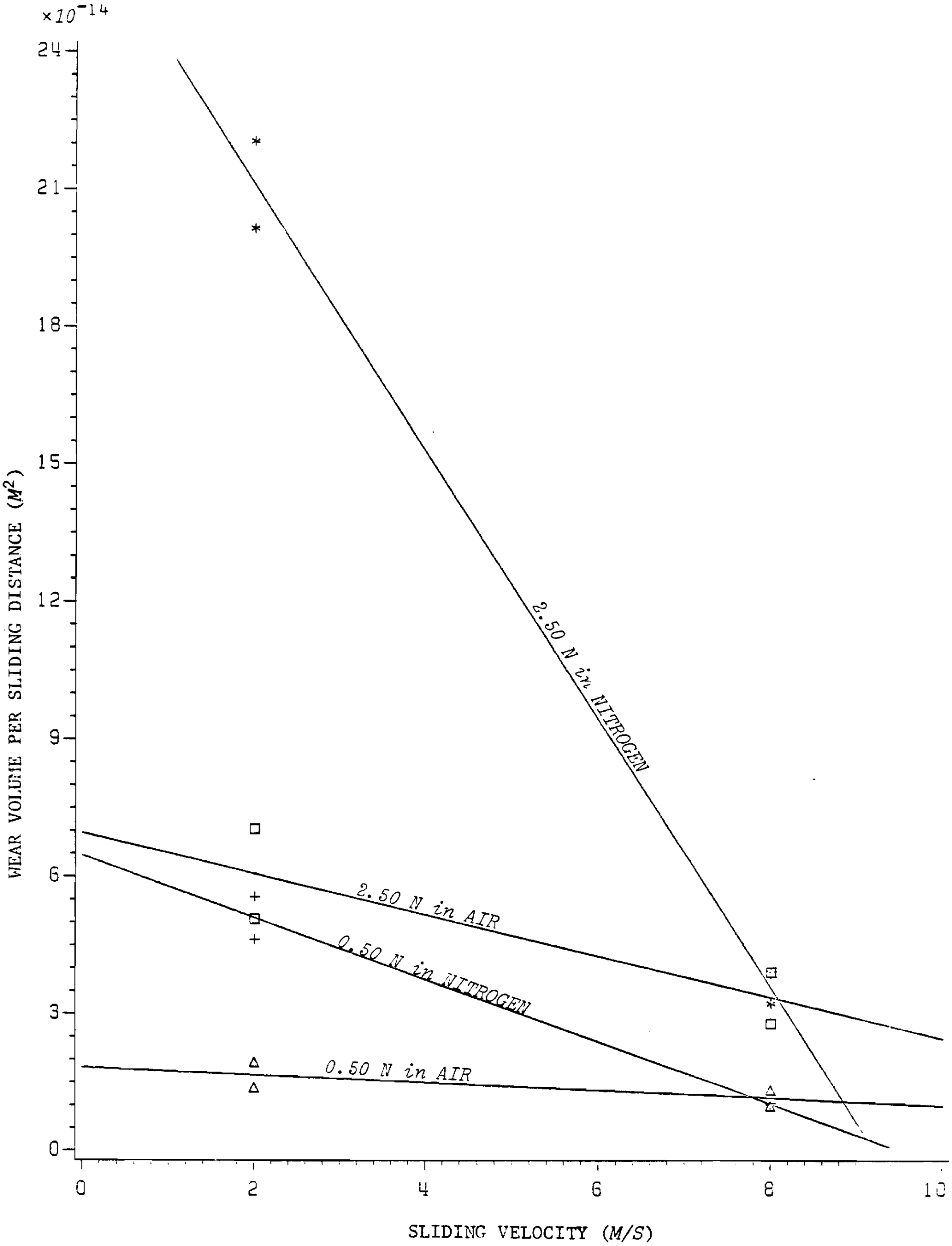

Figure 47 Trend of Wear Volume Per Sliding Distance Versus Sliding Velocity in Both Air and Nitrogen

DISCUSSION

The radiance data collected as a function of time presented useful observations which formed some basic assumptions used for estimating emissivity and calculating surface temperatures. The important observations made were:

1) the presence of rapid radiance fluctuations,
2) the quasi-steady state condition obtained after a run-in period (approximately two minutes),
3) the higher radiance levels generally recorded as a function of position for tests conducted in air, especially at lower loads and velocities,
4) the relatively constant radiance levels recorded, independent of position, for tests conducted in nitrogen, and
5) the general increase of radiance level with increasing velocity and load.

The occurrence of rapid radiance fluctuations recorded while taking measurements from a fixed target area may be explained by two phenomena -- a change in temperature or a change in emissivity. It is highly probable that changes in both will occur simultaneously.

Photographs taken at the end of each experiment showed formations of oxide at the interface for tests performed in air. Measurements of of the oxide layers revealed emissivity values of approximately *0.80*. However, clean iron surfaces have a measured emissivity of approximately *0.20*. Thus, a large change (400%) in radiance can occur during the wear process even if the surface temperature is held constant. In contrast, tests conducted in nitrogen have been shown to successfully inhibit oxidation on the interface surface, resulting in a much narrower range of possible emissivities. However, radiance fluctuations were still recorded though somewhat diminished in magnitude. It may be assumed that these fluctuations are due to temperature changes within the target area.

Although several hypotheses may account for the change in temperature within the target area, that caused by the migration of the contact area which occurs naturally by the wear process as discussed by Ling and Pu (32) seems most probable. As contacting areas wear, new areas in different locations come into contact. This would also include load-carrying wear particles as they traverse the contact region. Since the target area of the infrared microscope is very small ($\sim 2.5 \times 10^{-10} m^2$), it is possible for contacting areas to be outside this area. Therefore, radiance fluctuations will occur whenever an area of actual contact comes within the microscope's target spot. This total process would most likely occur within a short time period, relative to the size of the contact area. The fluctuations shown in Fig. 19 and 20 reveal an almost instantaneous rise followed by a rapid, exponential fall in radiance which may correspond to the rapid heating and cooling of an area which has come into sliding contact.

After a period of time (approximately two minutes), a quasi-steady state condition appeared to be reached in each test case. This condition may be characterized by stable wear processes and steady heat transfer from the system to the surrounding environment. In this state, a relatively prominent minimum and maximum radiance level was observed and recorded along with the average radiance level. These levels were shown in Fig. 33. These three values provide a qualitative measure of the radiance output behavior for each test.

Scanning within the wear area revealed that radiance level is a function of position for tests conducted in air, while in nitrogen, relatively constant radiance levels were recorded. The maximum radiance levels recorded in all tests in air was located between the center and trailing edge of the wear area, nearer the trailing edge, in most cases. Present evidence correlates the increased radiance levels to the presence of oxide layers which have a relatively high emissivity, as previously stated. Thus, emissivity was assumed to be a function of position within the wear area, at least for tests in air. Following the assumption that steady conditions exist, it was assumed that the distribution of emissivity over the wear area remains constant and, furthermore, repeatable for tests performed under identical conditions.

From the measurements of emissivity for each test condition, a distribution of the emissivity values can be determined within the wear area. However, to minimize the variance of this distribution, the wear area was divided into four equal sections, or positions, normal to the direction of sliding, as shown in Appendix J. Knowing the distribution of emissivity for each position, a mean temperature and its error can be calculated given the radiance level and the position from which the measurement was made.

To determine the mean emissivity and the variance for each test condition, multiple linear regression was implemented. This technique was used, not only to calculate the mean and the variance, but to generate an equation to fit the statistical data as a function of the significant parameters, i.e., position, load, and velocity. Thus, it would be possible to predict a mean emissivity and a variance for any combination of load, velocity, and position within the limits of the initial test conditions. This method was applied to data from both environments.

The statistical results supported the observation that emissivity is a function of position for tests performed in air but not in nitrogen. Therefore, the model for estimating emissivity in air is a function of load, velocity, and position, and the model for emissivity in nitrogen is only a function of load and velocity, given by equations {46} and {47}. It was determined that the proportion of the variation of emissivity explained is approximately *0.29* and *0.53* for tests conducted in air and nitrogen, respectively. Although the models are only fair in their predictive capabilities, it should be understood that this is not an exhaustive, but rather a preliminary investigation from which the results may provide insight to better designed experiments in the future.

The parameters used in both mathematical models were determined to be significant with *99%* confidence. Therefore, it would appear that other variables exist which were not accounted for in these tests. Future tests should include not only load, velocity, and position, but any other possible variables which may have an effect such as, time, laboratory environmental conditions, and variations in material properties due to temperature changes. It may also be necessary to determine a better method of assigning positions.

Comparing the results of the two environments may provide further insight. Even though the model for nitrogen tests is simpler than that for air, it explains almost twice the variation of emissivity. Obviously the principal cause is the lack of oxidation on the surface. Thus, parameters that affect oxidation should possibly be added to the model for tests in air. However, it would be an advantage is surface temperature measurements of readily oxidizable materials could be performed in nitrogen and still be representative of the surface temperatures generated in air.

The estimated mean emissivities were used to calculate the surface temperatures from the measured radiance levels. The variance associated with the estimated mean emissivities was found, in general, to affect the mean temperature by 1 or 2^{o} C which may be consider negligible in comparison to the total experimental error. Therefore, only the surface temperature calculated using the estimated mean emissivity is given in the numerical data in Appendix K. The measured bulk temperatures were subtracted from the measured surface temperatures to give the temperature rise. Figures 34 - 41 compared the range of normalized measured temperature rises of both environments to the theoretical mean temperature rise as a function of velocity and load. In general, the measured surface temperature rise was less than that predicted by Archard and Jaeger.

The plots of measured temperature rise reveal some interesting observations concerning the effects of load, velocity, and environment on surface temperature. In general, it can be seen that surface temperature increases with both velocity and load. However, changes in velocity have a more marked effect on surface temperature than changes in load. (This fact is supported later by the statistical results.) Theoretically, the surface temperature has been shown to be proportional to V and $\sqrt{W}$ although the measured values do not follow these relationships.

It can also be seen from the numerical temperature data that the range of measured surface temperatures becomes larger with increasing velocity and load. This increased difference of surface temperature is easily explained by the hypothesis that individual areas of contact are viewed as they migrate within the wear area. Heat is assumed to be generated at the contacting asperity tips and then conducted away into the bulk material. Therefore, the temperature will be much greater at the sites of contact than at those not in contact. Furthermore, this temperature gradient will increase as the heat input increases, i.e., at higher loads and velocities, resulting in a greater difference of temperatures.

The environmental effects are readily observable. In all tests conducted in nitrogen, the range of temperatures measured was less than the corresponding range of measurements in air. This may be a consequence of the narrower distribution of emissivity, due to the near absence of oxidation. However, as the load and velocity increased, the range and magnitude of the measured temperature rises in air approached those measured in nitrogen. This may be explained by the fact that the distribution of emissivity for tests run at higher loads and velocity in air approaches the distribution of emissivity in comparable tests performed in nitrogen. This may be seen by comparing Figs. 21-26 to Figs. 27-32. Thus, it might be assumed that at high loads and velocities, the surface temperature is not a function of the environment, i.e., air versus nitrogen. However, this is not conclusive.

A statistical treatment, the analysis of variance, was performed to determine whether a variation of conditions has a significant effect on surface temperature, coefficient of friction, and wear. The analysis of variance not only establishes the significance of the main effects, but also their interactions. Interaction is a measure of the change of the effect of one factor due to the presence of another factor. The interaction would be zero if the effect is independent of the second factor. For simple cases, plots of the data may reveal both main effects and interactions. For two level cases, a consistent change in slope may signal an interaction between factors. The final numerical results of the statistical analysis were summarized in Table 4, 5, and 6 and presented graphically in Figs. 43-47.

As expected, both load and velocity have a significant effect on surface temperature, with velocity having the greater effect (the larger F value). The interaction between load and velocity was also found to be significant with the highest surface temperatures measured at both high load and velocity. These effects can be seen in Figures 43 and 44. Environment was determined to be significant within 90% confidence. At this level of significance, it is difficult to definitely state that surface temperature is or is not a function of environment. Models having predictive capabilities of higher accuracy than the ones used in this study should establish whether any environmental effects exist.

Irrespective of the models used, the measured surface temperatures were consistently greater for tests performed in air than those performed in nitrogen. (See Figs. 43 and 44.) This trend occurs even though the energy input, as determined by frictional resistance, is greater in nitrogen, expecially at *2 m/s* as shown in Fig. 45. One possible reason may be due to the presence of oxide formation which is prevalent in the air tests. Iron oxide, having a lower thermal conductivity than pure iron, may form an insulating layer. This layer would decrease the amount of heat transferred across the interface, thus increasing the surface temperature of the specimen. A second reason may be that the increased energy input to the system in nitrogen is expended by the increased wear rate. Figures 46 and 47 show that wear is greater in nitrogen than air, especially at *2 m/s*.

The significant effects on friction (the coefficient of friction) was determined to be velocity, environment, and the interaction between these two variables. The trend of these effects can be seen graphically in Fig. 45. Higher friction coefficients in nitrogen, in contrast to air, was expected since the oxide film which acts as a protective layer was inhibited from forming, allowing greater adhesion between the specimen and sapphire disk. However, transfer from the specimen to the disk appeared minimal, though no actual measurements were made. The observed decrease in friction with an increase in velocity is definite; however, the reason for this effect is not known.

Wear was determined to be a function of load, velocity, and environment. All three variables, including their first and second order interactions were deemed highly significant (*99%* confident). The greatest wear was measured for tests performed in a nitrogen environment, at high load and low velocity conditions. The general effects can be seen in Fig. 46 and Fig. 47. The effect of load was as expected from equation {48}; however, the strong effect of velocity was not predicted. The actual cause for the decrease in wear (wear volume per sliding distance) with velocity is not known. Increased wear in the nitrogen environment was anticipated since adhesion at the sliding interface would most likely be greater than in air, as noted previously.

CONCLUSIONS

Surface temperatures generated by friction have been indirectly measured using an infrared radiometric microscope. The sliding system consisted of an Armco iron pin loaded against a rotating sapphire disk.

The temperatures were calculated from measured radiance levels emitted from the surface and estimated mean emissivity values. The presence of oxide formations for tests performed in air caused a wide variation in emissivity across the wear area. Repeated tests in nitrogen inhibited the formation of oxide layers. The resulting range of measured surface temperature rises was compared to the theoretical mean temperature rise, as determined by Jaeger and Archard theories.

Measurements of frictional resistance and wear were also made for each test run. A statistical study revealing the relative effects of load, velocity, and environment (air versus nitrogen) on surface temperature, friction, and wear was performed.

The following is a summary of the major findings in this experimental investigation.

1) The infrared radiometric microscope and system were successfully used to measure surface temperature, frictional resistance, and wear.

2) The radiance data revealed large fluctuations with time emitted from a fixed area within the general region of contact. These fluctuations were caused by changes in both emissivity and temperature.

3) Emissivity measurements and SEM photographs showed that emissivity is dependent on the oxide formations within the wear area for tests conducted in air.

4) Performing repeat test runs in a nitrogen environment successfully inhibited oxide formations.

5) From statistical results, emissivity was found to be a significant function (99% confident) of position, load, and velocity for tests in air. For tests in nitrogen, only load and velocity were significant.

6) A general increase in radiance level was observed with increasing velocity and load. The radiance level rise was associated with a rise in surface temperature.

7) Analysis of variance results verified that surface temperature is significantly effected by velocity and load with a confidence of 99%. However, environment was deemed only 90% significant.

8) Coefficient of friction was found to decrease with velocity for both environments with the decrease being greater in nitrogen. The coefficient of friction in nitrogen was higher than that for air at 2 m/s.

9) Data revealed that wear decreased with velocity and increased with load. Greater wear was measured for tests performed in a nitrogen environment. Statistics confirmed that velocity, load, and environment are significant, including their first

and second order interactions (all with 99% confidence).

10) In general, the measured surface temperature rises were less than those predicted by flash temperature theory.

RECOMMENDATIONS

The following recommendations for further study have been made based upon the results of this experimental investigation. It is sincerely hoped that the solutions to these problems may advance the present state of surface temperature measurement and the science of tribology.

1) Develop a more accurate mathematical model for estimating the emissivity and the variance. Answers must be found to questions such as: Does a quasi-steady state truly exist? Are the emissivity distributions actually repeatable? What other variables may affect emissivity than those already established?

2) Using the newly developed model, apply statistical methods to determine if surface temperature is a function of the environment (air versus nitrogen). If no function exists, surface temperature measurements can then be conducted in nitrogen, providing both fewer complicating factors and greater accuracy.

3) Expand the use of nitrogen in surface temperature measurements of other readily oxidizable materials and compare with similar tests in air. It would be advantageous to know if the effects of load, velocity, and environment are universal or only unique, being dependent upon the material chosen.

4) Improve the method for measuring radiance output. Employing more advanced techniques than measuring voltages from chart paper will help to reduce experimental error.

5) Relate the radiance frequency distribution to load, velocity, and environment. This may provide information concerning the number and size of contacting areas.

6) Determine any correlation between radiance and friction data. It may be possible that radiance fluctuations are a function of friction transients causing higher surface temperatures.

7) Further investigate the effect of sliding velocity on friction and wear. The discovered effect of decreased friction and wear with increased velocity may possibly be caused by a peculiarity of the system being used. If so, a design change may be necessary.

8) Observe, in more detail, the build-up of oxide layers at the trailing edge for tests performed in air. It has been shown that the oxide formation is a function of load and velocity. However, it should be determined what proportion of the load is carried by this layer at the trailing edge. Also, the effect of this oxide layer on conduction heat transfer should be established.

9) Design an experiment to relate wear and surface temperature. According to Quinn's oxidational wear mechanism (23), the wear rate should increase with surface temperature.

10) <u>Examine the possible effect of material transfer to the sapphire disk on external transmissivity</u>. A method is needed to monitor any significant reductions in radiance measurements caused by transfered materials.

REFERENCES

1. Chao, B. T., Li, H. L., and Trigger, K. J., "An Experimental Investigation of Temperature Distribution at Tool-Flank Surface", ASME Transactions, Journal of Engineering for Industry, November, 1961, pp. 496-504.

2. Snidle, R.W., "Contribution to the Theory of Frictional Heating and the Distribution of Temperature in Wires and Strips During Drawing", Wear, Vol. 44, 1977, pp. 279-294.

3. Blok, H., "The Flash Temperature Concept", Wear, Vol. 6, 1963, pp. 483-494

4. Niemann, G., and Lechner, G., "The Measurement of Surface Temperatures on Gear Teeth", ASME Transactions, Journal of Basic Engineering, September, 1965, pp. 641-654.

5. Al-Rubeye, H. S., "Friction, Wear, and Temperature in Sliding Contact", ASME Transactions, Journal of Lubrication Technology, Vol. 102, January, 1980, pp. 107-112.

6. Santini, J. J. and Kennedy, F. E. Jr., "An Experimental Investigation of Surface Temperatures and Wear in Disk Brakes", ASLE Preprint No. 74 LC-IB-3, 1974, pp. 1-7.

7. Rowson, D. M., "The Interfacial Surface Temperature of a Disk Brake", Wear, Vol. 47, 1978, pp. 323-328.

REFERENCES CONT.

8. Floquet, A., Play, D., and Godet, M., "Surface Temperatures in Distributed Contacts. Application to Bearing Design", ASME Transactions, Journal of Lubrication Technology, April, 1977, pp. 277-283.

9. Turchina, V., Sanborn, D. M., and Winer, W. O., "Temperature Measurements in Sliding Elastohydrodynamic Point Contacts", ASME Transactions, Journal of Lubrication Technology, July, 1974, pp. 464-471.

10. Furey, M. J., "The Formation of Polymeric Films Directly on Rubbing Surfaces to Reduce Wear", Wear, Vol. 26, 1973, pp. 369-392.

11. Wiggins, J. M., "An Experimental Method for Measuring Surface Temperatures Generated by Friction", Master of Science Thesis, Mechanical Engineering, Virginia Polytechnic Institute and State University, Blacksburg, Va, December 1974.

12. Omori, D. I., "Infrared Measurements of Surface Temperatures in an Unlubricated Sliding System", Master of Science Thesis, Mechanical Engineering, Virginia Polytechnic Institute and State University, Blacksburg, Va, August 1975.

13. Li, S. H., "Experimental Investigation of Surface Temperatures of Some Polymers in Unlubricated Sliding", Master of Science Thesis, Mechanical Engineering, Virginia Polytechnic Institute and State University, Blacksburg, Va, August 1976.

REFERENCES CONT.

14. Richardson, M. H., "An Experimental Investigation of the Surface Temperature of Graphite in a Sliding System Using an Infrared Microscope", Master of Science Thesis, Mechanical Engineering, Virginia Polytechnic Institute and State University, Blacksburg, Va, August 1976.

15. Furey, M. J., "Infrared Measurements of Surface Temperatures Produced in Tribological Processes", Third International Tribology Congress, Warsaw, Poland, September 1981.

16. Furey, M. J., "Infrared Measurements of Surface Temperatures Produced by Friction in Dry Sliding Contact", VPI & SU Research Proposal Submitted to the National Science Foundation, Washington D. C., October, 1980.

17. Spurr, R. T., "Temperatures Reached During Sliding", Wear, Vol. 55, 1979, pp. 289-293.

18. Earles, S. W. E., Hayler, M. G., and Powell, D. G., "A Comparison of Surface Temperature Theories and Experimental Results for High Speed Dry Sliding", ASLE Transactions, Vol. 14, 1970, pp. 135-143.

19. Ling, F. F., and Simkins, T. E., "Measurement of Pointwise Juncture Condition of Temperature at the Interface of Two Bodies in Sliding Contact", ASME Transactions, Journal of Basic Engineering, No. 62, 1962, pp. 1-5.

REFERENCES CONT.

20. Shore, H., "Thermoelectric Measurement of Cutting Tool Temperature", Journal Washington Academy of Science, Vol. 15, 1925, pp. 85-88.

21. Furey, M. J., "Surface Temperatures in Sliding Contact", ASLE Transactions, Vol. 7, 1964, pp. 133-146.

22. Uetz, H., and Sommer, K., "Investigations of the Effect of Surface Temperatures in Sliding Contact", Wear, Vol. 43, 1977, pp. 375-388.

23. Quinn, T. F. J., "The Dry Wear of Steel as Revealed by Electron Microscopy and X-Ray Diffraction", Proc. Institute Mechanical Engineers, Vol. 182, 1968, p. 201.

24. Parker, R. C., and Thomas, P. R., "The Measurement of the Temperature of Sliding Surfaces with Particular Reference to Railway Brake Blocks", Proc. Inst. Mechanical Engineers, Vol. 158, 1948, pp. 209-229.

25. Bowden, F. P., and Thomas, P. H., "The Surface Temperature of Sliding Solids", Royal Society of London Proceedings, A223, 1954, pp. 29-40.

26. Furey, M. J., "Recent Experimental Measurements of Surface Temperatures Using IR Methods", Lecture, Fifth Limits of Lubrication Conference, Imperial College, London, July 1977.

REFERENCES CONT.

27. Blok, H., "Theoretical Study of Temperature Rise at Surfaces of Actual Contact Under Oiliness Lubricating Conditions", Institute of Mechanical Engineers, Vol. 2, 1937, pp. 222-235.

28. Jaeger, J. C., "Moving Sources of Heat and the Temperature at Sliding Contacts", Proc. Royal Society, New South Wales, Vol. 56, 1942, pp. 204-224.

29. Carslaw, H. S., Introduction to the Mathematical Theory of the Conduction of Heat in Solids, MacMillan, London, 2nd Ed., 1921, p. 150.

30. Archard, J. F., "The Temperature of Rubbing Surfaces", Wear, Vol. 2, 1958, pp. 438-455.

31. Powell, D. G., and Earles, S. W. E., "An Assessment of Surface Temperature Predictions in High Speed Sliding of Unlubricated SAE 1113 Steel Surfaces", ASLE Transactions, Vol. 15, No. 2, 1971, pp. 103-112.

32. Ling, F. F., and Pu, S. L., "Probable Interface Temperature of Solids in Sliding Contact", Wear, Vol. 7, 1964, pp. 23-36.

33. Ling, F. F., and Rice, J. S., "Surface Temperature with Temperature-Dependent Thermal Properties", ASLE Transactions, Vol. 9, 1966, pp. 195-201.

REFERENCES CONT.

34. Francis, H. A., "Interfacial Temperature Distribution Within a Sliding Hertzian Contact", ASLE Transactions, Vol. 14, 1970, pp. 41-54.

35. Cook, N. H., and Bhushan, B., "Sliding Surface Interface Temperatures", ASME Transactions, Journal of Lubrication Technology, January, 1973, pp. 59-64.

36. Malkin, S., and Marmur, A., "Temperatures in Sliding and Machining Processes with Distributed Heat Sources in the Subsurface", Wear, Vol. 42, 1977, pp. 333-340.

37. Balakin, V. A., "Formation and Distribution of Heat in the Frictional Contact Zone Under Conditions of Non-Stationary Heat Exchange", Wear, Vol. 72, 1981, pp. 133-141.

38. Instruction Manual, Infrared Radiometric Microscope, Model RM-2A, BEC 06 200970, Barnes Engineering Company, Stamford, Conn.

39. Rogers, C. A., "An Experimental Investigation of the Effect of Subdivision of Contact Area on Surface Temperatures Generated by Friction", Master of Science Thesis, Mechanical Engineering, Virginia Polytechnic Institute and State University, Blacksburg, Va., December, 1982.

APPENDICES

APPENDIX A

CALIBRATION OF THE BARNES INFRARED RADIOMETRIC MICROSCOPE

The following procedure was used to calibrate the infrared microscope.

1. An instrument warm-up period of approximately 30 minutes was allowed.
2. The infrared microscope was focused on the calibration heat source (shown in Fig.A-1) at ambient temperature and the voltage output was zeroed by adjusting the zero set control knob. The microscope control unit was adjusted to measure radiance according to the procedure in the instruction manual for the microscope (38). The radiation scale was set on *10X* and the voltage output was measured from the "recorder" output jack set on "HI" impedance. Note: For all radiance measurements, the adjustable ring on the *36X* objective must be set on *"0"*.
3. With the microscope positioned away from the aperture of the calibration heat source, the source was allowed to heat to a given temperature. The microscope was then positioned over the heat source and the voltage output was recorded.
4. Step (3) was repeated for each temperature setting. The resulting calibration curve is shown in Fig. A-2.

The listing of instrumentation is given in Table A-1.

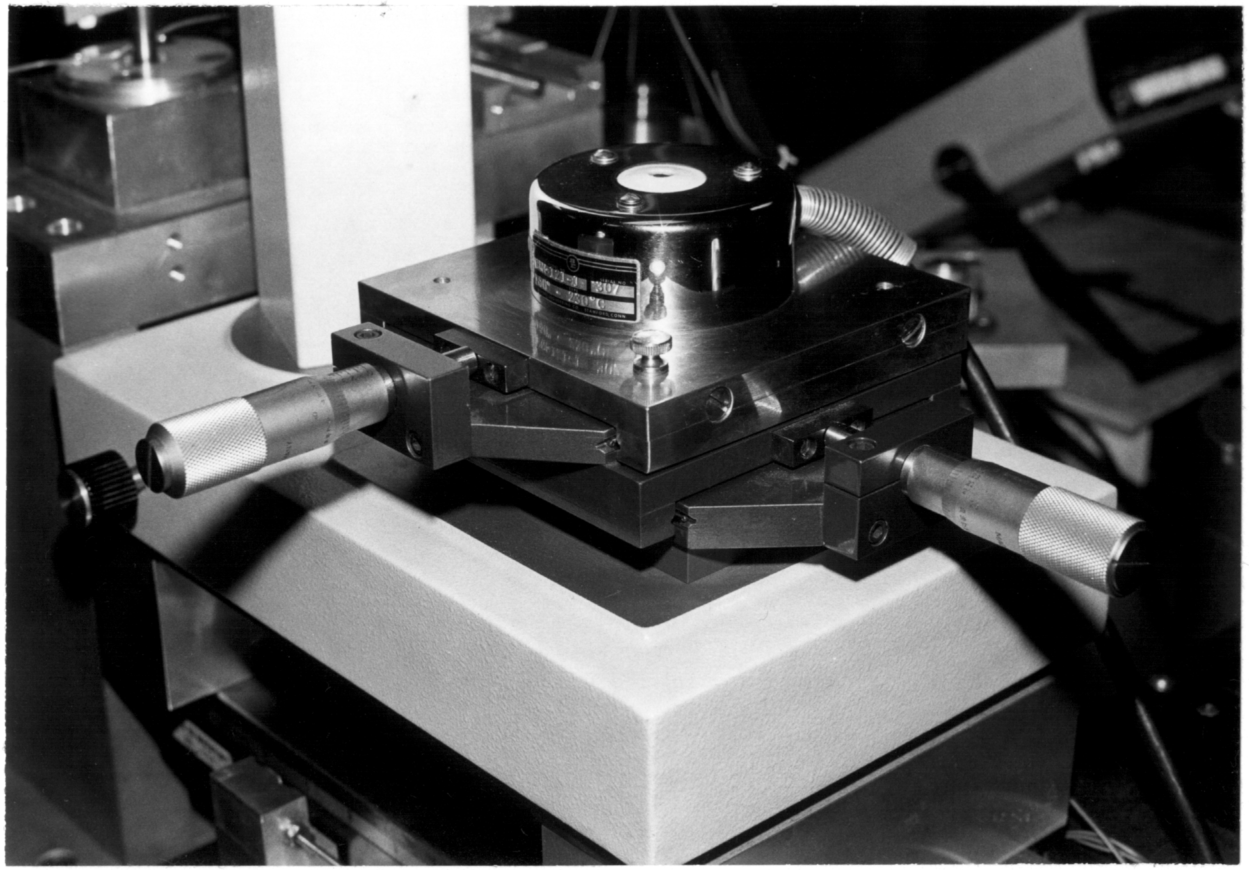

Figure A-1 Calibration Heat Source

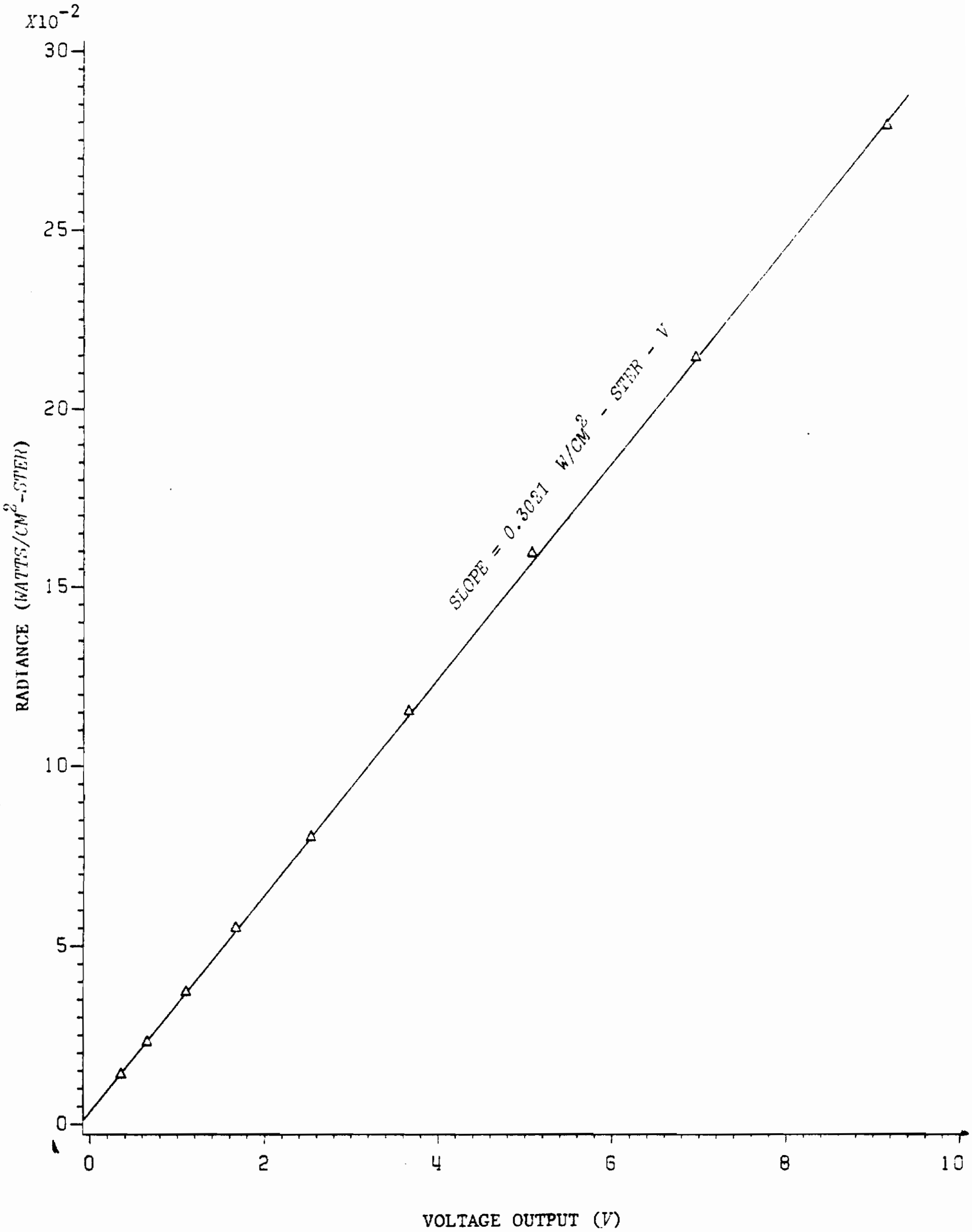

Figure A-2 Calibration Curve of RM-2A Infrared Microscope

TABLE A-1

INSTRUMENTATION

Barnes Infrared Radiometric Microscope
and Control Unit
Model RM-2A
Serial No. 421

Beck Reflecting Objective (*36X*)
Model RM-121
Serial No. 255

Calibration Heat Source and Controller
Model RM-121
Serial No. 307

Keithley Digital Multimeter
Model 168
Serial No. 31533

APPENDIX B

CALIBRATION OF THE LINEAR VARIABLE DIFFERENTIAL TRANSFORMER

The following procedure was used to calibrate the linear variable differential transformer (LVDT).

1. The LVDT was connected to a power supply adjusted to *20.0 V DC* output with the LVDT output connected to a digital voltmeter.
2. With the LVDT output initially set at *0.000* volts, the microscope assembly was displaced in definite increments by the precision *X-Y* table. The voltage output was recorded for each increment.
3. The above procedure was performed for both the tangential and radial LVDTs.
4. The calibration curve for the tangential LVDT and the radial LVDT are shown in Fig. B-1 and Fig. B-2 , respectively.

The listing of instrumentation is given in Table B-1.

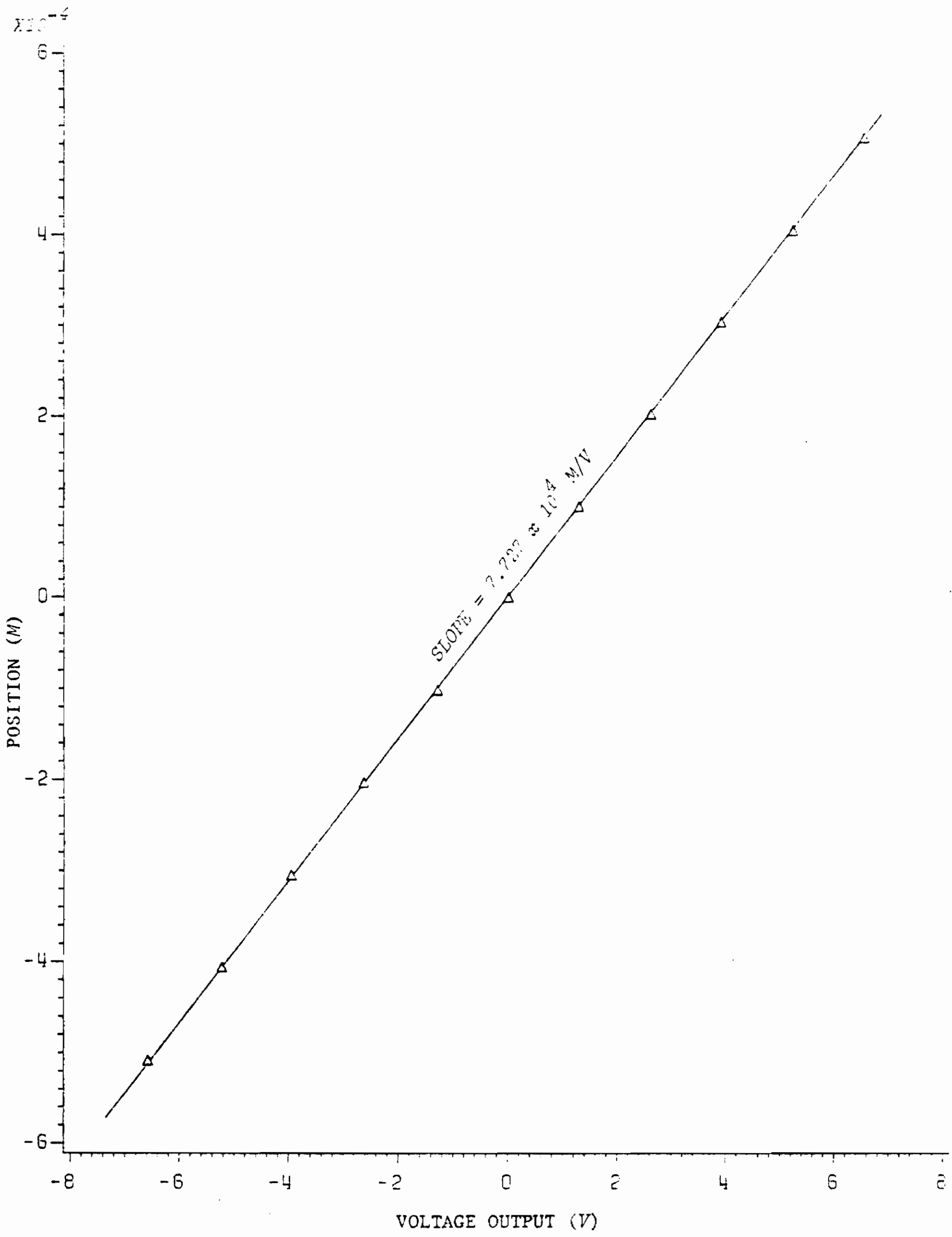

Figure B-1 Calibration Curve for Tangential LVDT

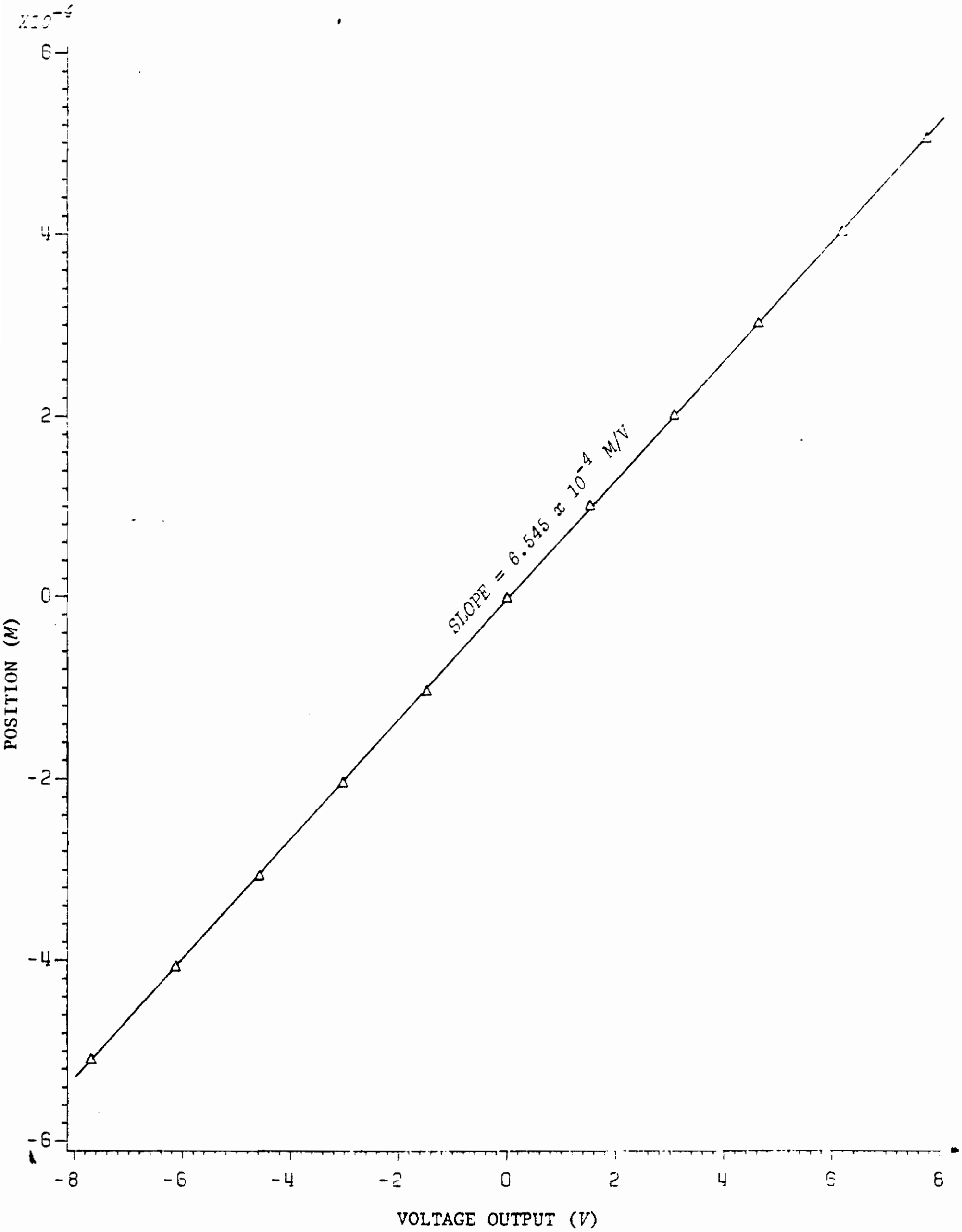

Figure B-2 Calibration Curve for Radial LVDT

TABLE B-1

INSTRUMENTATION

Schaevitz Linear Variable Differential Transformer

Model Type 100 HR-DC

Serial No. 1502

Hewlett-Packard Power Supply

Model 6218A

Serial No. 1148A04947

Keithley Digital Multimeter

Model 168

Serial No. 31533

APPENDIX C

CALIBRATION OF THE LEBOW TORQUE TRANSDUCER

The following procedure was used to calibrate the Lebow miniature torque transducer.

1. The provided calibration hardware which includes two sets of pulleys, a spacer block, an aluminum disk (*0.0508 m* in diameter) with screw, and clamp was installed as shown in Fig. C-1. The clamp prevents movement of the torque transducer's lower input shaft.
2. A length of nylon monofilament was attached to the screw positioned edgewise in the aluminum disk. A pan was attached at one end of the monofilament while a counterweight was attached at the other end.
3. With the monofilament positioned horizontally over the pulleys, lead shot was added until the pan weight was nulled. The transducer's output was *0.000* volts as measured by a digital voltmeter. Power was supplied by a *12V* battery with the voltage adjusted to *10.00 V* by a variable resistor. The output signal of the transducer was amplified *1000X*.
4. Laboratory weights were placed on the pan to produce a known applied torque to the transducer. To overcome the static friction between the slip rings and brushes, the brushes were opened then closed after each weight was added. The voltage output was recored for each torque value.
5. The calibration curve in Fig. C-2 was obtained showing the linear torque/voltage relationship.

The listing of instrumentation is given in Table C-1.

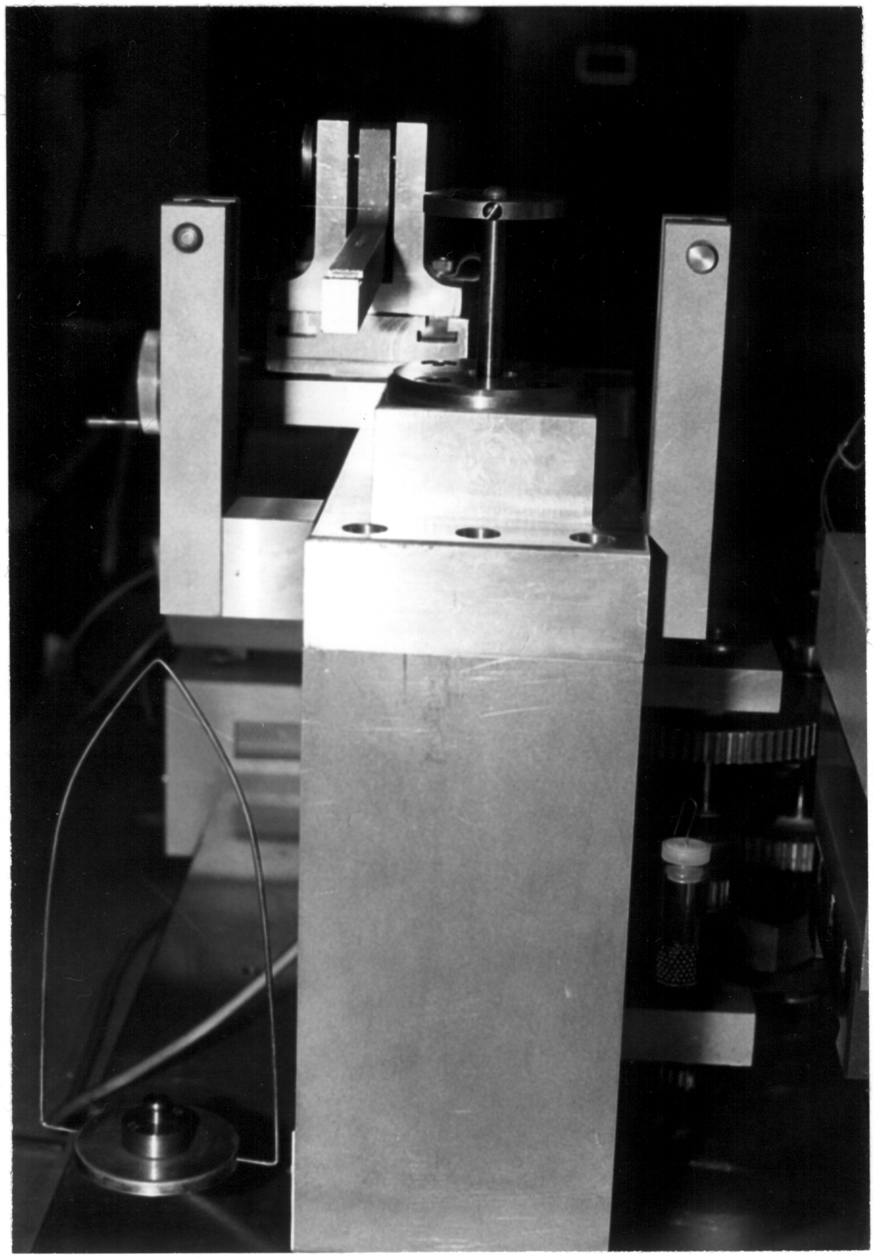

Figure C-1   Attachments for Calibrating Torque Transducer

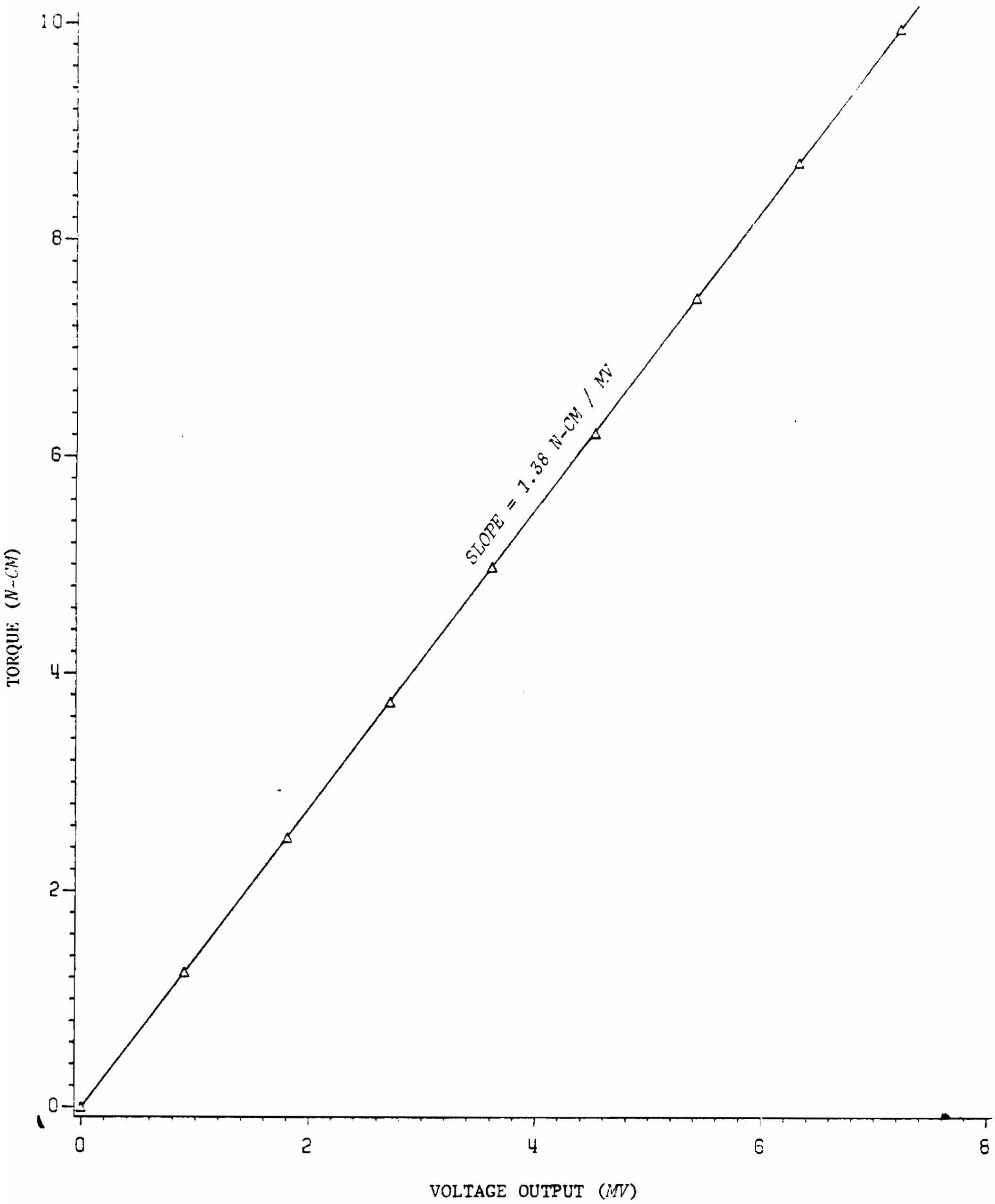

Figure C-2 Calibration Curve for Lebow Torque Transducer

TABLE C-1

INSTRUMENTATION

Lebow Miniature Rotary Torque Transducer

Model 1102-50

Serial No. 752

Keithley Digital Multimeter

Model 168

Serial No. 31533

Hewlett-Packard Amplifier

Model 2470A

Serial No. 553-00061

12 V Ray-O-Vac Battery

Model 922

APPENDIX D

CALCULATION OF THE COEFFICIENT OF FRICTION

The following procedure was used to derive the frictional coefficient from the torque transducer output.

1. The voltage output as recorded from the torque transducer during a test was converted to torque output by multiplying by the slope of the calibration curve (1.38×10^{-2} *N-m/mV*). The transducer signal was amplified by *1000X*, thus, the actual voltage recorded corresponds to millivolt output.
2. The inherent torque of the system (without an externally applied torque) was subtracted from the above recorded torque. This torque was measured prior to each test run and has been found to be dependent upon the rotational velocity of the torque transducer.
3. The resulting torque is that due to the sliding resistance of the specimen alone.
4. To calculate the frictional coefficient, the torque applied by the specimen was divided by both the applied normal load and the radial position of the specimen on the disk.

Example

A test was performed at *4.0 m/s* sliding velocity with a *1.0 N* normal load. The drive shaft was rotating at *188.5 rad/s*. The recorded voltage was *0.607 V*. The internal torque was measured to be 2.0×10^{-3} *N-m*.

The preceding method was followed.

1. Since the torque transducer signal was amplified by *1000X*, the actual transducer output was *0.607 mV*. Converting the output voltage to torque gives

   $$(0.607\ \mathrm{mV}) \times (1.38 \times 10^{-2}\mathrm{N\text{-}m/mV}) = 8.37 \times 10^{-3}\mathrm{N\text{-}m}.$$

2. Subtracting the internal torque results in

   $$(8.37 \times 10^{-3}\mathrm{N\text{-}m}) - (2.0 \times 10^{-3}\mathrm{N\text{-}m}) = 6.37 \times 10^{-3}\mathrm{N\text{-}m}.$$

3. Thus, the externally applied torque is $6.37 \times 10^{-3} N\text{-}m$.

4. The radial position of the specimen can be determined from the sliding velocity and the angular velocity. This is found to be

   $$(4.0\ \mathrm{m/s}) \ / \ (188.5\ \mathrm{rad/s}) = 2.122 \times 10^{-2}\mathrm{m}.$$

   Thus, the coefficient of friction is determined to be

   $$(6.37 \times 10^{-3}\mathrm{N\text{-}m}) \ / \ (1.0\mathrm{N} \times 2.122 \times 10^{-2}\mathrm{m}) = 0.30.$$

APPENDIX E

RADIANCE VERSUS TEMPERATURE CURVES

FOR BLACK EMITTER

(Reproduced from reference 38)

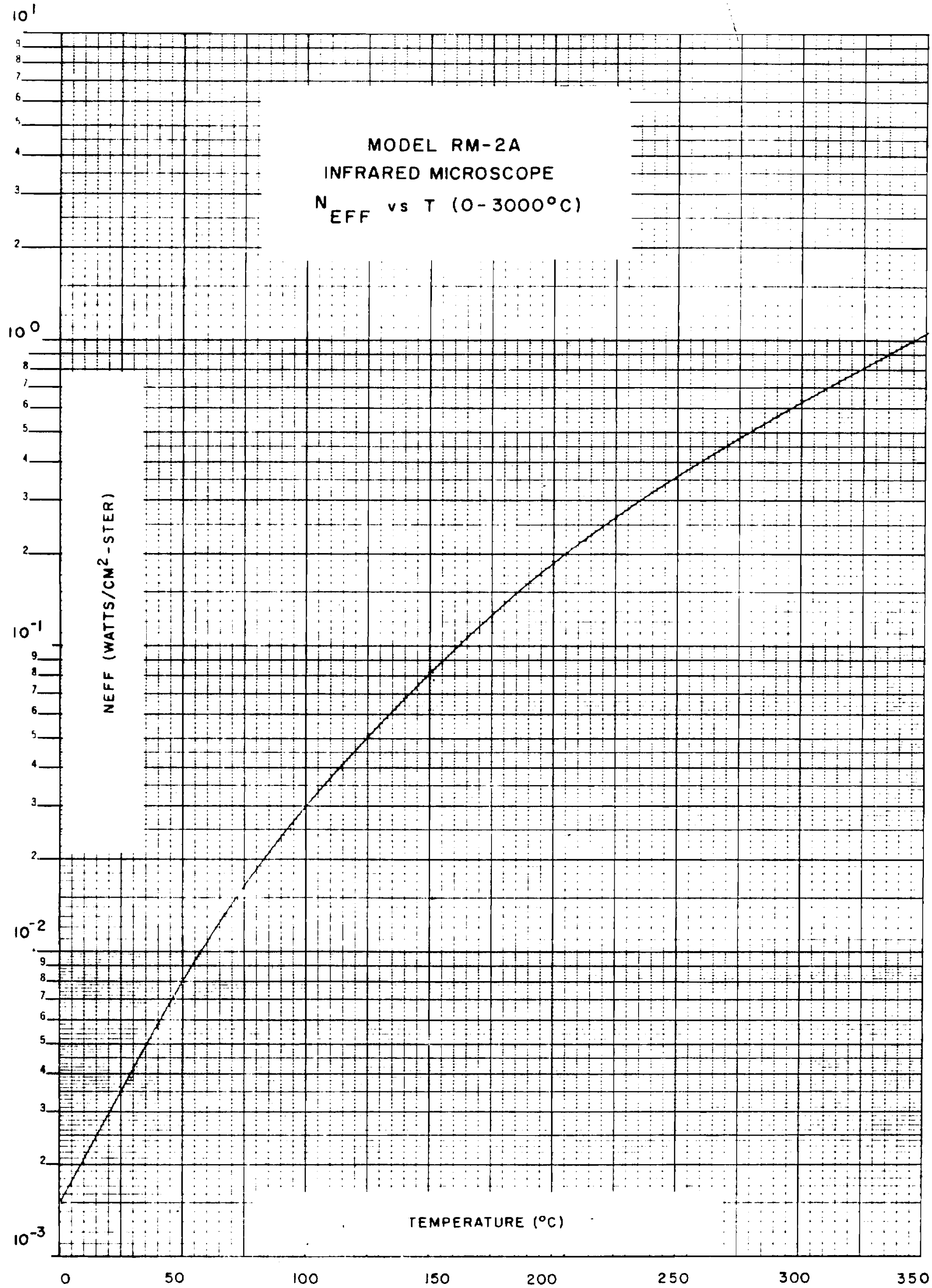
MODEL RM-2A
INFRARED MICROSCOPE
N_{EFF} vs T (0-3000°C)
NEFF (WATTS/CM^2-STER)
TEMPERATURE (°C)
10^1
10^0
10^{-1}
10^{-2}
10^{-3}
0
50
100
150
200
250
300
350

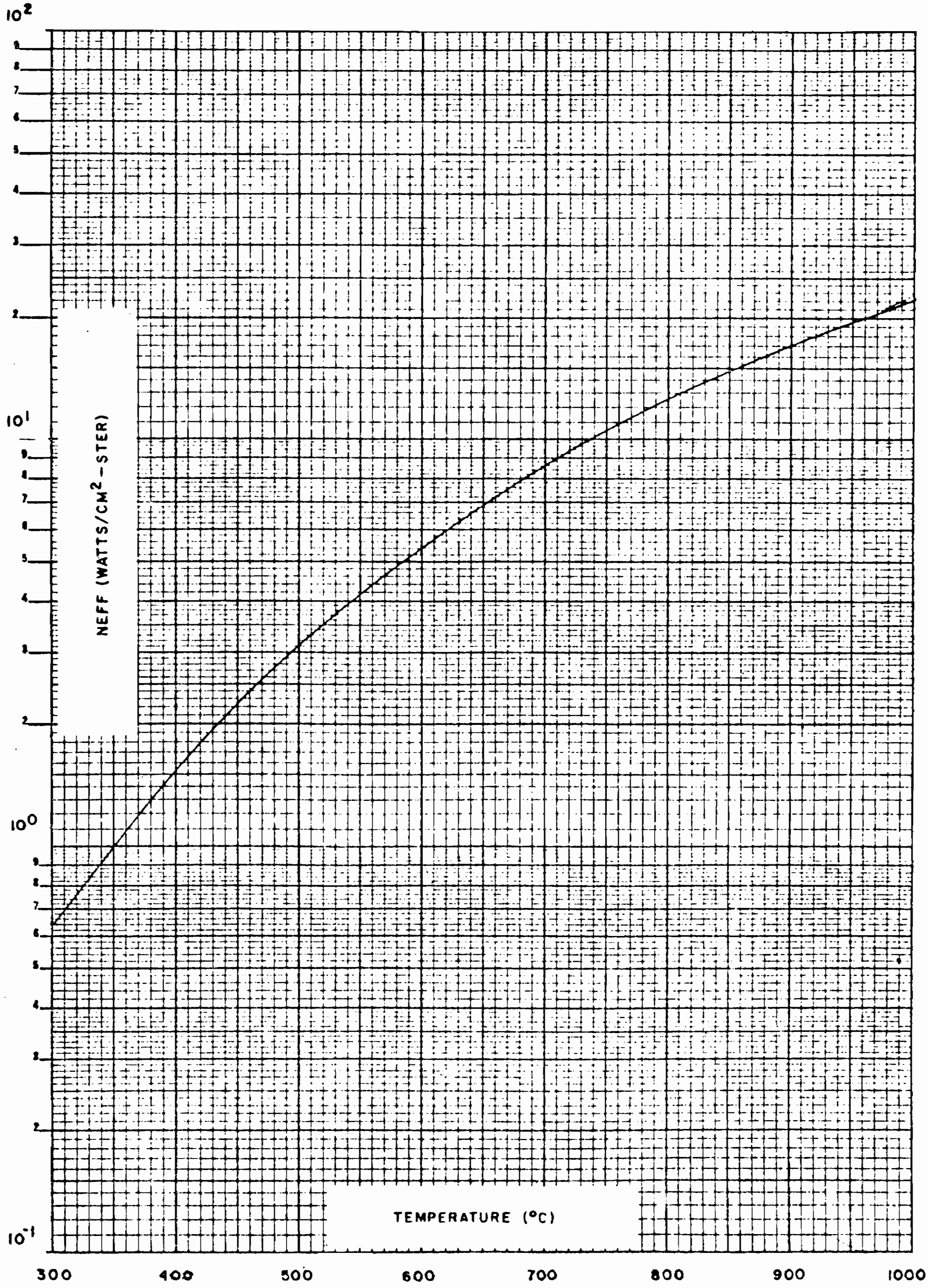
NEFF (WATTS/CM² - STER)
TEMPERATURE (°C)
10²
10¹
10⁰
10⁻¹
300
400
500
600
700
800
900
1000

APPENDIX F

CLEANING PROCEDURE FOR TEST SPECIMENS AND SAPPHIRE DISK

Test Specimens

The following procedure was used to clean the Armco iron test specimens:

1. The specimens were scrubbed with a paper towel saturated with a 4% concentrated solution of tri-sodium phosphate detergent in distilled water.
2. The specimens were rinsed with distilled water.
3. The remaining water was removed by a methanol rinse.
4. After drying by evaporation, the specimens were placed in clean glass containers and put in a desiccator.

Sapphire Disk

The following procedure was used to remove iron and iron oxide from the disk:

1. The disk was scrubbed with a cotton-tipped applicator saturated with diluted hydrochloric acid. When removal was difficult, the disk was immersed edge-wise in diluted hydrochloric acid. Acid contact with the resin epoxy was prevented.
2. The remaining acid was removed by rinsing with distilled water.
3. The disk was scrubbed with a paper towel saturated with a 4% concentrated solution of tri-sodium phosphate detergent.
4. Distilled water was used to remove the detergent.

5. The disk was then rinsed with methanol.
6. After drying by evaporation, the disk was placed in a clean container in a desiccator.

APPENDIX G

PROCEDURE FOR DETERMINING THE EMISSIVITY WITHIN THE WEAR AREA

The following procedure was used to measure the emissivity of any location in the wear area.

1. A specially designed heater for this purpose as shown in Fig.18 was placed on the microscope's substage and allowed to reach a steady temperature. The temperature was controlled by regulating the input voltage by a variable transformer and measured by a copper-constantan thermocouple.
2. After removing the heater cover, the test specimen was positioned as desired in the holder, adjusted to the same height as the black standard specimen, and held in place with a setscrew. The cover was replaced quickly to minimize heat loss.
3. Equilibrium was allowed to be reached.
4. The infrared microscope output was zeroed by focusing on the black calibration heat source at ambient temperature. The output voltage was measured by a digital voltmeter.
5. The microscope was focused on the black standard specimen and the output voltage was recorded.
6. The microscope was then focused on a predetermined reference point on the wear area of the specimen. The X and Y position of the specimen as measured by the substage micrometers was recorded.

7. The specimen was displaced by definite increments relative to the reference point with the microscope output voltage being recorded at each position. The output voltage from the microscope was amplified.
8. Since the microscope was zeroed at ambient temperature, the emissivity was determined as the ratio of the voltage measured from the specimen to that from the black standard.

The listing of instrumentation is given in Table G-1.

TABLE G-1

INSTRUMENTATION

Barnes Infrared Radiometric Microscope
and Control Unit
Model RM-2A
Serial No. 412

Beck Reflecting Objective (*36X*)
Model RM-163
Serial No. 255

Heater for Emissivity Measurements
Model Special

Powerstat Variable Transformer
Model S649

Calibration Heat Source
Model RM-121
Serial No. 307

Keithley Digital Multimeter
Model 168
Serial No. 31533

Dynamics Amplifier

Model 7521B 7914D/NR

Serial No. 3124

APPENDIX H

COMPUTER PROGRAM FOR CONVERTING INFRARED MICROSCOPE VOLTAGE OUTPUT TO RADIANCE AND TEMPERATURE

```
      REAL IR,NS,NO
C
C *****************************************************************
C *****************************************************************
C
C                 ***CONVERSION OF INFRARED MICROSCOPE
C                 VOLTAGE OUTPUT TO BLACKBODY RADIANCE
C              EMITTED FROM THE SPECIMEN AND TEMPERATURE ***
C
C *****************************************************************
C
C    THIS PROGRAM CONVERTS THE VOLTAGE OUTPUT FROM
C    THE BARNES MODEL RM-2A INFRARED RADIAMETRIC
C    MICROSCOPE TO EFFECTIVE BLACKBODY RADIANCE
C    EMITTED FROM THE SPECIMEN AND ITS TEMPERATURE.
C    INPUT PARAMETERS NEEDED ARE THE EXPERIMENTALLY
C    DETERMINED EMISSIVITY, THE VOLTAGE OUTPUT OF THE
C    MICROSCOPE AND THE GAIN SETTING OF ANY EXTERNAL
C    AMPLIFIER.  THE OUTPUT CONTAINS THE FRESNEL
C    REFLECTION COEFFICIENT, THE EMISSIVITY OF THE
C    SPECIMEN, THE SPECIMEN SURFACE REFLECTIVITY AND
C    THE ATTENUATION FACTORS OF BOTH THE AMBIENT RADIATION
C    AND THAT EMITTED FROM THE SPECIMEN.  PROGRAM
C    WRITTEN BY C.A. ROGERS.
C
C *****************************************************************
C
      DIMENSION ANAME(10),VOLT(20),EMISS(20),RADINT(250),TAU(250)
C
C *****************************************************************
C
C    READS THE POWER OF THE MICROSCOPE
C    OBJECTIVE USED WHERE:
C       OBJ = MICROSCOPE OBJECTIVE
C               (36X OR 15X)
C
C *****************************************************************
C
      READ (5,5) OBJ
5     FORMAT(F3.0)
C
C *****************************************************************
C
C    READS THE DATA FROM DATA CARD
C    NUMBER 2 WHERE:
C         ANAME = SPECIMEN MATERIAL
C         GAIN  = EXTERNAL AMPLIFIER GAIN
C         AMB   = AMBIENT RADIATION (M/CM-STER)
C
C *****************************************************************
C
      READ (5,10) (ANAME(I),I=1,10),GAIN,AMB
10    FORMAT (10A1,F6.1,F9.7,F5.3)
C
C *****************************************************************
```

```
C
C   READS THE DATA FROM DATA CARD
C   NUMBER 3 WHERE:
C           NE = NUMBER OF EMISSIVITIES TO BE EVALUATED
C           NV = NUMBER OF VOLTAGES TO BE EVALUATED
C
C ******************************************************************
C
      READ (5,20) NE,NV
20    FORMAT (2I3)
      WRITE (6,30)
      WRITE (6,40)
      WRITE (6,50)
      WRITE (6,30)
30    FORMAT('*****************************************************'/)
40    FORMAT(1H1,10X,'CALCULATION OF THE EMITTED BLACKBODY')
50    FORMAT(15X,'RADIATION FROM THE SPECIMEN'/)
C
C ******************************************************************
C
C   READS THE DATA FROM CARD
C   NUMBER 4 WHERE:
C       EMISS = EMISSIVITY OF THE SPECIMEN SURFACE
C
C ******************************************************************
C
      READ (5,60) (EMISS(I),I=1,NE)
C
C ******************************************************************
C
C   READS THE DATA FROM DATA
C   CARD NUMBER 5 WHERE:
C       VOLT = VOLTAGE OUTPUT FROM MICROSCOPE AND ANY
C                 EXTERNAL AMPLIFIER
C
C ******************************************************************
C
      READ (5,60) (VOLT(I),I=1,NV)
60    FORMAT (20F6.3)
C
C ******************************************************************
C
C   THIS DO-LOOP EVALUATES EACH EMISSIVITY
C   FOR EVERY VOLTAGE OUTPUT IN THE DATA
C
C ******************************************************************
C
      DO 120 I=1,NE
      WRITE (6,70)
70    FORMAT (///)
C
C ******************************************************************
C
C   THIS EXPRESSION EVALUATES THE SURFACE
C   REFLECTIVITY OF THE SPECIMEN AS
```

```
C    (1-EMISSIVITY) WHERE:
C          SURF = SURFACE REFLECTIVITY
C
C ******************************************************************
C
       SURF=1.0-EMISS(I)
C
C ******************************************************************
C
C    THE NEXT DECLARATION SETS THE INDEX
C    OF REFRACTION TO A GIVEN VALUE WHERE:
C          IR = INDEX OR REFRACTION OF THE SAPPHIRE
C
C ******************************************************************
C
       IR=1.65
C
C
C ******************************************************************
C
C    THE NEXT EXPRESSION CALCULATES THE
C    FRESNEL REFLECTION COEFFICIENT FROM
C    THE INDEX OF REFRACTION GIVEN ABOVE
C
C ******************************************************************
C
       FRES=(IR-1.0)**2/((IR+1.0)**2)
C
C ******************************************************************
C
C    THE NEXT SECTION CALCULATES THE
C    INTERNAL TRANSMISSIVITY BASED ON THE
C    DECLARED INDEX OF REFRACTION AND THE
C    EXPERIMENTALLY DETERMINED EXTERNAL
C    TRANSMITTANCE WHERE:
C          EXTER = EXTERNAL TRANSMITTANCE
C          TRANS = INTERNAL TRANSMISSIVITY
C
C ******************************************************************
C
       EXTER=0.8539
       TRANS=EXTER/((1-FRES)/(1+FRES))
C
C ******************************************************************
C
C    THIS SECTION CREATES A TABLE OF IMPORTANT
C    DATA FOR EACH NEW EMISSIVITY EVALUATED
C
C ******************************************************************
C
       WRITE (6,80) EMISS(I),IR,SURF,FRES,TRANS,GAIN,OBJ
80     FORMAT (1X,'EMISSIVITY OF THE SPECIMEN       ',F6.4/1X,
     2            'INDEX OF REFRACTION              ',F6.4/1X,
     3            'SPECIMEN REFLECTIVITY            ',F6.4/1X,
     4            'FRESNEL REFLECTION               ',F6.4/1X,
```

```
     5              'INTERNAL TRANSMISSIVITY          ',F6.4/1X,
     6              'AMPLIFIER GAIN                  ',F4.0/1X,
     7              'MICROSCOPE OBJECTIVE             ',F3.0,'X'///)
      WRITE (6,90)
90    FORMAT(1X,'VOLTAGE',4X,'SPECIMEN',8X,'AMBIENT',6X,'AMBIENT',
     1 8X,'SPECIMEN',6X,'SPECIMEN'/1X
     2'OUTPUT',4X,'ATTENUATION',4X,'ATTENUATION',3X,'RADIATION',7X,
     3'BLACKBODY',3X,'TEMPERATURE',/13X,
     3'FACTOR',9X,'FACTOR',22X,'RADIATION',6X,'DEG. C',/1X
     4'-------------------------------------------------------------
     5------------'/)
C
C *******************************************************************
C
C   THIS DO-LOOP CONVERTS EVERY VOLTAGE
C   OUTPUT TO BLACKBODY RADIANCE OF THE
C   SPECIMEN WITH THE EMISSIVITY
C   DETERMINED BY THE OUTSIDE DO-LOOP
C
C *******************************************************************
C
      DO 110 J=1,NV
C
C *******************************************************************
C
C   CONVERTS THE VOLTAGE OUTPUT TO
C   RADIANCE WHERE:
C        0.312 = THE CALIBRATION CONSTANT FOR THE
C                     MICROSCOPE WITH A 36X OBJECTIVE
C        0.171 = THE CALIBRATION CONSTANT FOR THE
C                     MICROSCOPE WITH A 15X OBJECTIVE
C
C *******************************************************************
C
      IF(OBJ.EQ.15.)CAL=.171
      IF(OBJ.EQ.36.)CAL=.312
      VOUT=VOLT(J)*CAL/GAIN
C
C *******************************************************************
C
C   THE NEXT SECTION CALCULATES THE FRACTION
C   OF SPECIMEN AND AMBIENT RADIATION THAT
C   IMPINGES ON THE INFRARED DETECTOR;I.E.
C        REFLS1 = FRACTION OF SPECIMEN RADIATION DUE
C                     TO REFLECTION NUMBER 1
C        REFLA3 = FRACTION OF AMBIENT RADIATION DUE
C                     TO REFLECTION NUMBER 3
C
C *******************************************************************
C
      REFLS1=(1-FRES)*TRANS
      REFLS2=(1-FRES)*SURF*FRES*(TRANS**3)
      REFLA1=FRES
      REFLA2=(1-FRES)**2*SURF*(TRANS**2)
      REFLA3=(1-FRES)**2*(SURF**2)*FRES*(TRANS**4)
```

```
C
C ********************************************************************
C
C   THE ATTENUATION FACTORS ARE THE SUM OF
C   THE APPROPRIATE REFLECTION FRACTIONS WHERE:
C       NO = AMBIENT ATTENUATION FACTOR
C       NS = SPECIMEN ATTENUATION FACTOR
C
C ********************************************************************
C
      NS=REFLS1+REFLS2
      NO=REFLA1+REFLA2+REFLA3
C
C ********************************************************************
C
C   THE NEXT EXPRESSION CALCULATES THE BLACK-
C   BODY RADIANCE EMITTED FROM THE
C   SPECIMEN WHERE:
C        RAD = BLACKBODY RADIANCE
C
C ********************************************************************
C
      RAD=(VOUT+AMB-(NO*AMB))/(EMISS(I)*NS)
C
C ********************************************************************
C
C   THE NEXT STATEMENT GIVES THE FOLLOWING
C   SUBROUTINE TEMPER, AN INITIAL GUESS OF
C   THE TEMPERATURE OF THE SPECIMENS.
C
C ********************************************************************
C
      TEMP=10.
C
C ********************************************************************
C
C   SUBROUTINE TEMPER CALCULATES THE
C   SPECIMEN TEMPERATURE
C
C ********************************************************************
C
      CALL TEMPER(RAD,TEMP,TEMPC,DLMDA,TAU,ICOUN)
      WRITE(6,100) VOLT(J),NS,NO,AMB,RAD,TEMPC
100   FORMAT (2X,F6.3,5X,F7.3,8X,F7.3,3X,2(E12.4,5X),F7.2)
110   CONTINUE
120   CONTINUE
      WRITE (6,130)
130   FORMAT (1H1)
C
C ********************************************************************
C
C   SUBROUTINE RESPON PLOTS THE SPECTRAL
C   RESPONSE CURVE USED IN THE CALCULATION
C   OF TEMPERATURE
C
```

```
C *******************************************************************
C
      CALL RESPON(TAU,DLMDA,ICOUN)
      STOP
      END
C
C
C
C
C *******************************************************************
C *******************************************************************
C *******************************************************************
C
C                        SUBROUTINE TEMPER
C
C   SUBROUTINE TEMPER TAKES THE EXPERIMENTAL SPECIMEN EFFECTIVE
C   BLACKBODY RADIANCE AND THEN CALCULATES THE CORRESPONDING
C   TEMPERATURE. THIS IS DONE BY GUESSING A TEMPERATURE AND THEN
C   CALCULATING THE MONOCHROMATIC BLACKBODY RADIANT INTENSITY FOR
C   THE BANDWIDTH OF THE MICROSCOPE. THE RADIANT INTENSITIES ARE
C   THEN MULTIPLIED BY THE SPECTRAL RESPONSE OF THE MICROSCOPE.
C   BY NUMERICAL INTEGRATION THE AREA UNDER THIS CURVE IS CALCULATED
C   AND REPRESENTS THE ACTUAL RADIATION RECEIVED BY THE MICROSCOPE.
C   THIS VALUE IS CORRECTED FOR THE ELECTRICAL CONSTANTS AFFECTING
C   THE OUTPUT AND THEN COMPARED WITH EXPERIMENTAL VALUE. AN
C   ITERATIVE PROCESS IS USED TO CONVERGE TO THE PROPER TEMPERATURE.
C
C
C *******************************************************************
C *******************************************************************
C *******************************************************************
C
C
      SUBROUTINE TEMPER(RAD,TEMP,TEMPC,DLMDA,TAU,ICOUN)
      DIMENSION RADINT(250),TAU(250),X(250),Y1(250),Y2(250),WAVE(250)
      DIMENSION RADI(250),RADY(250)
      TEMPK=TEMP+273.
1     DLMDA=0.022
      WAV=1.6-DLMDA
      ICOUN=0
C
C *******************************************************************
C
C   THE NEXT SECTION CALCULATES THE NORMALIZED
C   SPECTRAL RESPONSE OF THE MICROSCOPE FOR A GIVEN
C   WAVELENGTH, WHERE:
C         TTAU=NORMALIZED SPECTRAL RESPONSE
C         TAU=MATRIX CONTAINING TTAU
C
C *******************************************************************
C
2     ICOUN=ICOUN+1
      WAV=WAV+DLMDA
      IF(WAV.GT.6.2) GO TO 3
      IF(WAV.GE.1.6.AND.WAV.LT.2.0) TTAU=.75*WAV-1.2
```

```
      IF(WAV.GE.2.0.AND.WAV.LT.2.2) TTAU=-.10*WAV+.50
      IF(WAV.GE.2.2.AND.WAV.LT.2.4) TTAU=0.0375*WAV+.1975
      IF(WAV.GE.2.4.AND.WAV.LT.2.6) TTAU=.1125*WAV+0.0175
      IF(WAV.GE.2.6.AND.WAV.LT.2.8) TTAU=.20*WAV-.21
      IF(WAV.GE.2.8.AND.WAV.LT.3.0) TTAU=.25*WAV-.35
      IF(WAV.GE.3.0.AND.WAV.LT.3.2) TTAU=.30*WAV-.50
      IF(WAV.GE.3.2.AND.WAV.LT.3.4) TTAU=.425*WAV-.90
      IF(WAV.GE.3.4.AND.WAV.LT.4.2) TTAU=.375*WAV-.73
      IF(WAV.GE.4.2.AND.WAV.LT.4.8) TTAU=.225*WAV-.10
      IF(WAV.GE.4.8.AND.WAV.LT.5.0) TTAU=.10*WAV+.50
      IF(WAV.GE.5.0.AND.WAV.LT.5.2) TTAU=-.60*WAV+4
      IF(WAV.GE.5.2.AND.WAV.LT.5.4) TTAU=-1.30*WAV+7.64
      IF(WAV.GE.5.4.AND.WAV.LT.5.6) TTAU=-2.35*WAV+13.31
      IF(WAV.GE.5.6.AND.WAV.LT.5.8) TTAU=-.45*WAV+2.67
      IF(WAV.GE.5.8.AND.WAV.LT.6.0) TTAU=-.25*WAV+1.51
      IF(WAV.GE.6.0.AND.WAV.LT.6.2) TTAU=-.05*WAV+.31
      TAU(ICOUN)=TTAU
      WAVE(ICOUN)=WAV
      GO TO 2
C
C ***********************************************************************
C
C   THE FOLLOWING SECTION CALCULATES THE
C   MONOCHROMATIC BLACKBODY RADIANT INTENSITY
C   IN WATTS/CM**2-STER
C
C ***********************************************************************
C
3     CONTINUE
      ICOUN=ICOUN-1
      WAV=1.6-DLMDA
      DO 7 I=1,ICOUN
      A=14388/(WAV*TEMPK)
      IF(A-86.)4,4,5
4     RADI(I)=((11909/WAV**5)*(1./(EXP(A)-1.)))
      RADINT(I)=((11909/WAV**5)*(1/(EXP(A)-1.)))*TAU(I)
      RADY(I)=RADINT(I)
      GO TO 6
C
C ***********************************************************************
C
C   THE FOLLOWING SECTION CALCULATES THE TOTAL
C   BLACKBODY RADIANT INTENSITY BY USING
C   SIMPSON'S RULE OF NUMERICAL INTEGRATION
C
C ***********************************************************************
C
5     RADINT(I)=0.0
      RADY(I)=0.0
      RADI(I)=0.0
6     WAV=WAV+DLMDA
7     CONTINUE
      RADF=RADINT(1)+RADINT(ICOUN)
      EVEN=0.0
      ODD=0.0
```

```
      M=ICOUN-1
      DO 8 K=2,M,2
      ODD=RADINT(K)+ODD
8     CONTINUE
      L=ICOUN-2
      DO 9 K=3,L,2
      EVEN=RADINT(K)+EVEN
9     CONTINUE
      EFRAD=(DLMDA/3.0)*(RADF+4.0*ODD+2.0*EVEN)
C
C ********************************************************************
C
C    THE NEXT STATEMENT CONVERTS THE ACTUAL RADIANCE
C    TO THAT READ BY THE MICROSCOPE DUE TO THE
C    MICROSCOPE'S ELECTRICAL SYSTEM (PER CONVERSATION
C    WITH NELSON ENGBORG OF BARNES ENGINEERING CO.)
C
C ********************************************************************
C
      EFFRAD=EFRAD*13.50
      TEMPC=TEMPK-273.
C
C ********************************************************************
C
C    THIS SECTION PERFORMS THE ITERATION OF THE
C    TEMPERATURE TO CONVERGENCE. CONVERGENCE IS
C    ACHEIVED WHEN THE CALCULATED RADIANCE EQUALS
C    THE EXPERIMENTAL RADIANCE + OR - 1.5 PERCENT.
C    AN ERROR RANGE LESS THAN THIS CAUSES NO
C    CONVERGENCE FOR SOME TEMPERATURES BECAUSE THE
C    TEMPERATURE IS INCREMENTED IN WHOLE NUMBERS AND
C    THE RADIANCE CHANGES LESS THAN THE ERROR
C
C ********************************************************************
C
      IF(TEMPC.LT.160.) GO TO 22
      ERROR=RAD*0.0075
      GO TO 33
22    ERROR=RAD*.0200
33    CONTINUE
      HIGH=EFFRAD-RAD
      ELOW=RAD-EFFRAD
      IF(HIGH.GT.ERROR) GO TO 10
      IF(ELOW.GT.ERROR) GO TO 11
      GO TO 12
10    TEMPK=TEMPK-1.
      GO TO 1
11    TEMPK=TEMPK+10.
      GO TO 1
12    CONTINUE
      CALL INTENT(WAVE,RADY,RADI,ICOUN,TEMPC)
      RETURN
      END
C
C
```

APPENDIX I

SURFACE TEMPERATURE CALCULATION

COMPUTER PROGRAM

```
      REAL KB,KC,MU,LE,LP,L,N,JE,JP,JAVG,NUM
C
C *******************************************************************
C *******************************************************************
C
C
C           ***SURFACE TEMPERATURE CALCULATION PROGRAM***
C
C             THIS PROGRAM CALCULATES SURFACE TEMPERATURES
C             GENERATED BY FRICTION USING BOTH ARCHARD'S
C             AND JAEGERS'S MEAN TEMPERATURE THEORIES.
C             THE TEMPERATURES ARE CALCULATED BY ASSUMING
C             PLASTIC AND ELASTIC DEFORMATION WHICH DETERMINES
C             CONTACT AREA.
C
C
C             THIS PROGRAM WAS WRITTEN BY CRAIG A. ROGERS.
C             REVISED BY STEVE C. MOYER (SEPT. 1982).
C
C
C *******************************************************************
C *******************************************************************
C
C
C
C *******************************************************************
C
C             THE FOLLOWING STATEMENT CREATES A MATRIX
C             WHICH HOLDS THE NAMES OF THE MATERIALS
C             WHICH ARE TO BE READ FROM DATA CARDS.
C
C *******************************************************************
C
      DIMENSION X(100),Y1(100),Y2(100),BNAME(10), CNAME(10)
      READ(5,10) (BNAME(I),I=1,3),EB,RHOB,CB,KB,PMB,TMB,POISB
      READ(5,10) (CNAME(I),I=1,3),EC,RHOC,CC,KC,PMC,TMC,POISC
10    FORMAT(3A4,7F9.7)
C
C *******************************************************************
C
C     THE FOLLOWING SECTION CREATES THE TITLE
C     AND MATERIAL PROPERTY TABLE WHERE:
C          EB,EC=MODULUS OF ELASTICITY OF THE TWO BODIES
C          RHOB,RHOC=DENSITY OF THE TWO BODIES
C          CB,CC=SPECIFIC HEAT OF THE TWO BODIES
C          KB,KC=THERMAL CONDUCTIVITY OF THE TWO BODIES
C          PMB,PMC=HARDNESS OR FLOW STRENGTH
C          TMB,TMC=MELTING POINT OF THE TWO BODIES
C          POISB,POISC=POISSON'S RATIO OF THE TWO BODIES
C
C *******************************************************************
C
      WRITE (6,270)
      WRITE(6,22)
      WRITE(6,20)
```

```
      WRITE(6,22)
20    FORMAT(20X,'CALCULATION OF SURFACE TEMPERATURES'//)
22    FORMAT(14X,'**********************************************'/)
      WRITE(6,40)
      WRITE(6,30)
30    FORMAT(1H+,30X,'__________',5X,'__________'/)
40    FORMAT(1H ,28X,'    SPHERE',5X,'     PLANE')
      WRITE(6,50)(BNAME(I),I=1,3),(CNAME(I),I=1,3),EB,EC,RHOB,RHOC,CB,
     2 CC,KB,KC,PMB,PMC,TMB,TMC,POISB,POISC
50    FORMAT(1X,'MATERIAL                          ',3A4,5X,3A4/1X,
     2         'MODULUS OF ELASTICITY(N/M**2)  ',1PE10.4,5X,1PE10.4/1X,
     3         'DENSITY(KG/M**3)               ',1PE10.4,5X,1PE10.4/1X,
     4         'SPECIFIC HEAT(JOULES/KG-C)     ',1PE10.4,5X,1PE10.4/1X,
     5         'CONDUCTIVITY(JOULES/SEC-M-C)   ',1PE10.4,5X,1PE10.4/1X,
     6         'HARDNESS(N/M**2)               ',1PE10.4,5X,1PE10.4/1X,
     7         'MELTING POINT(C)               ',1PE10.4,5X,1PE10.4/1X,
     8         'POISSONS RATIO                 ',1PE10.4,5X,1PE10.4/)
C
C ******************************************************************
C
C     FROM THE DATA:  THE NORMAL LOAD,WT (NEWTONS),THE
C     COEFFICIENT OF FRICTION, MU, AND THE RADIUS OF
C     THE SPECIMEN,R (METERS), IS READ.
C
C ******************************************************************
C
60    READ(5,70) WT,MU,R
      K=1
      IF (WT.EQ.0.0) GO TO 260
      I=0
70    FORMAT(3F10.5)
      WRITE(6,80)WT,MU,R
80    FORMAT(//' LOAD =',F6.2,' N',5X,'COEFF. OF FRICTION =',F5.3,
     2   5X,' RADIUS = ',1PE12.6,'  M'//)
C
C ******************************************************************
C
C     CALCULATES THE RADIUS OF THE ELASTIC AREA
C     OF CONTACT, AE.
C
C            AP2=PLASTIC AREA OF CONTACT
C            AE2=ELASTIC AREA OF CONTACT
C
C ******************************************************************
C
      AE=((((1.-POISB*POISB)/EB)+((1.-POISC*POISC)/EC))*.75*WT*R)**.33333
C
C ******************************************************************
C
C     DETERMINES THE HARDEST MATERIAL AND THEN USES
C     ITS HARDNESS IN THE PLASTIC DEFORMATION THEORY
C
C ******************************************************************
C
      PM=PMC
```

```
      IF(PMC.GT.PMB) PM=PMB
      AP=SQRT(WT/(3.14159*PM))
      AP2=WT/PM
      AE2=3.14159*AE*AE
      WRITE(6,90) AE2,AP2
90    FORMAT(1X,'ELASTIC AREA OF CONTACT =',1PE12.4,' M**2'//1X,
     2          'PLASTIC AREA OF CONTACT =',1PE12.4,' M**2'/)
C
C *****************************************************************
C
C     DETERMINES THE MATERIAL WITH THE
C     LOWEST MELTING POINT. THE PROGRAM
C     WILL STOP WHEN IT CALCULATES A
C     TEMPERATURE GREATER THAN THIS MELTING
C     POINT
C
C *****************************************************************
C
      IF(TMB.GT.TMC)TM=TMC
      IF(TMC.GE.TMB)TM=TMB
C
C *****************************************************************
C
C      DIF EQUALS THE THERMAL DIFFUSIVITY
C
C *****************************************************************
C
      DIF=KC/(RHOC*CC)
      V=0.
      WRITE(6,100)
100   FORMAT(43X,'ARCHARDS THEORY',5X,'JAEGERS THEORY'/23X,
     2'PECLET NUMBER',15X,'TEMPERATURE RISE (C)'//1X,
     3'SLIDING SPEED(M/S)',3X,'ELASTIC',3X,'PLASTIC',3X,'ELASTIC',
     43X,'PLASTIC',3X,'ELASTIC',3X,'PLASTIC'/)
C
C *****************************************************************
C
C      INCREMENTS THE VELOCITY BY 0.2 M/S.
C
C *****************************************************************
C
110   IF(V.GT.9.9 ) GO TO 250
      V = V+0.2
C
C *****************************************************************
C
C      CALCULATES THE PECLET NUMBER FOR THE ELASTIC
C      AND PLASTIC AREA OF CONTACT.
C
C              LE=PECLET NUMBER USING ELASTIC DEFORMATION
C              LP=PECLET NUMBER USING PLASTIC DEFORMATION
C
C *****************************************************************
C
170   LE=V*AE/(2.*DIF)
```

```
      LP=V*AP/(2.*DIF)
C
C ********************************************************************
C
C      CALCULATES THE HEAT INPUT TO THE SYSTEM
C
C           Q=HEAT INPUT
C
C ********************************************************************
C
      Q=MU*WT*V
C
C ********************************************************************
C
C     DETERMINES WHICH OF THE THREE EQUATIONS
C     SHOULD BE USED BASED ON THE SPEED CRITERION
C     OR THE PECLET NUMBER.
C
C ********************************************************************
C
180   IFLAG=1
      IF (LP.LT..1) GO TO 220
      IF (LP.GT.5.) GO TO 230
      IF (LP.GE..1.AND.LP.LE.5.) GO TO 240
190   IFLAG=2
      IF (LE.LT..1) GO TO 220
      IF (LE.GT.5.) GO TO 230
      IF (LE.GE..1.AND.LE.LE.5.) GO TO 240
200   WRITE(6,210) V,LE,LP,TME,TMP,JE,JP
210   FORMAT(6X,F7.3,7X,F8.4,3X,F7.4,4(4X,F6.1))
      K=K+1
      X(K)=V
      Y1(K)=JP
      Y2(K)=TMP
      GO TO 110
C
C ********************************************************************
C
C      CALCULATES THE SURFACE TEMPERATURE WHEN
C      L IS LESS THAN 0.1 USING THE SLOW SPEED
C      EQUATIONS
C
C ********************************************************************
C
220   IF(IFLAG.EQ.1) RAD=AP
      IF(IFLAG.EQ.2) RAD=AE
C
C ********************************************************************
C
C       TAVG IS THE MEAN TEMPERATURE ACROSS
C         THE HEAT SOURCE USING ARCHARD'S EQUATION
C       JAVG IS THE MEAN TEMPERATURE USING
C         JAEGER'S THEORY
C
C ********************************************************************
```

```
C
      TAVG=(1./(KB+KC))*Q/(4*RAD)
      JAVG=0.946*Q/(4*RAD*(KB+KC))
      IF (IFLAG.NE.1) GO TO 111
      TMP=TAVG
      JP=JAVG
      GO TO 190
111   IF (IFLAG.NE.2) GO TO 222
      TME=TAVG
      JE=JAVG
222   IF (TME.GE.TM) GO TO 250
      GO TO 200
C
C ******************************************************************
C
C     CALCULATES THE SURFACE TEMPERATURE
C     WHEN L IS GREATER THAN 5 USING THE
C     HIGH SPEED ARCHARD EQUATION
C
C ******************************************************************
230   IF (IFLAG.EQ.1) RAD=AP
      IF (IFLAG.EQ.2) RAD=AE
      TAVG=.31*Q*SQRT(DIF/(V*RAD))/(KC*RAD)
C
C ******************************************************************
C
C      NUM IS THE NUMERATOR AND DEN IS
C      THE DENOMINATOR OF THE JAEGER
C      EQUATIONS.
C
C ******************************************************************
C
      NUM=1.064*(Q/(3.1417*RAD))*(DIF**0.5)
      DEN=(1.125*KB*DIF**0.5)+(KC*(RAD*V)**0.5)
      JAVG=NUM/DEN
      IF (IFLAG.NE.1) GO TO 333
      TMP=TAVG
      JP=JAVG
      GO TO 190
333   IF (IFLAG.NE.2) GO TO 444
      TME=TAVG
      JE=JAVG
444   IF (TME.GE.TM) GO TO 250
      GO TO 200
C ******************************************************************
C
C     CALCULATES THE SURFACE TEMPERATURE
C     WHEN L IS BETWEEN 0.1 AND 5, USING
C     THE INTERMEDIATE SPEED-ARCHARD EQUATION
C     WITH ALPHA DERIVED FROM FIGURE 7 OF
C     JAEGER'S PAPER
C
C ******************************************************************
C
240   IF (IFLAG.EQ.1) L=LP
```

```
      IF (IFLAG.EQ.2) L=LE
C
C    THESE NEXT FIVE EQUATIONS REPRESENT
C    THE CURVE OF FIGURE 7 OF JAEGER'S
C    PAPER BY APPROXIMATING THE CURVE
C    AS 5 DIFFERENT STRAIGHT LINE SEGMENTS
C
      IF (L.GE.0.1.AND.L.LE..5) Y=2.25*L-0.025
      IF (L.GT.0.5.AND.L.LE.1.0) Y=1.50*L+0.35
      IF (L.GT.1.0.AND.L.LE.2.0) Y=1.05*L+0.80
      IF (L.GT.2.0.AND.L.LE.3.0) Y=0.80*L+1.30
      IF (L.GT.3.0.AND.L.LE.5.0) Y=0.60*L+1.90
      ALPHA=(4*Y)/(3.14159**2*L)
      IF (IFLAG.EQ.1) RAD=AP
      IF (IFLAG.EQ.2) RAD=AE
      NB=Q/(RAD**2*RHOB*CB*V)
      NC=Q/(RAD**2*RHOC*CC*V)
C
C    TEMPB IS CALCULATED USING THE ARCHARD STATIONARY
C    HEAT SOURCE EQUATION
C
      TEMPB=0.5*NB*L
C
C    TEMPC IS CALCULATED USING THE ARCHARD INTERMEDIATE
C    SPEED EQUATION
C
      TEMPC=0.5*ALPHA*NC*L
C
C    THE AVERAGE TEMPERATURE ACROSS THE
C    HEAT SOURCE IS FOUND BY
C      1/TAVG=(1/TEMPB)+(1/TEMPC)
C
      TAVG=1/((1/TEMPB)+(1/TEMPC))
      NUM=0.946*DIF*Y*Q/(3.1417*RAD)
      DEN=(1.486*RAD*KC*V)+(DIF*KB*Y)
      JAVG=NUM/DEN
      IF (IFLAG.NE.1) GO TO 555
      TMP=TAVG
      JP=JAVG
      GO TO 190
555   IF (IFLAG.NE.2) GO TO 666
      TME=TAVG
      JE=JAVG
666   IF (TME.GE.TM) GO TO 250
      GO TO 2OC
250   X(1)=K-1
      Y1(1)=K-1
      Y2(1)=K-1
      CALL INITT(120)
      CALL BINITT
      CALL XTYPE(1)
      CALL YTYPE(1)
      CALL XFRM(2)
      CALL YFRM(2)
       CALL LINE(3)
```

```
      CALL CHECK(X,Y1)
      CALL DSPLAY(X,Y2)
      CALL LINE(0)
      CALL CPLOT(X,Y1)
      CALL FRAME
C
      CALL LABLE3(35,265,1.25,90.,29,'Mean Temperature Rise, deg. C')
      CALL LABLE3(375,50,1.25,0.,23,'Sliding Velocity, m/sec')
      CALL LABLE3(175,550,1.25,0.,6,'Load =')
      CALL LABLE3(175,525,1.25,0.,16,'Friction Coef. =')
      CALL RLOUT(235,550,WT,6,3)
      CALL RLOUT(375,525,MU,4,3)
      CALL LABLE3(350,550,1.25,0.,7,'Newtons')
       CALL LABLE3(400,650,1.0,0.,12,BNAME)
       CALL LABLE3(460,625,1.0,0,4,'-ON-')
       CALL LABLE3(400,600,1.0,0.,12,CNAME)
      CALL MOVABS(550,200)
      CALL DSHABS(650,200,3)
      CALL LABLE3(650,200,1.25,0.,16,'  Archard Theory')
      CALL MOVABS(550,250)
      CALL DRWABS(650,250)
      CALL LABLE3(650,250,1.25,0.,15,'  Jaeger Theory')
      CALL MOVABS(0,780)
      CALL ANMODE
      WRITE(3,510)
 510  FORMAT(10X,'DO YOU WISH TO GET A HARDCOPY OF THIS PLOT?',
     +/,10X,'TYPE 1 TO GET A HARDCOPY OR 2 FOR NO HARDCOPY.')
      IHARD = IVET(1,2,IE)
      IF(IHARD .EQ. 2) GO TO 520
      CALL PLSAVE
      CALL ERASE
520   CONTINUE
C
260   IF (WT.NE.0.0) GO TO 60
      WRITE(6,270)
270   FORMAT(1H1)
      CALL FINITT(0,700)
      STOP
      END
```

APPENDIX J

KEY TO NOTATION

Test Number

A - 4 - 150 - 1

- 1 — Test Run Number
- 150 — Normal Load ($\times 10^{-2}$ N)
- 4 — Sliding Velocity (m/s)
- A — Environment A=Air N=Nitrogen

Position

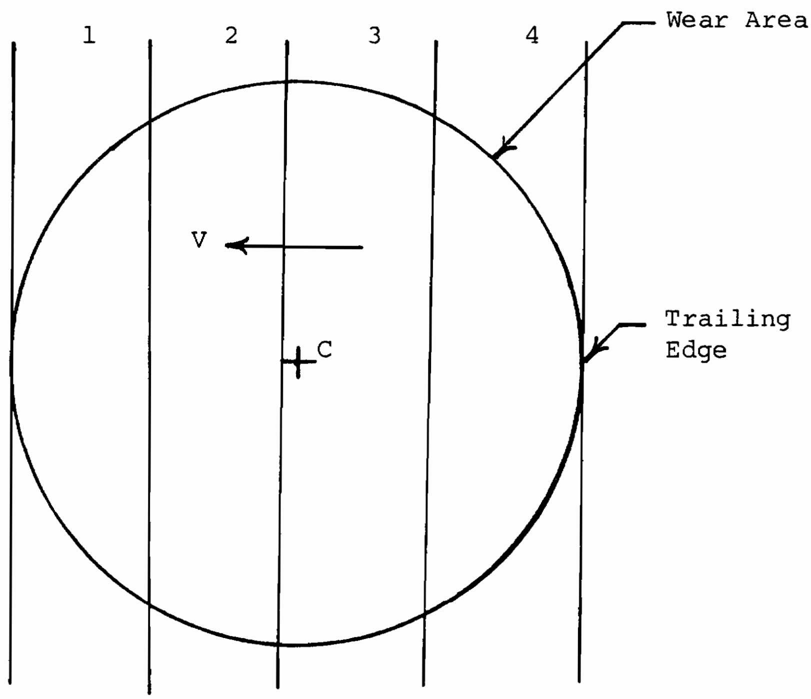

APPENDIX K

TEMPERATURE DATA

TEMPERATURE DATA

[1]Test No.	[1]Position	Radiance [2]Microscope Output (mV)			[3]Emissivity	Bulk Temp.(C)	Calculated Temperature Rise (C)		
		max.	min.	avg.			max.	min.	avg.
A-2-50-1	3	9.8	2.4	4.0	0.46-0.51	24	36	15	20
	4	16.0	2.4	10.4	0.53-0.59	24	44	14	33
A-2-50-2	3	10.7	4.4	7.4	0.46-0.51	25	37	20	29
	4	10.7	4.4	7.4	0.53-0.59	25	34	18	26
A-2-100-1	3	8.3	3.8	5.5	0.39-0.44	25	35	21	27
	4	18.0	6.0	12.0	0.46-0.52	25	50	25	40
A-2-100-2	3	25.8	3.0	8.8	0.39-0.44	26	67	17	36
	4	25.8	3.0	8.8	0.46-0.52	26	61	14	31
A-2-150-1	3	5.5	1.9	3.3	0.35-0.42	26	26	13	19
	4	33.6	10.3	14.0	0.42-0.49	26	73	36	44
A-2-150-2	3	38.0	4.4	10.4	0.35-0.42	27	83	22	40
	4	38.0	4.4	10.4	0.42-0.49	27	76	19	36

[1]See Appendix J for key.

[2]Gain adjusted to 1X.

[3]Calculated 95% confidence interval about estimated mean emissivity.

TEMPERATURE DATA CONT.

Test No.	Position	Radiance Microscope Output (mV)			Emissivity	Bulk Temp. (C)	Calculated Temperature Rise (C)		
		max.	min.	avg.			max.	min.	avg.
A-2-200-1	3	5.9	3.5	4.1	0.37-0.42	25	29	20	23
	4	46.5	8.3	15.0	0.44-0.50	25	85	31	46
A-2-200-2	3	3.2	1.6	2.8	0.37-0.42	27	17	10	16
	4	10.0	3.9	5.5	0.44-0.50	27	34	17	22
A-2-250-1	3	8.0	3.8	4.8	0.42-0.48	27	31	17	21
	4	23.8	6.3	13.5	0.49-0.55	27	55	28	38
A-2-250-2	3	4.0	2.6	3.3	0.42-0.48	28	17	12	15
	4	21.0	4.0	10.0	0.49-0.55	28	50	15	30
A-4-50-1	3	20.0	3.4	8.2	0.46-0.51	25	53	17	31
	4	28.0	3.4	8.2	0.53-0.59	25	60	14	28
A-4-50-2	3	19.2	4.0	10.4	0.46-0.51	25	52	19	36
	4	30.4	4.0	10.4	0.53-0.59	25	63	16	32
A-4-100-1	3	2.8	1.6	1.9	0.36-0.41	26	17	11	13
	4	17.8	6.6	9.6	0.43-0.49	26	50	26	35
A-4-100-2	3	9.1	1.3	3.9	0.36-0.41	27	36	9	21
	4	15.9	2.6	3.9	0.43-0.49	27	47	12	17
A-4-150-1	3	5.0	3.5	4.3	0.35-0.41	27	25	19	22
	4	42.0	13.0	23.0	0.42-0.49	27	80	41	58

TEMPERATURE DATA CONT.

Test No.	Position	Radiance Microscope Output (mV)			Emissivity	Bulk Temp.(C)	Calculated Temperature Rise (C)		
		max.	min.	avg.			max.	min.	avg.
A-4-150-2	3	7.6	3.8	5.0	0.35-0.41	29	31	18	22
	4	23.0	3.8	5.0	0.42-0.49	29	56	15	19
A-4-200-1	3	57.0	9.0	15.0	0.39-0.44	26	99	35	49
	4	57.0	9.0	15.0	0.46-0.52	26	91	32	44
A-4-200-2	3	30.0	2.6	5.7	0.39-0.44	29	69	12	23
	4	60.0	2.6	5.7	0.46-0.52	29	79	13	23
A-4-250-1	3	21.5	8.5	11.0	0.47-0.51	31	49	25	31
	4	44.0	9.5	13.0	0.54-0.59	31	70	25	31
A-4-250-2	3	26.0	9.0	15.3	0.47-0.51	32	55	26	38
	4	50.0	12.5	21.0	0.54-0.59	32	74	29	43
A-8-50-1	3	14.8	5.5	7.5	0.32-0.38	25	55	30	37
	4	24.0	6.3	12.5	0.39-0.45	25	65	29	45
A-8-50-2	3	15.0	3.5	7.5	0.32-0.38	27	53	20	35
	4	50.0	3.5	22.5	0.39-0.45	27	92	18	61
A-8-100-1	3	55.0	6.5	13.5	0.31-0.37	30	102	29	47
	4	55.0	6.5	13.5	0.38-0.45	30	94	25	43
A-8-100-2	3	95.0	8.0	35.0	0.31-0.37	30	111	34	82
	4	95.0	8.0	35.0	0.38-0.45	30	121	29	74

TEMPERATURE DATA CONT.

Test No.	Position	Radiance Microscope Output (mV)			Emissivity	Bulk Temp. (C)	Calculated Temperature Rise (C)		
		max.	min.	avg.			max.	min.	avg.
A-8-150-1	3	150.0	13.0	43.0	0.33-0.41	34	150	43	84
	4	150.0	13.0	43.0	0.41-0.48	34	139	35	76
A-8-150-2	3	160.0	14.0	42.0	0.33-0.41	34	99	46	83
	4	160.0	14.0	42.0	0.41-0.48	34	142	37	75
A-8-200-1	3	113.0	30.0	55.0	0.41-0.48	34	122	62	87
	4	113.0	30.0	55.0	0.48-0.55	34	115	57	80
A-8-200-2	3	158.0	28.0	66.0	0.41-0.48	40	135	53	89
	4	158.0	28.0	66.0	0.48-0.55	40	127	48	81
A-8-250-1	3	180.0	30.0	55.0	0.53-0.59	42	127	45	68
	4	180.0	30.0	55.0	0.60-0.67	42	120	41	64
A-8-250-2	3	130.0	36.0	72.0	0.53-0.59	42	111	52	80
	4	130.0	36.0	72.0	0.60-0.67	42	103	47	75
N-2-50-1	*	4.4	1.0	1.7	0.34-0.37	32	46	10	17
N-2-50-2	*	5.2	0.7	2.0	0.34-0.65	29	46	19	26
N-2-250-1	*	24.4	4.6	7.2	0.57-0.65	26	20	13	16

* condition does not apply

TEMPERATURE DATA CONT.

Test No.	Position	Radiance Microscope Output (mV)			Emissivity	Bulk Temp. (C)	Calculated Temperature Rise (C)		
		max.	min.	avg.			max.	min.	avg.
N-2-250-2	*	22.5	7.0	10.3	0.57-0.65	29	46	19	26
N-4-50-1	*	2.6	1.3	1.8	0.28-0.30	26	20	13	16
N-4-100-1	*	11.3	4.5	6.0	0.35-0.38	27	44	23	29
N-4-150-1	*	15.4	6.8	9.9	0.41-0.44	29	46	26	34
N-4-200-1	*	17.7	7.2	11.8	0.46-0.48	33	43	21	31
N-4-250-1	*	37.0	16.0	21.0	0.49-0.52	36	63	35	43
N-8-50-1	*	27.0	8.0	15.2	0.38-0.42	26	70	34	51
N-8-50-2	*	20.5	5.5	11.0	0.38-0.42	26	60	26	41
N-8-250-1	*	164.0	74.4	116.0	0.50-0.54	44	124	83	104
N-8-250-2	*	104.0	50.0	68.0	0.50-0.54	44	100	65	78

APPENDIX L

FRICTION DATA

FRICTION DATA

[1]Test No.	Torque (N-cm)	Radius (cm)	Coefficient of Friction
A-2-50-1	0.131	1.06	0.25
A-2-50-2	0.145	1.06	0.27
A-2-100-1	0.338	1.06	0.32
A-2-100-2	0.338	1.06	0.32
A-2-150-1	0.421	1.06	0.26
A-2-150-2	0.531	1.06	0.33
A-2-200-1	0.711	1.06	0.34
A-2-200-2	0.697	1.06	0.33
A-2-250-1	0.911	1.06	0.27
A-2-250-2	0.821	1.06	0.31
A-4-50-1	0.318	2.12	0.30
A-4-50-2	0.289	2.12	0.27
A-4-100-1	0.545	2.12	0.26
A-4-100-2	0.518	2.12	0.24
A-4-150-1	0.766	2.12	0.24
A-4-150-2	0.904	2.12	0.28
A-4-200-1	1.263	2.12	0.30
A-4-200-2	1.400	2.12	0.33

[1]See Appendix J for key.

FRICTION DATA CONT.

Test No.	Torque (N-cm)	Radius (cm)	Coefficient of Friction
A-4-250-1	1.867	2.12	0.35
A-4-250-2	1.880	2.12	0.32
A-8-50-1	0.115	1.06	0.22
A-8-50-2	0.130	1.06	0.25
A-8-100-1	0.366	1.06	0.34
A-8-100-2	0.345	1.06	0.33
A-8-150-1	0.455	1.06	0.29
A-8-150-2	0.469	1.06	0.29
A-8-200-1	0.568	1.06	0.27
A-8-200-2	0.508	1.06	0.24
A-8-250-1	0.681	1.06	0.26
A-8-250-2	0.584	1.06	0.22
N-2-50-1	0.214	1.06	0.40
N-2-50-2	0.211	1.06	0.40
N-2-250-1	0.959	1.06	0.36
N-2-250-2	1.042	1.06	0.39
N-4-50-1	0.393	2.12	0.37
N-4-100-1	0.766	2.12	0.36

FRICTION DATA CONT.

Test No.	Torque (N-cm)	Radius (cm)	Coefficient of Friction
N-4-150-1	1.152	2.12	0.36
N-4-200-1	1.511	2.12	0.36
N-4-250-1	1.760	2.12	0.33
N-8-50-1	0.115	1.06	0.22
N-8-50-2	0.129	1.06	0.24
N-8-250-1	0.653	1.06	0.25
N-8-250-2	0.722	1.06	0.27

APPENDIX M

WEAR DATA

WEAR DATA

[1]Test No.	Δ Weight (mg)	Wear Vol. ($\times 10^{-11} m^3$)	Sliding Distance (m)	Wear V/L ($\times 10^{-14} m^2$)	K($\times 10^{-5}$)
A-2-50-1	*0.078*	*0.99*	*717.3*	*1.4*	*2.5*
A-2-50-2	*0.102*	*1.30*	*668.0*	*1.95*	*1.75*
A-2-100-1	*N/A*	- -	- -	- -	- -
A-2-100-2	*0.102*	*1.30*	*548.9*	*2.37*	*2.13*
A-2-150-1	*0.249*	*3.17*	*575.3*	*5.51*	*3.30*
A-2-150-2	*0.061*	*0.78*	*560.5*	*1.4*	*0.83*
A-2-200-1	*0.167*	*2.13*	*755.3*	*2.81*	*1.27*
A-2-200-2	*0.134*	*1.71*	*614.1*	*2.78*	*1.25*
A-2-250-1	*0.278*	*3.54*	*502.5*	*7.04*	*2.53*
A-2-250-2	*0.198*	*2.56*	*496.1*	*5.08*	*1.83*
A-4-50-1	*0.119*	*1.51*	*1040.1*	*1.46*	*2.62*
A-4-50-2	*0.131*	*1.67*	*1036.1*	*1.61*	*2.90*
A-4-100-1	*N/A*	- -	- -	- -	- -
A-4-100-2	*0.068*	*0.87*	*880.1*	*0.98*	*0.89*
A-4-150-1	*N/A*	- -	- -	- -	- -
A-4-150-2	*0.337*	*4.29*	*1093.9*	*3.92*	*2.35*
A-4-200-1	*N/A*	- -	- -	- -	- -
A-4-200-2	*9,229*	*2.91*	*1579.7*	*1.84*	*0.83*

[1]See Appendix J for key.

WEAR DATA CONT.

Test No.	Δ Weight (mg)	Wear Vol. ($\times 10^{-11} m^3$)	Sliding Distance (m)	Wear V/L ($\times 10^{-14} m^2$)	K($\times 10^{-5}$)
A-4-250-1	0.316	4.2	1103.3	3.64	1.31
A-4-250-2	0.361	4.59	1059.9	4.33	1.56
A-8-50-1	0.291	3.70	2788.5	1.33	2.39
A-8-50-2	0.184	2.34	2372.0	0.99	1.78
A-8-100-1	0.196	2.49	2185.3	1.14	1.03
A-8-100-2	0.231	2.94	1962.6	1.50	1.35
A-8-150-1	0.309	3.93	2009.4	1.96	1.17
A-8-150-2	0.339	4.31	2250.4	1.92	1.15
A-8-200-1	0.662	8.42	2331.9	3.61	1.63
A-8-200-1	N/A	- -	- -	- -	- -
A-8-250-1	0.692	8.80	3153.3	2.79	1.01
A-8-250-2	0.687	8.74	2230.1	3.92	1.41
N-2-50-1	0.256	3.26	703.1	4.63	8.34
N-2-50-2	0.295	3.75	674.5	5.56	10.00
N-2-250-1	0.804	10.2	507.6	20.2	7.25
N-2-250-2	1.158	14.7	666.0	22.1	7.95
N-4-50-1	N/A	- -	- -	- -	- -
N-4-100-1	N/A	- -	- -	- -	- -
N-4-150-1	N/A	- -	- -	- -	- -

WEAR DATA CONT.

Test No.	ΔWeight (mg)	Wear Vol. ($\times 10^{-11} m^3$)	Sliding Distance (m)	Wear V/L ($\times 10^{-14} m^2$)	K($\times 10^{-5}$)
N-4-200-1	*N/A*	- -	- -	- -	- -
N-4-250-1	*N/A*	- -	- -	- -	- -
N-8-50-1	*0.174*	*2.21*	*2186.5*	*1.01*	*1.82*
N-8-50-2	*0.200*	*2.55*	*2432.2*	*1.05*	*1.88*
N-8-250-1	*0.745*	*9.48*	*2937.1*	*3.23*	*1.16*
N-8-250-2	*0.755*	*9.61*	*2462.7*	*3.90*	*1.40*

VITA

Steven Craig Moyer was born in Anthony, Kansas on April 15, 1958, to Mr. and Mrs. S. Jay Moyer. He attended the public schools in Argonia, Kansas, and graduated from Argonia High School in May, 1976. In the fall of 1976, he began his college education at Wichita State University in Wichita, Kansas, where he pursued a course of study leading to a Bachelor of Science degree in Mechanical Engineering. On May 26, 1979, Mr. Moyer was married to Miss Llewellyn McCoy. Graduating in May, 1981, he began his graduate education at Virginia Polytechnic Institute and State University in September, 1981, with the expectation of obtaining a Master of Science degree in Mechanical Engineering. Mr. Moyer is currently an Engineer-in-Training in the State of Kansas and an associate member of the American Society of Mechanical Engineers.

Steve C. Moyer

Steve C. Moyer